# METHODOLOGY FOR ON-LINE BATTERY HEALTH MONITORING

by

Lalit Prakash Mandal

A dissertation submitted to the faculty of
The University of North Carolina at Charlotte
in partial fulfillment of the requirements
for the degree of Doctor of Philosophy in
Electrical Engineering

Charlotte

2012

Approved by:

_____
Dr. Robert W. Cox

_____
Dr. Yogendra Kakad

_____
Dr. Jonathan Bird

_____
Dr. Na Lu

ABSTRACT

LALIT PRAKASH MANDAL. Methodology for on-line battery health monitoring.
(Under the direction of DR. ROBERT W. COX)

The growing demand for electric vehicles and renewable energy sources has increased the need for safe, reliable, and cost-effective energy-storage systems, many of which include batteries. The reliability and efficiency of these battery-based systems can be significantly improved using intelligent energy-management systems that effectively indicate battery health in real time. On-line monitoring can be difficult, however, because batteries are non-linear and time-varying systems whose characteristics depend on temperature, usage history, and other factors. The key metrics of interest in a battery are its remaining capacity and health. Most of the current methods require off-line measurement, and even the available on-line methods are only good in laboratory conditions. This thesis provides an enhanced streamlined framework for on-line monitoring. In this methodology, a non-intrusive test signal is superimposed upon a battery load which causes transient dynamics inside the battery. The resulting voltage and current are used as test data and the estimation is done in two parts. First, a non-linear least-squares routine is used to estimate the electrical parameters of a battery model. Second, a state-estimation algorithm is used to estimate the open-circuit voltage. Experimental results obtained at consistent temperatures demonstrate that the open-circuit voltage and parameter values together can combine to provide capacity and health measurements. This approach requires minimal hardware and could form the basis for a robust on-line monitoring system.

## DEDICATION

I would like to dedicate this work to my beloved mother who could not live to see this day, but whose blessings and memories always guide me.

# ACKNOWLEDGMENTS

I would like to thank my advisor Prof. Dr. Robert Cox for his guidance and support. His incisive comments and ideas were instrumental in bringing out this work and I deeply appreciate the opportunity to work under him. I am grateful to Prof. Dr. Yogendra Kakad for accepting to be in my thesis committee graciously. I would also like to thank Prof. Dr. Jonathan Bird and Prof. Dr. Na Lu for reviewing my thesis and giving many valuable suggestions. Thanks goes to all my present and past labmates at NC Laboratory of Energy Efficient Systems. I also extend my sincere gratitude to Ms. Pat Winter in the department and Ms. Marian Beane in the International Student Office for always helping me find resources and stay legally footed in the University System. Lastly I thank my family for their love and encouragement all these years.

TABLE OF CONTENTS

LIST OF FIGURES

LIST OF TABLES

CHAPTER 1: INTRODUCTION

The battery market is rapidly growing and is expected to reach \$50 billions by 2015 [1]. Most of the growth is driven by increasing use of batteries in automobiles, portable electronics and medical devices, and renewable energy sources. As it becomes one of the important sources of energy storage and back-up supply for the majority of applications, it becomes imperative that the batteries are monitored continuously and efficiently. Some of the prominent usages of battery are given below.

- Use of battery in automobiles

The increasing demand to improve fuel economy and reduce emission in present automobiles has accelerated the development of propulsion drives beyond the conventional internal combustion engine (ICE). Such system combines ICE with other forms of energy storage most commonly with battery. A battery or a stack of batteries in a hybrid and electric vehicle enables an electric motor to store braking energy in the battery during regeneration. During driving, the electric motor utilizes the stored energy in a battery to propel the engine in the absence of the ICE. Several kinds of battery are used for automotive applications like lead-acid, nickel-cadmium, and lithium-ion etc. Because of its usage in critical vehicle operation, it is important that the batteries are monitored regularly to provide an analogous form to the 'fuel gauge' of a conventional vehicle.

- Use of battery in uninterruptible power supply (UPS)

The rise of internet and wireless communication has created thousands of data centers and uninterruptible power supply (UPS) system around the world, in which the battery is used as a back-up power supply. Since the battery is one of the important components in a UPS system, its reliable functioning is needed for the overall functioning of the system. For example, as reported in [2], a single lead-acid battery is used in each of the thousands of servers that Google uses for its operation. This serves as an example of critical application of a battery. With the increasing trend of computing over internet, and more data being stored online, the number of data centers are only going to increase. The timely functioning of battery would be one of the indispensable attributes for the UPS system in future and is a major concern for companies around the world.

- Use of battery in electronic devices

Batteries are used to power most of the electronic and portable devices in use today. A malfunctioning of the battery may cause such system to stop working. Furthermore, a lack of accurate monitoring of the battery may cause a device to provide unreliable information. Such an issue may create a lack of confidence among consumers and may bring upon a huge loss to a company [3]. Because more devices are going wireless and more people are using them, the importance of reliable monitoring of the battery is only growing. One major question in such appliances is to find out the available power from the battery on a continuous basis. An effective monitoring mechanism can not only provide this information but also can yield the maximum power and longest life to the device.

In addition,the battery is one of the attractive options for energy storage for distributed energy sources like wind and solar in which the energy is required to be stored for the period when the energy production in not on. For large scale production of energy by such sources, equally large and reliable storage mechanism has to be put in place for which a cost-effective and reliable battery monitoring mechanism would be an important component.

Because of the diverse applications of batteries, an inexpensive and minimally intrusive monitoring system would be invaluable in terms of providing reliable power and timely replacement. Any such monitoring system would have to be independent in the sense of being self-contained, requiring minimal physical presence and no reconfiguration of the automated system.

## 1.1   Battery Monitoring

The primary terminologies used to describe the battery capacity and health are state-of-charge (SOC) and state-of-health (SOH) respectively [4, 5, 6]. The SOC refers to the total charge stored in a battery relative to what is available immediately after the battery is fully charged. In other words, it is the percentage of charge available with respect to the stage when the battery is fully charged and the SOC is considered a unity. In general, the SOC may be considered as the remaining capacity or analogous to "fuel gauge" in a vehicle. Similarly, the SOH is the measure of the degree of degradation of a battery with respect to the condition of a fresh or good battery. Generally, the purpose of SOH is to find out whether the battery needs to be replaced. Most of the monitoring methods tend to assess either SOC or SOH or a

combination of both.

The diverse applications of battery and hence the need to monitor it efficiently requires a method which is simple to use and requires minimal inputs, and provides lucid results. Moreover, a monitoring may be sought in diverse operating conditions. Some of these conditions are given below [4].

1) The battery is only partially charged. In other words, the discharge may not start from a fully charged stage or unity SOC.

2) The charging is done at different current rates for unequal durations. One instance of charging may not bring the battery to its unity SOC. In addition, once the charging is done, the settling time may vary depending upon the operation.

3) Discharge is done at different current rates with varying interval between discharges. Also the duration of discharge may fluctuate.

4) Full discharge or the run-down discharge is performed by drawing a large current for a long time.

5) The operating temperature is anywhere between -30C to 50C.

6) The process to initiate a test is easy and short.

7) The raw data obtained from the battery is processed and the result is presented in a simple way.

The above cases are few of the conditions in which a monitoring method has to provide an assessment. Ideally, such method should also provide a mechanism to control voltage and current, and charging status, and give an assessment of operating range of SOC, temperature, and any indication of unwanted situation that may have adverse impact on the battery life. The method should read available data like current and

voltage easily, and also be flexible in terms of giving the prediction for near term, medium term, or long term. Specifically, the two factors that such method has to predict reliably are SOC and SOH. However, estimating SOC or SOH independently may not be enough for a robust assessment because the measures of SOC and SOH give different but complementing information about the battery. For example, a new battery with high SOH can still be operated in low SOC range, and an old battery with poor SOH can be acceptable if it is in high SOC range. Hence both measures in combination may be required to provide a good assessment. A combination of SOH and SOC can be used to calculate a figure of merit that would provide an unequivocal measure and which is observable in all operating conditions [4].

## 1.2    Contribution

The tasks required for an effective battery monitoring, as outlined above, are broad and dynamic. Because of their important and pervasive applications, a method that would monitor the battery status in real time have been widely explored. However, in the context of efficient nonintrusive battery monitoring, there are unique issues.

A primary problem is the lack of uniformity in modeling of the electrochemical behavior of a battery. Batteries are extremely complex systems whose characteristics are nonlinear, time-variant, changing with respect to aging, operating conditions, charge/discharge rates, temperature and other structural and environmental based factors. Conventionally, researchers have tried to model the electrochemical behavior of a battery by an equivalent lumped element electrical circuit. However, most of the models have been chosen arbitrarily under the constraints of the laboratory conditions

at a fixed operating condition. Since the batteries are operated at various conditions as outlined above, the ease of model specification is essential to make a nonintrusive online battery monitoring working in a wide range of applications in a simplistic way.

Electrochemical impedance spectroscopy (EIS) is a powerful mathematical tool for modeling the behavior of a system [7, 8, 9]. Since the concept and steps are widely understood and recognized, the researchers have long used it to study a battery. Such methodology relies on the fact that there is resistance to flow of charge inside a battery showing a resistive and a combination of capacitive and inductive characteristics. However, the impedance spectrum over the full range of SOC merely changes minimally and this makes it difficult to differentiate distinctly the different SOCs. In addition, the variation in complex impedance may take place due to several external factors such as temperature, aging and depth of discharge. Furthermore, an expert understanding of EIS and detailed experimental setup used by researchers in the past have made it impractical for the common method of battery monitoring.

The search of an effective method has led researchers to the use of non-linear estimation techniques. However, one primary issue is that the iterative optimization techniques often used to estimate parameters require a good initial guess. For an online device designed to handle a range of operating conditions, this can be an issue. Another aspect of the problem unique to the nonintrusive battery monitoring is the availability of data for the pattern matching processes. A variety of batteries with different capacity ratings and chemistries make it a daunting task practically. Moreover, many such methods are computationally expensive and time consuming.

This thesis provides a new streamlined framework for enhanced battery monitoring

based on modeling of its behavior and estimation of parameters, with a focus on simplistic nonintrusive on-line methodology. This framework is designed with commonly available batteries such as lead-acid and lithium-ion and is established with general battery applications.

## 1.3  Organization

A detailed overview of prior works in the area of battery monitoring is presented in Chapter 2. Chapter 3 presents the modeling of a battery behavior based on an equivalent electric and simplistic model. Chapter 4 covers the nonlinear estimation technique used for the estimation of parameters of the simplified battery model. Chapter 5 provides an adaptive state-estimation technique used to measure the open-circuit voltage of the battery. Chapter 6 provides experimental results and validation tests and chapter 7 gives conclusion and recommendations for future works.

# CHAPTER 2: BATTERY MONITORING

Several methods have been developed to determine the health of a battery in the past two decades. These methods rely on various parameter measurements. Many techniques, for instance, directly aim to determine the state-of-charge (SOC), while others aim to determine explicit values for individual model elements. Using individual parameter values, researchers have been able to track both state-of-charge and overall health or state-of-health (SOH). Almost all of the available health-monitoring methods are time-consuming and require specific, off-line tests. Many other on-line methods are only good in laboratory conditions under test data. This section reviews the most popular health-monitoring methods in use today.

## 2.1    Background

Measurement of electrolyte specific gravity (SG) is the conventional approach used to determine SOC . In this technique, the specific gravity of a battery's electrolyte is measured using a hydrometer [10]. The SG of a chemical solution is defined as the ratio of the density of the chemical substance to the density of water available per unit solution. A hydrometer is a common instrument that can be dipped inside the chemical solution to measure the SG. Specific gravity readings can be translated into SOC values using data tables. The advantage of the specific gravity method is its simplicity. The procedure is easy to carry out, and anyone with limited training can

do it. However, this method does have several important drawbacks. The first and most important is the fact that measurements cannot be recorded while the battery is in use as the electrolytic solution must be at rest for at least 3 hours before an accurate reading can be taken. In addition, most batteries in use these days are sealed, making SG measurements very difficult to obtain. Moreover, it is relatively dangerous to draw some electrolyte from an open battery.

The other old method is the use of the stabilized float current for determining if a battery is fully charged [11]. This technique, which is only usable during charging, exploits the fact that most lead-acid battery chargers maintain a constant and stable current into a battery once it approaches full charge. This method is commonly used in generating stations and substations that feature batteries for back-up systems . Although this method has been found extremely reliable, it is impractical in any mobile situation in which the battery is not being constantly charged. Furthermore, it does not provide a running indicator of SOC, only an indication that the battery has returned to full capacity.

Yet in another method, the battery is left to rest for a long time in the range of 3 hours, and the open-circuit voltage is measured from the open ends of the battery. The value of open-circuit voltage is subsequently tallied to its SOC value from a pre-calibrated table [12].

Most of these old methods of SOC estimation are stationary ones. Such methods like electrolyte specific gravity, stabilized float current, open circuit battery voltage measurement etc. require a long testing time and the battery needs to be off-loaded. Since the battery operation has to be interrupted before SOC estimation is done,

such methods are not suitable for practical purposes in modern battery applications and hence are not relevant in the review here. Only those methods that estimate the SOC non-intrusively in a relatively short span of time are reviewed here.

All the attempted methods to model the battery behavior and estimate the SOC can be broadly divided into four categories. Each of these methods with its advantages and disadvantages is reviewed in details here.

## 2.2    Impedance Spectroscopy Method

Electrochemical impedance spectroscopy (EIS) is a well established mathematical tool in which a small sinusoidal current signal superimposed on a larger direct current is sent to a battery, and the resulting responses of voltage and phase are measured. By the complex division of ac voltage by ac current, the impedance of the battery is measured [9], and it is repeated for all meaningful frequencies. This is a useful tool to measure the impedance of a battery and is quite prevalent among the researchers [13, 14, 15, 16, 17, 18, 19, 20]. The first such experiment on a battery seems to go back as far as 1941 [21] and the preliminary record of impedance data seems to be given first by [22], in which the impedance measurement is performed at a wide range of frequencies recording the variation among the impedances at different frequencies. Although no apparent interpretation of impedance data was floated by [22], it was clearly shown that the impedance varies with the depth of discharge and in fact varies in greater magnitude than the corresponding change in the open-circuit voltage of the battery. This paves the way for use of battery impedance as a possible tool to predict the battery status. In another early work in [18], the

kinetics of the electrochemical process inside the battery is modeled by equivalent electrical components like inductor, capacitor and resistor. It was established that the battery can be represented by an ideal voltage source in series with a combination of a resistance and a reactance, mostly capacitive reactance. A continuous shift in the impedance parameters in the frequency range 15 to 200 Hz with SOC was observed, but the nature of the curves was shown to be parabolic which could not directly be used to correlate with the SOC of battery due to the nonlinear nature.

Another attempt was made to measure the residual capacity of a lead-acid battery by the use of EIS in [17, 19, 23]. First, an equivalent electrical circuit was established to describe the impedance of the battery. Second, it was shown that the components do not vary smoothly and consistently enough with residual capacity to provide a basis for a test nor was it suitable to use a single frequency to measure the system impedance. However, it was shown that the combination of charge-transfer resistance and the double layer capacitance which makes the time-constant of the $R$-$C$ network in the battery model decreases sharply and smoothly between 50 and 100% SOC range and could form a basis for a test. It was further found that there exists a basic difference in the complex impedance of a battery with a differently aged and differently treated cell and this feature could form a basis for SOH of a battery. However, an extensive requirement of circuitry needed to carry out the experiment was acknowledged as the hindrance for the extensive use of this method. Following up with similar experiment in [24], it was further supported that there exists a unique value of combined charge-transfer resistance and double-layer capacitance, which could be a basis for a test. However, it was acknowledged that the variations in the complex

impedances of the battery at a different frequencies are not enough and unique in nature to determine the SOC of a battery distinctively. A further analysis of impedance spectroscopy of a battery was done by [14]. It was shown that the Nyquist plot of the complex impedance at different frequencies of a battery is semi-circle in nature. The values of basic circuit elements like the charge-transfer resistance and the double-layer capacitance are subsequently estimated from the plot. However, it was agreed that the variations in operating conditions and rated capacities of battery make it hard to use impedance spectroscopy on a consistent basis for the battery assessment.

In contrast to many experiments in the preceding references which showed that the parameters of a battery are non-linear in nature, a dynamic model for battery kinetics was presented in [16]. Again the method of impedance spectroscopy was used to find the parameters of the equivalent circuit model. However, it also showed the complex circuit model comprising of several components when the varying kinetics inside battery is represented by equivalent circuit model. A review of the issues associated with the use of impedance spectroscopy to assess the battery was further presented by [13]. They explained the challenges of this method into three categories. First, *nonlinearity* is an issue when the batteries are operated at relative high current during which the transport and reaction processes inside the battery are non-linear in nature and cannot be neglected. Second, *nonstationarity* is another issue by which the structures inside battery changes during charging or discharging processes. *Nonideality* is the third issue which occurs because reaction kinetics and mass transport inside a battery varies from one battery to the other making it hard to come up with a method that works well for all operating conditions. These above issues were cited to limit the

scope to EIS for most practical usages. A further attempt was made in [15] to model the parameters of the porous electrode structure, the reaction kinetics, electrolyte transport, and failure mechanism inside battery, but still the results do not show any apparent consistent way by which SOH and SOC would be measured consistently by this method. To match as closely as possible the varying complex impedances at different frequencies, the author in [8] used an extended double-electrode lumped electrical model of battery. In order to provide a quantitative measure of SOC and SOH, the author in [8] used nonlinear estimation method. Similarly, an extended modeling of complex impedance of battery was done by [25], but it was made more computationally challenging to calculate the parameters of lumped electrical model and it further showed the difficulty of modeling impedance spectrum of battery by equivalent lumped electrical circuits. A similar attempt to do extending modeling of complex impedance of battery was also done by [26]. However, only one lumped equivalent parameter is ultimately considered for battery health measure. Such limitation contained the use of this method and was further argued by [27], in which the concluding argument seems to be that EIS is helpful only in certain operating conditions for particular purpose and the overall assessment of battery health has to combine EIS with some additional evaluation scheme. A similar conclusion is also drawn by [20] in a recent paper.

In summary, EIS was invariably the first mathematical tool adopted by researchers with an expectation to model the battery kinetics. Since it has been an established tool to study the behavior of a system for a long time, it was natural to look into it. However, extremely complex kinetics of electrochemical processes inside a battery

render the EIS method to have very limited use in practice. Apparently it is difficult to determine SOC in all operating conditions based on its impedance spectra only. However, the variation in the complex impedance through an entire SOC discharge process can be a tool for SOH assessment. Yet it could still be a useful tool to study the battery kinetics and especially use it to compare an equivalent electrical model of battery.

## 2.3    Current Integration Method

Current integration or Coulometric measurement is the most commonly used method to measure the SOC of a battery [7, 28, 29, 30, 31]. This method uses the dynamic measurement of the battery current, and integrates it for a finite interval giving the direct assessment of the remaining SOC. Although this method sounds intuitively straightforward, it has a number of practical limitations. First, it requires the initial level of SOC to be known before the current integration is performed. Any wrong initial value of SOC keeps accumulating in the subsequent measurements of SOC. Since SOC is a dynamic quantity which depends upon the temperature, operating conditions, aging etc., it is a difficult task to calibrate SOC at regular intervals correctly. Moreover, there may arise error in the terminal measurement of current due to noise, resolution, and rounding off. Furthermore, the available capacity depends on the rate of discharge, and it also decreases with aging and the number of cycles in use. Although it has been a popular method to estimate the remaining capacity of battery, there is a good consensus that it is not the most effective one[29]. Especially in electric vehicle operations, in which the recurrent cycles of charging/discharing is a

norm, implementing this method would be more difficult. This method may work for short charging/discharing load especially when the flow of current is unidirectional and constant supported by accurate current reading and controlled temperature setting. For the diverse applications of battery currently, this requirements can not be fulfilled. For example, one practical problem that arises with this method is described here from [29] and shown in Fig. 1. The top graph shows the SOC estimation based
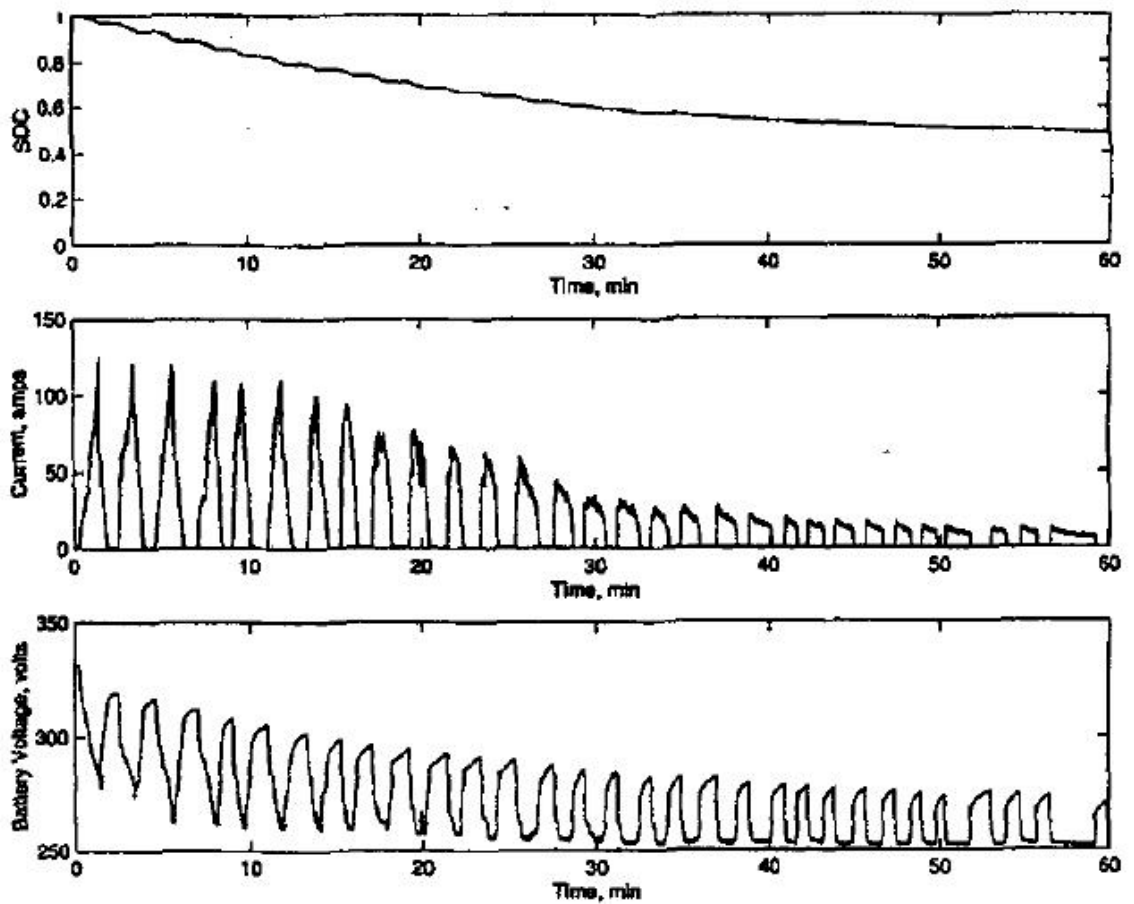


Figure 1: Top:- SOC estimate by the current integration method; Middle:- terminal current from the battery; Bottom:- battery terminal voltage [29].

on the current integration, assuming the starting SOC to be 100%. The center graph shows the current drawn from the battery, and the bottom graph show the voltage

drawn from the battery. Although the voltage has decreased substantially, and the drawn-out current from the battery pack is very low, the estimated SOC level is still high, giving inaccurate assessment of battery capacity. In this sense, the current integration method is analogous to open loop because the SOC estimation does not take into account the battery parameters such as the open-circuit voltage [29]. The method is also dependent upon accurate initial value of SOC and discharge rate which varies by usage and time resulting into big mistake in the SOC estimation[**?**]. Such problem is considered typical for this method.

In summary, the current integration method may work well for estimating SOC for short charging/discharing profiles especially when the flow of current is unidirectional, and constant and the accurate measurement of current is taken and the experiment is done in a controlled environment. For diverse operating conditions of battery, this may not be a suitable method. In addition, it does not provide any basis for the SOH measure.

## 2.4    Kalman Filter Method

Another method is state-estimation technique such as Kalman Filter (KF), Extended Kalman Filter (EKF) etc. for real-time prediction of SOC and SOH [29, 32, 33, 34, 35, 36]. The Kalman Filter is a least squares optimal estimator for discrete time linear systems, which may contain noise and are stochastic in nature. The algorithm iteratively estimates the optimal state vector at each time step by estimating first the state vector at the previous time step and covariance based on a state-space model and then correcting this estimate in a least-square sense using the latest measurement

of output from the actual system. The EKF extends this algorithm to the nonlinear dynamic systems. The state variables are still estimated using a system model, but to estimate covariance and correct state estimate, the model is linearized around the latest estimate of the state variables [34].

Using this approach, the authors in [29] have presented a measure of state variables to indicate SOC. Using a non-linear time-varying state-space model, states are modeled as first-ordered Markov color-noise processes. The system of equations is then linearized, and the extended Kalman filter algorithm is used to implement a state estimator for the resulting linear and time-varying equations. They show that this method could be a feasible way to estimate SOC under constant-temperature conditions, although the authors were not able to achieve accurate estimates of the parameter values (i.e. $R_d$, $R_b$, and $C$). The authors in [33] used the same non-linear time-varying state-space model and proposed a deterministic method for determining the open-circuit voltage $V_{oc}$ by assuming that the state variables do not vary over time. As a prerequisite, the authors assume that the current has a quadratic dependence on time. The authors clearly show that the observability of the overall model relies on this quadratic dependence. They do not show, however, whether or not higher-order dependence will affect observability. In order to demonstrate that their method is feasible, they determined $V_{oc}$, but they arbitrarily reset their estimate to the measured terminal voltage approximately 100 seconds after each discharge was ended. The authors justify this resetting operation because they assume that the states are constant. Note that this decision amounts to stating that the parameters $R_d$, $R_b$, and $C$ are constant. Since these parameters vary with other factors,

such as temperature and age, the proposed estimation method could lead to arbitrary biases. Similarly, the authors in [32] have used the Kalman filter approach to measure SOC, but their battery model does not seem to follow the output terminal voltage completely. Moreover, the authors have used a pulse current to generate a voltage profile from a battery for the testing purpose, but it is not supported for diverse current profiles. In a similar use of this method in [37], extensive modeling is done to represent the electrochemical phenomena of a battery. However, such an extensive electrical model with several parameters are computationally challenging. Furthermore, the use of EKF is poor in transients and it needs long time to adapt the parameters to get small error[38]. Also, the SOC range used in [37] is from 50% to 90% which seems to under-utilize the operating range of SOC. Since the accuracy of the battery model is crucial for the accuracy of the estimator, a new battery model was proposed by [34]. However, a model has to be widely accepted and applicable in all practical conditions. Similarly, extensive modeling based on other variables of the battery such as over-potential, concentrations and current distribution across the electrodes is presented in [35]. Such a large set of parameters from a model may bring a huge overhead, and may make the result analysis difficult. In another recent work of [36], EKF is used along with neural networks, which works only in a controlled environment and the performance may not be robust for all battery chemistries.

In summary, although KF and EKF are popular tools to estimate state variables, it would require an accurate dynamic model of the battery. Since battery dynamics depends upon several factors such as operating conditions, discharge rates, temperature, electrochemical reaction etc., an effective model which will fit all operating conditions

is difficult to implement. If modeling is extended with the addition of several lumped electrical components, the estimates of parameters will be computationally more challenging. Accurate initial guess for these parameters are also important which may pose a challenge too.

## 2.5    Miscellaneous Methods

The lack of a robust method for estimating the SOC of the battery has given rise to several new ideas over the years. A number of these works are focused on modeling battery with different lumped-electrical circuit, presenting a new algorithm, or using statistical approach. One such early approach was *coup de fouet* method [39, 40] in which the beginning sag in the open-circuit voltage of battery is used to assess the battery capacity empirically. However, the battery SOC being dependent upon so many variables, it makes it impractical for the majority of applications. In another such work in [41], a simplified battery model is used along with voltage and current to estimate parameters, which would form a basis for battery of monitoring. A similar idea is presented by [42] in which one of the parameters in the form of a double-layer capacitance is used to estimate the battery capacity. However, this method is shown being used only at a constant current discharge. In [43], a method is presented in which the reserve time with respect to the SOC of the battery is found out irrespective of capacity, discharge rate, operating condition, and ambient temperature. In this method, the initial open-circuit voltage of the battery is normalized with respect to an assumed base voltage, and a unified characteristic curve is produced for the total discharge at the given current. However, the normalization is not practical because

the open-circuit voltage does not stay constant and any error in it would accrue over time. Furthermore, the range of voltage change allowed for operations from a battery is normally a small one close to about one volt for a battery with a nominal voltage of 12 V. Any wrong assumption about the base voltage can give an inaccurate estimation of the reserve time. Moreover, it is not clear how to proceed when the discharge rate is not constant. An analytical method is presented in [44], but it is only meant for portable electronic devices with generally low battery capacity, and it is not clear how it would function for the higher rating industrial batteries.

An early statistical method is presented in [45], in which the open-circuit voltage is estimated by using a record of charging profiles. Since battery charge/discharge depends upon many variables, any such method would be difficult to implement in practice. Furthermore, rapid charging/discharging from a battery may not show the full voltage profile for use in a statistical analysis. An effort to model other variables like temperature is shown in [46], in which they present a temperature dependant battery model, but they have only provided simulated results. SOC estimation from the combination of impedance, open-circuit voltage and discharge current is presented in [47]. However, the combination of all three factors may make it difficult for analysis, and they also used an extended battery model which contains several parameters and seems to have little support elsewhere in literature.

Presenting yet another new approach, the authors in [48] used an artificial neural networks (ANN) to estimate SOC. However, the use of ANN may still have limitations because of the dependency of SOC on various factors and the difficulty in giving accurate input data. A nonlinear dynamic modeling of a battery is presented in

[49] for NiMH battery. However, it is not clear whether it would support other battery chemistries and operating conditions. In [50], they used an impulse response to estimate the open-circuit voltage. However, an accurate impulse response from a battery is always challenging and it may not be the optimal method for different discharge currents. Nonlinear modeling for battery discharges is also presented in [51] using few sets of discharge currents. However, they have not shown whether they are valid when other variables like temperature is considered. A new model of a battery based on partial differential equations is presented in [52]. However, how effective the model is yet to be verified.

Similarly, a novel idea of applying the Bayesian theory for managing uncertainty and complexity in battery modeling is floated by [53, 54, 55]. Bayesian tools like Relevance Vector Machine (RVM), and particle filters (PF) are used to measure the remaining useful life ( RUL) and SOH. However, most of these methods have been used for batteries in space application, which are different in size, weight, capacity and cost. It is yet to be supported for other batteries with larger capacity, discharge rates and availability. In addition, they do not seem to present a direct method to estimate SOC, but rather they focus estimating the remaining useful life (RUL).

## 2.6    Summary

The lack of a robust monitoring method has given rise to plenty of research and experiments especially in the last several years. Researchers have tried to come up with new methods to enhance the battery monitoring method. However, any new method needs to be tested for all operating conditions and be easy to implement. The

right approach may be a trade-off between the complexity in the battery modeling,

the parameter estimation process, and its simplicity to use and analyze the results.

CHAPTER 3: BATTERY MODELING

Numerous studies on the kinetics of electrochemical processes inside battery have been reported in the literature [9, 21, 8, 42, 14, 56, 57]. Equivalent electrical circuits have been developed to model these processes. Based upon several assumptions that are applicable to battery characteristics, simplified electrical circuits are presented. Subsequently, a simplified electrical circuit is derived and used for either lead-acid or lithium-ion chemistries. Such an equivalent electrical model broadly supports the characteristics a battery exhibits during discharge, charge or rest.

### 3.1 Detailed Electrical Equivalent Circuit

Fig. 2 shows a detailed model that has been widely reported [9, 21]. Note that this model separately describes processes occurring at the individual electrodes, hence the use of the subscripts $p$ and $n$.
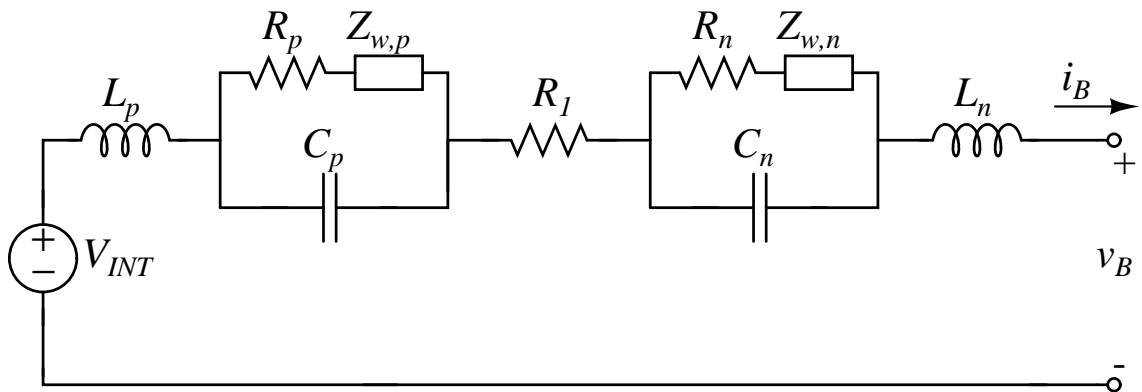


Figure 2: Detailed electrical equivalent circuit for a lead-acid battery.

A physical explanation can be provided for each of the components in Fig. 2. $L_p$ and $L_n$, for instance, model the inductive behavior caused by the porosity of the individual electrodes [9, 21]. $R_1$, on the other hand, represents the combined resistances of the electrolyte, the contacts, and the crystallized lead-sulphate layer on the electrodes [9, 21]. The resistances $R_n$ and $R_p$ model losses due to charge transfer at the electrodes, and $C_p$ and $C_n$ are the capacitances arising from space-charge distribution in the electrochemical double layers [9, 21]. The terms $Z_{w,p}$ and $Z_{w,n}$ represent the so-called Warburg impedances caused by ion diffusion in the electrolyte and in the electrode pores. These impedances are of the form

$$Z_w = \frac{\sigma}{\omega^{1/2}} + \frac{\sigma}{\jmath\omega^{1/2}}, \tag{1}$$

where $\sigma$ is a coefficient related to the various physical properties of the electrodes [21]. The model also includes an internal source $V_{INT}$ which is observable at the terminals under open-circuit conditions.

### 3.2    Modified Electrical Circuit

The detailed equivalent circuit in Fig. 2 was developed from physical arguments and validated using impedance spectroscopy [9, 21, 8, 42, 14]. With certain simplifying assumptions, the model can be reduced to a simpler circuit having a similar impedance spectrum. Because the impedances of the cathode and anode are nearly identical, for instance, they cannot be clearly resolved experimentally [9, 21]. It is thus reasonable to combine the electrode impedances into a single group. Similarly, the inductive reactance is typically only noticeable at very high frequencies [9, 21]. Since we will

ultimately avoid excitation in this range, these terms can be neglected. Fig. 3 presents

a simplified model. The composite terms $R_2$, $C$, and $Z_w$ represent the combined effects

of the two electrodes.
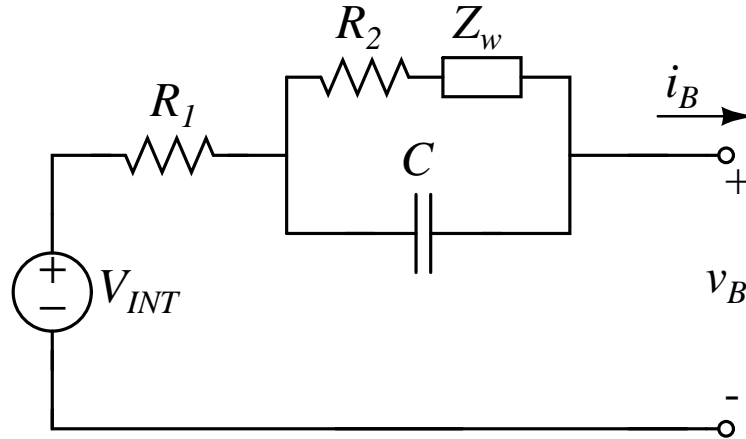


Figure 3: Modified lead-acid battery model with the electrode impedances combined and the inductive effects neglected.

### 3.3    Simplified Electrical Circuit

The Warburg impedance in Fig. 3 can also be neglected in many cases. This circuit

component models the effects of the time-dependent diffusion layer created when a

low frequency AC signal is impressed upon the battery [21].
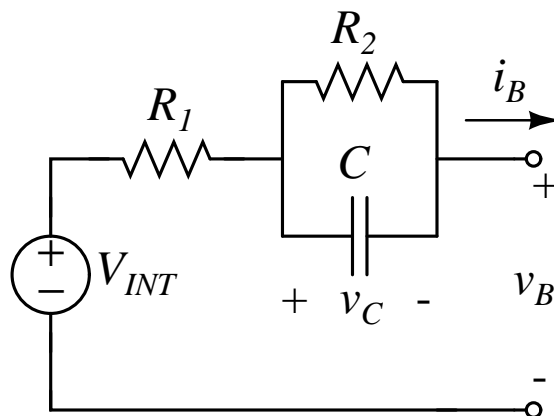


Figure 4: The simplified series-capacitor model of a battery.

Empirical evidence has shown that this impedance is negligible for frequencies above several hundred microHertz [16]. Because such frequencies correspond to periods much longer than those considered in this paper, the Warburg impedance is removed and the circuit is further simplified as shown in Fig. 4.

Similar models have been reported throughout the literature [9, 21]. Parameter estimation proceeds using this simplified equivalent circuit.

### 3.4    Model Simulation

The simulation of the battery model is performed by recording a sample discharge from a lead-acid battery for an of-the-shelf load such as a headlight of a car. Fig. 5 shows such a discharge profile. Note that the current rises sharply at the outset and then falls to a steady level. This rapid change in current is a result of the inner physics of the lamp. Note that the battery voltage displays a sharp initial drop and then falls exponentially. To obtain a result via simulation as shown in Fig. 6, a constant set of parameters was selected, and the model was excited using the terminal current shown in Fig. 5. Parameter values were selected by the grid search method, and the set was chosen which had the minimum root mean squares (RMS) value for the modeling error. The result in Fig. 6 closely matches the plot of Fig. 5, which supports the battery model in use. Similarly, for a lithium-ion battery, Fig. 7 shows a sample discharge curve when a heater is turned on by a 3.6 Volt nominal 18650-model lithium-ion battery.

Using the terminal battery current from the same discharge on the battery model of Fig. 4, the simulated voltage is obtained and the result is shown in Fig. 8. Note

that the parameters $R_1$, $R_2$ and $C$ used in the model are chosen by the grid search method where the set was chosen based on the minimum root mean square (RMS) value from the modeling error.

### 3.5    Model Validation by Impedance Spectroscopy

Electrochemical impedance spectroscopy (EIS) is a powerful mathematical tool for studying the behavior of a system. In general, this method involves determination of a complex impedance by superimposing a small ac signal on top of a DC current over a range of frequencies. The resulting voltage and current data are recorded, and the complex division of voltage by current gives the impedance. Thus calculated impedances in the form of real and imaginary components and phase angle over a range of relevant frequencies are recorded, and plotted over x-y axis to obtain the broad contour formed by the impedance profile. Such a contour may, in general terms, support the chosen model of the battery in Fig. 4. However, note that the EIS of a battery may reveal all the inner dynamics of a battery in a particular operating condition. For establishing a simplified model, the plot especially in the range of frequencies of interest rather than the detailed plot from the complete range of frequencies is scrutinized more closely to check whether the simplified battery model makes sense. The method of EIS is nondestructive in nature since the polarization applied through it is so low that the linear polarization conditions created by load currents are not affected. With the ease of measurement processes made possible by the advent of computer-controlled equipments over the years, EIS is comparatively easier to implement now than it was in the past. EIS was performed on an automotive

lead-acid battery to study the model behavior.

### 3.5.1    Electrochemical Impedance

The dynamic behavior of a battery can be explained by its electrochemical impedance, which is obtained from the response of an excitation of small signal [9]. Although any type of excitation signal like sine wave, step, noise etc. may be used, sine waves are most commonly used signal for the system excitation. In one such scheme, an experiment is performed in the galvanostatic mode in which the d.c. load current from the battery is kept constant and a sinusoidal current in the form of

$$\triangle I = I_{max} \sin(2\pi f t), \tag{2}$$

at frequency $f$, is superimposed on the d.c. signal $I$, resulting in a sinusoidal voltage response

$$\triangle V = V_{max} \sin(2\pi f t + \phi) \tag{3}$$

around the d.c. voltage $V$ at the terminals of the battery. Then the impedance of the system is defined by

$$Z(f) = \frac{V_{max}}{I_{max}} e^{\jmath \phi}. \tag{4}$$

Hence the electrochemical impedance of a battery is a frequency-dependant complex number characterized by its real and imaginary parts, or by its modulus $|Z| = \frac{V_{max}}{I_{max}}$ and its phase angle $\phi$.

### 3.5.2 Complex Impedance of the Battery Model

For the chosen equivalent electrical model of the battery as shown in Fig. 9, the complex impedance is

$$Z_{total} = R_1 + R2 || \frac{1}{\jmath\omega C}. \tag{5}$$

Eq. 5 can be represented as

$$Z_{total} = R_1 + \frac{R_2 \cdot \frac{1}{\jmath\omega C}}{R_2 + \frac{1}{\jmath\omega C}}, \tag{6}$$

which can be further simplified as

$$Z_{total} = R_1 + \frac{R_2}{(1 + \jmath\omega R_2 C)}. \tag{7}$$

Simplifying the complex number in Eq. 5 yields to

$$Z_{total} = R_1 + \frac{R_2(1 - \jmath\omega R_2 C)}{(1 + (\omega R_2 C)^2)}. \tag{8}$$

The final equation can be further written as

$$Z_{total} = R_1 + \frac{R_2}{(1 + \omega R_2 C)^2} - \jmath\frac{\omega R_2^2 C}{(1 + \omega R_2 C)^2}, \tag{9}$$

which is in the form of

$$Z_{total} = \{\text{real part}\} + \jmath \{\text{imaginary part}\}. \tag{10}$$

To see how the complex impedance of the battery model varies over a range of frequencies, A Nyquist plot for a full spectrum of frequencies is plotted and shown in Fig. 10. As the figure shows $R_1$ is the high frequency part with almost negligible

imaginary part, and the $R - C$ network of the battery model forms the shape of a semi-circle with increasing impedance at decreasing frequencies. Note that the values of the parameters used to plot the Fig. 10 is estimated by the nonlinear least squares method described in this thesis in Chapter IV.

### 3.5.3 Battery EIS Plot

An Agilent function generator is used to send a series of ac signals superimposed on a fixed dc current controlled by an electronic load. The resulting voltage and current are recorded and such a sample data is shown in Fig. 11. Fig. 12 is the zoomed-in version of the data of Fig. 11, in which the insets show the details of the voltage and current data. Performing the Fast Fourier Transform (FFT) on the obtained voltage and current data gives each component of voltage and current signals. Using the equations from the section 3.5.2, the result for EIS is obtained, and Fig. 13 shows one such plot for a 12 V lead-acid car battery. The plot is approximately close in nature with the theoretical Nyquist plot of Fig. 10 especially in the range of frequencies of interest and is also similar in nature to the diagram given in [9]. Note that the inductive effect of the battery has started to show at the high frequencies which is in line with the explanation of detailed battery model explained in above section. Since the real impedance diagram shows the detailed model of the battery, and it consists of more components than the simplified model of Fig. 4, the purpose here is to show that the impedance diagram broadly supports the simplified model of the battery especially in the range of frequencies of interest in which the test would be conducted.

Note that the parameters obtained from the EIS method may not necessarily be equal to the parameters from other methods, because the polarization created by an a.c. current is non-destructive and very small such that it does not disturb the polarization created by a dc current, which increases the polarization linearly.

## 3.6    Summary

Fig. 4 is the most commonly accepted model of a battery. The key advantage is that it represents approximately the chemical kinematics of a battery in its simplified form. It is a simple electrical equivalent circuit with few components which is helpful for the system modeling and parameter estimation process. Electrochemical impedance spectroscopy (EIS) still stands as one of the most reliable options to study the behavior of a battery. EIS is performed on a lead-acid battery to study its behavior and its plot broadly supports the simplified electrical model especially in the range of frequencies of interest. However, to study the inner-dynamics of the battery by EIS, low frequency signals need to be sent out, for which the measurement time is long. Because of this reason, it may not be the quickest way to estimate the impedance of a battery.
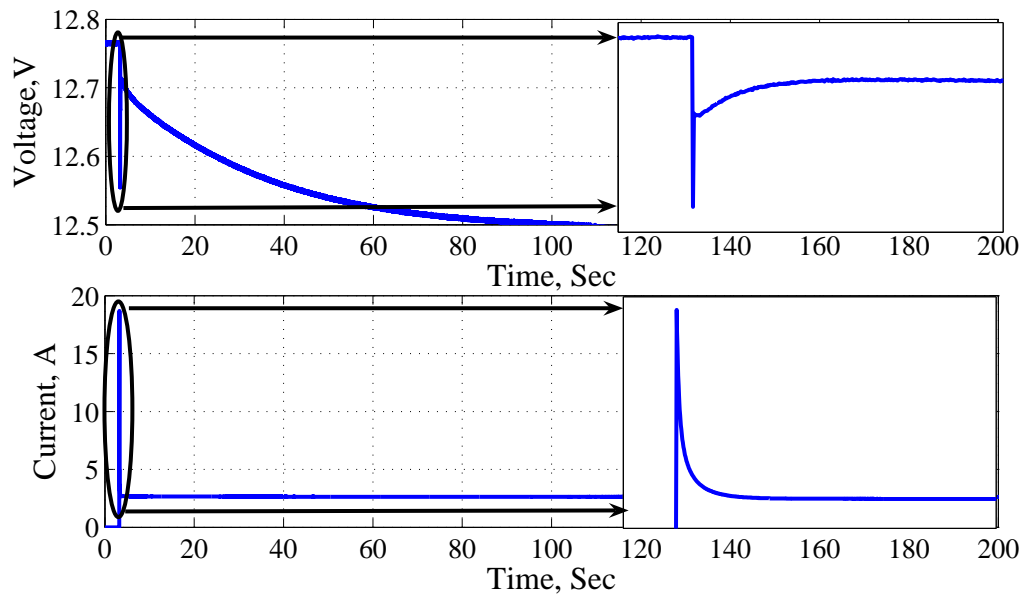
Figure 5: The measured terminal voltage of the battery when connected to a head-lamp. Upper trace: the voltage measured at the battery terminals. Bottom trace: the measured terminal current.
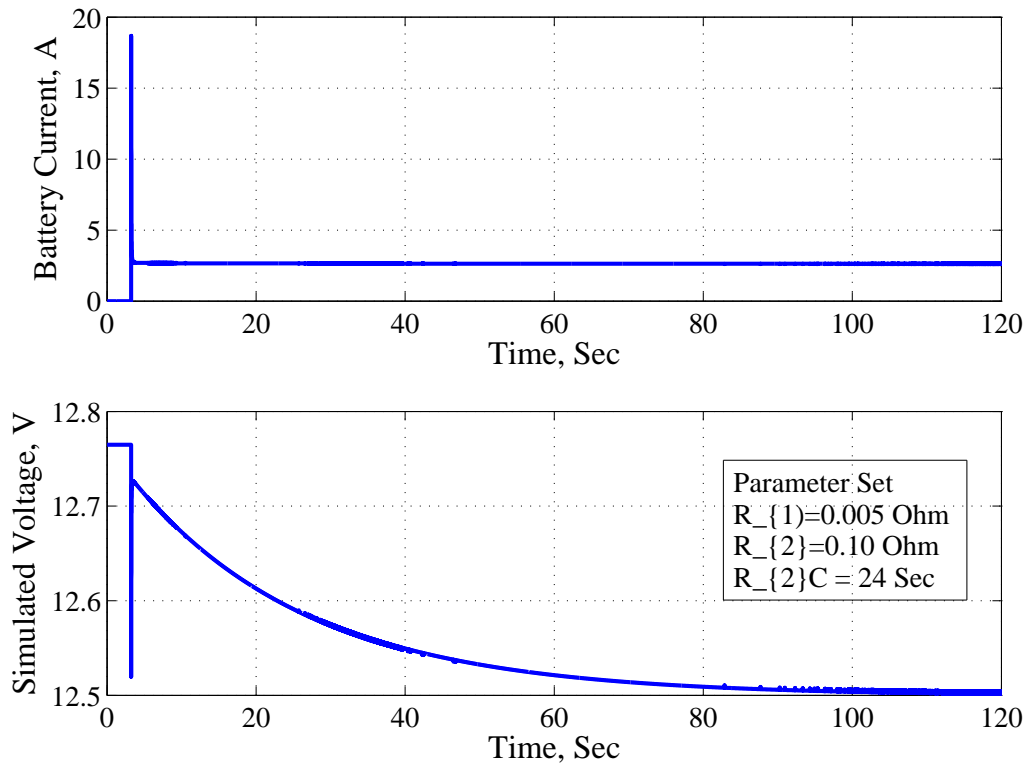


Figure 6: The simulated voltage from the battery model for the real battery current in Fig. 5.
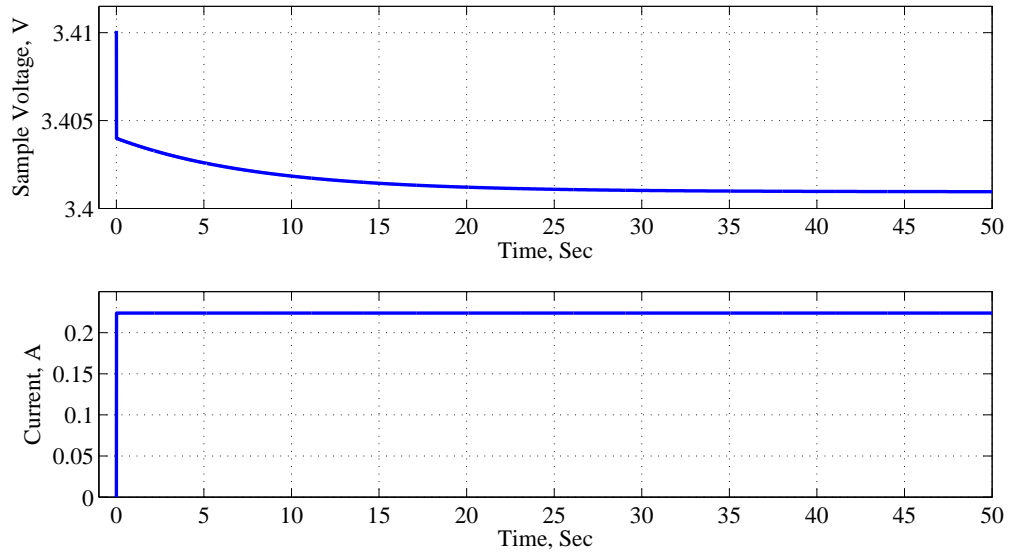
Figure 7: The measured terminal voltage of a 3.6 Volt 18650-model lithium-ion battery when connected to a heater. Upper trace: the voltage measured at the battery terminals. Bottom trace: the measured terminal current. Note that the current rises sharply at the outset and then reaches to a steady level in a step-like manner. Note that the battery voltage displays a sharp initial drop and then falls exponentially.
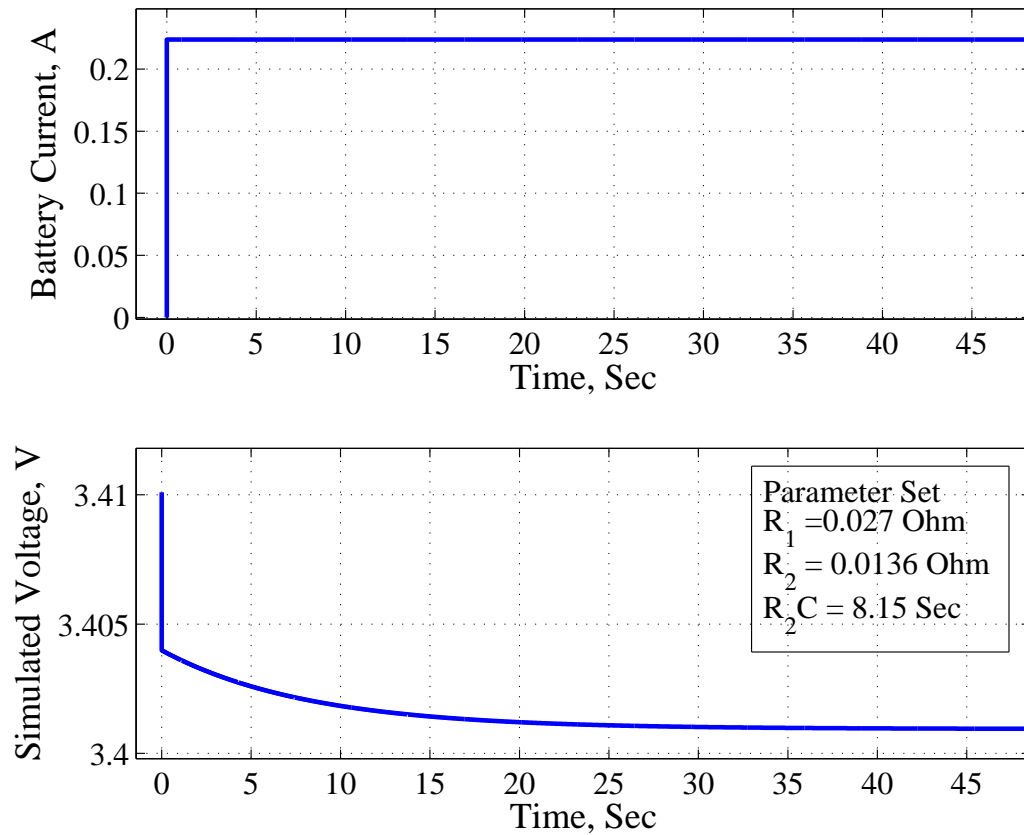


Figure 8: The simulated voltage from the battery model for the real battery current.
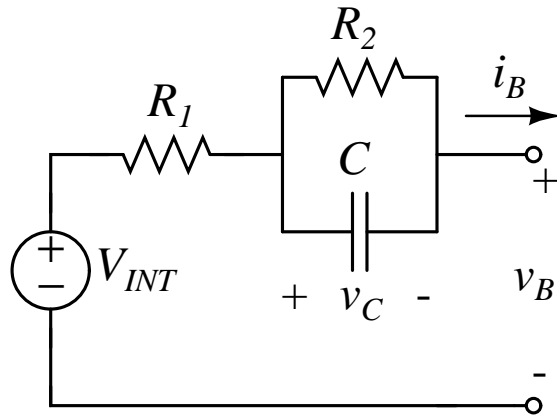
Figure 9: The chosen series-capacitor model of a battery.
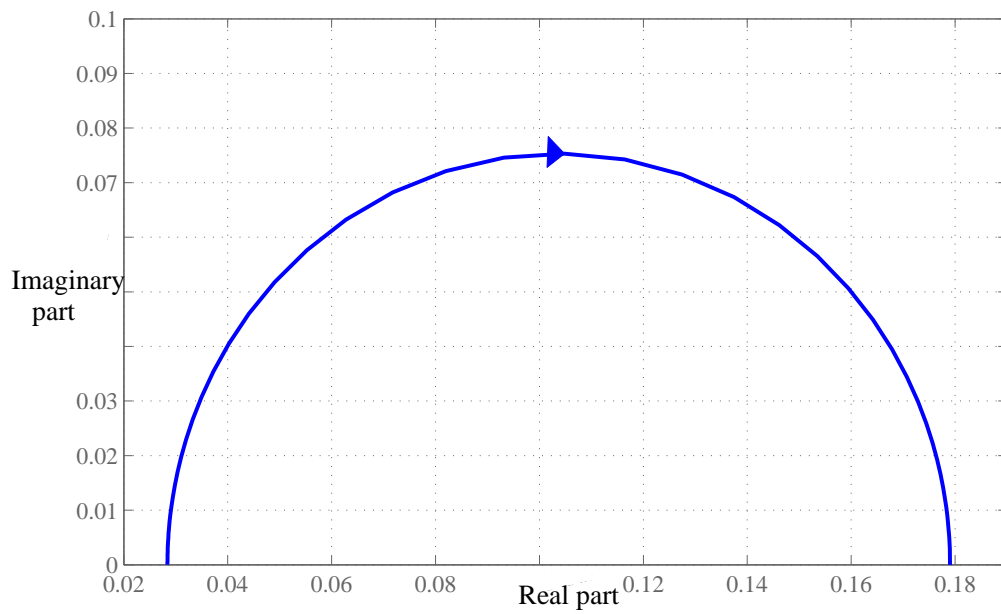


Figure 10: The Nyquist plot showing the nature of complex impedance for chosen series-capacitor model of a battery, in which $R_1 = 0.03$ Ohm is the starting point of the circle and $R_2 = 0.15$ Ohm is the diameter along x-axis.
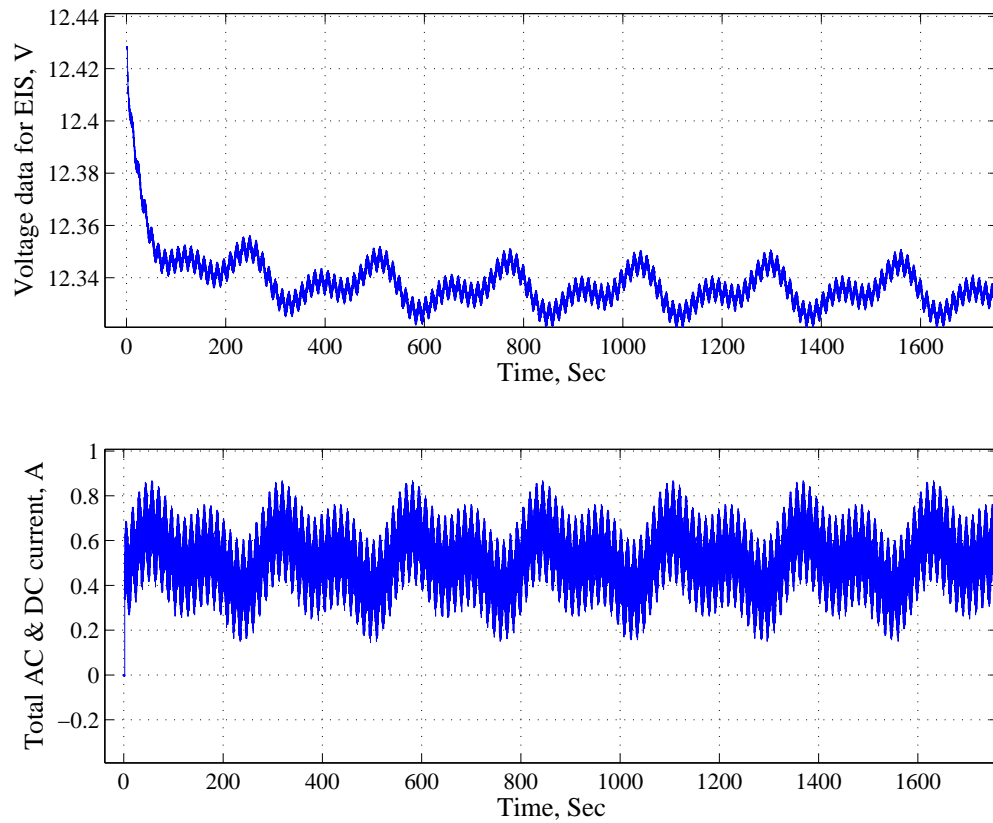
Figure 11: The sample voltage and current data used to estimate the complex impedance from a 12 Volt lead-acid battery. The current signal has a.c. signals in the range from 0.000761 Hz to 76.1 Hz superimposed on a 0.5 Ampere d.c. current and the voltage data is response of the current signal. Note the phase shift between the voltage and current data.
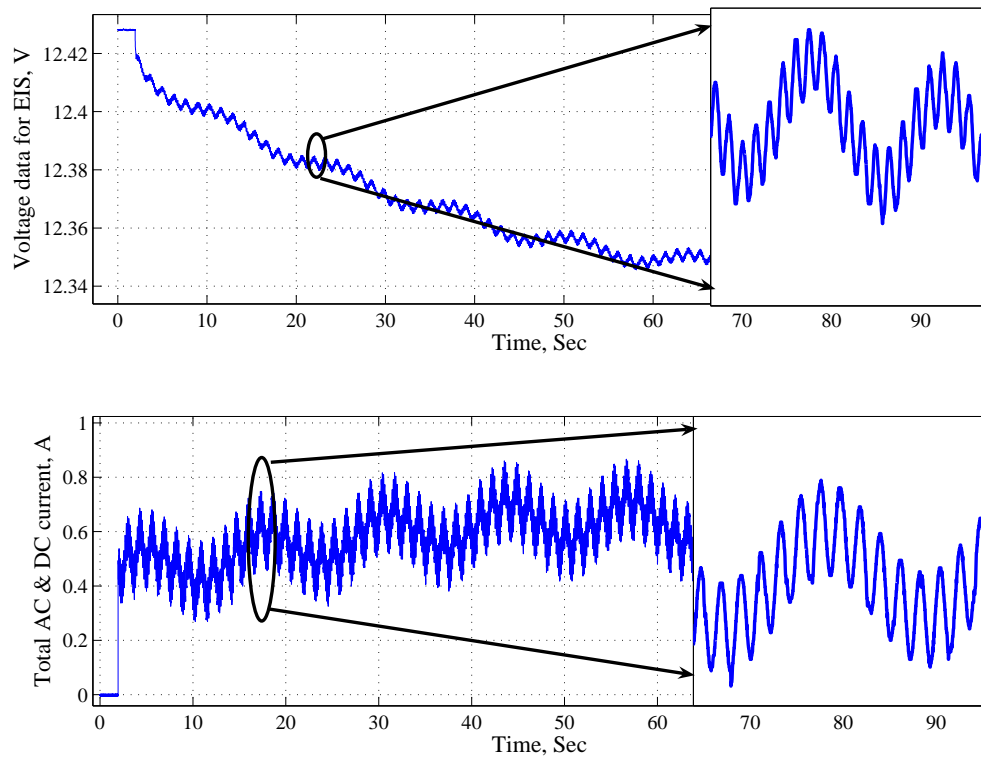
Figure 12: The zoomed in version of voltage and current data of Fig. 11. The insets shows the details of the data.
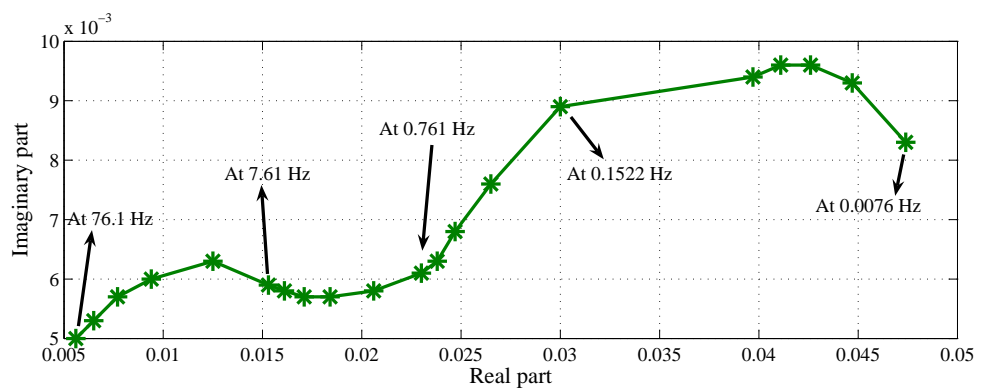


Figure 13: The impedance spectrum obtained for a 12V lead-acid battery.

## CHAPTER 4: A TRANSIENT-BASED PARAMETER ESTIMATION

Nonlinear least squares methods are the popular tools used to estimate the parameters of dynamic models. Such a method may be an attractive option for the estimation of parameters for a dynamic system like a battery. However, conventional methods tend to be susceptible to local minima and may not converge to the global minimum. Moreover, such a method may have unpredictable performances for initial guesses that are far from the optimal values. Others may have high computational overhead and can take a long time to converge. Therefore, it is essential to choose the right method suitable for the applications at hand. The method chosen for this thesis takes advantage of the structure of residuals in data fitting. Such a method is an excellent choice because it tends to converge for a wide range of initial guesses to the desired minimum than the standard techniques such as Levenburg-Marquardt or Gauss-Newton methods do [58].

## 4.1    Gauss-Newton Method with Linearization Approach

A nonlinear least squares problem involves finding an $m$ dimensional vector estimate $\hat{\mu}$ of $\mu$ satisfying in the least squared sense the $n$ equations

$$
f_1(u_1; \mu) = y_1
$$

$$
f_2(u_2; \mu) = y_2
$$

$$
\vdots
$$

$$
f_n(u_n; \mu) = y_n,
$$

(11)

where $u_k$ is the $k$'th input, $y_k$ is the $k$'th observation, $f_k$ is the $k$'th function relating these quantities, $\mu$ is the parameter vector, and $n > m$ [58, 59]. The $f_k$ are considered nonlinear by the way that $\mu$ are related to $y$. The use of semi-colon in Eq. 11 separates parameters from inputs in the arguments of the function.

Then the objective of the nonlinear least squares problem is the minimization of a loss function over parameter vectors $\mu$

$$
\hat{\mu} = \arg\min_{\mu} V(\mu).
$$

(12)

The notation in Eq. 12 implies that the final estimate $\hat{\mu}$ is the value of $\mu$ for which the loss function $V(\mu)$ attains a minimum. For the least squares problem represented by Eq. 11, the loss function may be defined as [58]

$$
V(\mu) = \frac{1}{2} \sum_{k=1}^{n} (y_k - f_k(u_k; \mu))^2.
$$

(13)

The loss function can also be written as

$$V(\mu) = \frac{1}{2}r'r \qquad (14)$$

where $r$ is the $n$ dimensional residual

$$r = y - f(u; \mu), \qquad (15)$$

where lack of subscripts is interpreted so that

$$r_k = y_k - f_k(u_k; \mu). \qquad (16)$$

The Gauss-Newton method iteratively finds a solution to the nonlinear least squares problem by updating $\hat{\mu}$ with a step $\delta_{GN}$ [58, 59]

$$\mu^{(\hat{i}+1)} = \mu^{\hat{(i)}} + \delta_{GN}^{(i)}, \qquad (17)$$

where $\mu^{\hat{(i)}}$ is the estimate of the parameters at the $i$'th iteration. At each iteration, $\delta_{GN}$ is computed as the least-squares solutions to the linear problem

$$J\delta_{GN} = r, \qquad (18)$$

where $J$ is the $n$ by $m$ Jacobian evaluated at $\hat{\mu}$ with elements

$$J_{k,i} = -\left.\frac{\partial r_k}{\partial \mu_i}\right|_{\hat{\mu}}, \qquad (19)$$

and $r$ is the residual defined in Eq. 15. In the linearization approach, a linear Taylor series approximation to $f(u; \mu)$ is considered. For simplicity, the dependence on $\mu$ is neglected here. Then at each iteration, this linearization should be in the neighbor-

hood of the current estimate $\hat{\mu}$ [58]

$$f(\hat{\mu} + \delta) \approx f(\hat{\mu}) + \nabla f(\hat{\mu})\delta, \tag{20}$$

where $\nabla f(\hat{\mu})$ is the $m$ dimensional row vector of partial derivatives

$$\nabla f(\hat{\mu}) = \left( \left.\frac{\partial f}{\partial \mu_1}\right|_{\hat{\mu}} \quad \left.\frac{\partial f}{\partial \mu_2}\right|_{\hat{\mu}} \quad \cdots \quad \left.\frac{\partial f}{\partial \mu_m}\right|_{\hat{\mu}} \right). \tag{21}$$

Then the goal is to obtain a $\delta$ to compute the next parameter estimate $(\hat{\mu} + \delta)$ by combining the linearization of Eq. 20 with the constraints. Substituting Eq. 11 by the proposed update $(\hat{\mu} + \delta)$ gives

$$
\begin{aligned}
f_1(\hat{\mu}) + \nabla f_1(\hat{\mu})\delta &= y_1 \\
f_2(\hat{\mu}) + \nabla f_2(\hat{\mu})\delta &= y_2 \\
&\vdots \\
f_n(\hat{\mu}) + \nabla f_n(\hat{\mu})\delta &= y_n
\end{aligned}
\tag{22}
$$

where the term $\nabla f_k(\hat{\mu})$ is the $k$'th row of $J$ defined by Eq. 19. Subtracting the $f_k$'s from both sides of equation, Eq. 22 can be written as the linear system

$$J\delta = r. \tag{23}$$

Multiplying both sides by $J'$ gives the Gauss-Newton step,

$$J'J\delta_{GN} = J'r, \tag{24}$$

which could be solved as

$$\delta_{GN} = (J'J)^{-1}J'r. \tag{25}$$

## 4.2  Parameter Estimation

The non-linear problem for the battery model is formulated in the following way.

### 4.2.1  Battery Nonlinear Problem

The model for the battery shown in Fig. 14 consists of the state equation
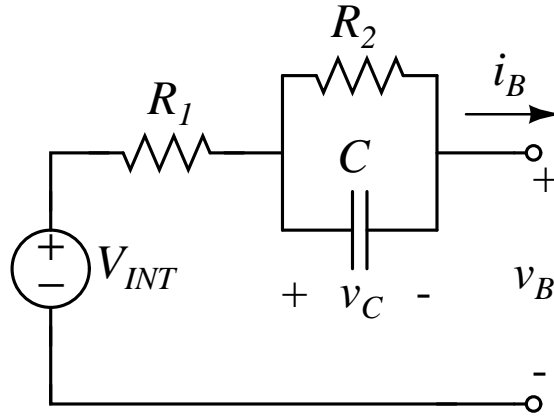


Figure 14: The simplified series-capacitor model of a battery.

$$\frac{dv_C}{dt} = \frac{i_B}{C} - \frac{v_C}{R_2 C} \tag{26}$$

and the output equation

$$v_B = V_{INT} - i_B R_1 - v_C. \tag{27}$$

For simplicity, the model is reformulated in terms of a vector of composite parameters, i.e.

$$\frac{dv_C}{dt} = \mu_1 i_B - \mu_2 v_C \tag{28}$$

and

$$v_B = V_{INT} - \mu_3 i_B - v_C, \tag{29}$$

where $\mu_1 = 1/C$, $\mu_2 = 1/(R_2 C)$, and $\mu_3 = R_1$. Then the parameter estimates $\hat{\mu}$ solve the equation

$$\hat{\mu} = \arg\min_{\mu} \mathbf{r}^T \mathbf{r}, \tag{30}$$

where the residual vector $\mathbf{r}$ is the difference between the model response $\hat{\mathbf{v}}_\mathbf{B}$ and the measured values $\mathbf{v}_\mathbf{B}$ as given in Eq. 31

$$\mathbf{r} = \hat{\mathbf{v}}_\mathbf{B} - \mathbf{v}_\mathbf{B}. \tag{31}$$

Note that vector notation has been used because we are considering a series of values observed at discrete time steps. The model response is determined via simulation. Parameter estimation proceeds in several steps. At the outset, initial guesses are generated from circuit considerations. A time-domain simulation then uses these guesses to generate an estimated voltage vector $\hat{\mathbf{v}}_\mathbf{B}$. A modified Gauss-Newton method then determines if the parameter values can be improved. If so, another simulation is performed using the updated parameter values. This process repeats until Eq. 30 is satisfied. The exact details are presented below.

Throughout this section, it is assumed that the data needed for parameter estimation is obtained by connecting a small load that sufficiently excites the dynamics of the battery. For convenience, off-the-shelf devices such as headlamps and resistance heaters are used. Other more complicated loads could be considered, but the choice

of loads are selected based on commonly used parts in vehicles and other battery-powered systems.

It should be noted that the internal source $V_{INT}$ is not considered a parameter to be estimated at this stage. That is the objective of the next chapter in this thesis. The value of $V_{INT}$ is determined by measuring the open-circuit voltage prior to the connection of the load (i.e. with $i_B = 0$). Over time, the value of $V_{INT}$ will decrease, but if the load connected to the terminals is small, the drop will not be significant during the measurement interval. In this sense, loads such as the head lamp can be viewed as "small-signal" sources.

### 4.2.2    Pre-Estimation

To generate initial guesses for the parameters $\mu_1$, $\mu_2$, and $\mu_3$, the load is first modeled as a current source connected across the battery terminals. Basic circuit considerations are then used to determine initial values for $R_1$, $R_2$, and $C$. These values are combined to obtain guesses for the composite parameters.

Pre-estimates for $R_1$ and $R_2$ are very easily determined by considering how the capacitor steers current through the circuit under different conditions. A load with a step-like behavior, for instance, causes a rapid initial change in terminal current. As this happens, the voltage across the capacitor must remain continuous. The result is that the capacitor appears as a short-circuit, forcing all of the terminal current to flow through it. If the capacitor is initially discharged, an initial guess for $R_1$ can thus be obtained by solving the equation

$$V_{INT} - i_B(0^+)R_1 = v_B(0^+), \tag{32}$$

where $i_B(0^+)$ and $v_B(0^+)$ are measurements of the current and voltage immediately

following the connection of the load. In steady state, the capacitor's behavior is quite

different. In that situation, the capacitor blocks the flow of DC current, thus forcing it

through $R_2$. An estimate for this resistance is then generated by solving the equation

$$v_{final} = V_{INT} - i_{final}(R_1 + R_2), \tag{33}$$

where $v_{final}$ and $i_{final}$ are the steady-state values of the terminal voltage and current,

respectively. Note that Eq. 33 must be solved in combination with the value of $R_1$.

To obtain a pre-estimate for the capacitance $C$, we begin with the notion that a

pure current step causes an exponential response of the form

$$v_B = v_{initial} - (v_{initial} - v_{final}) \left(1 - e^{-t/R_2C}\right), \tag{34}$$

where $v_{initial}$ and $v_{final}$ are the initial and final values of the terminal voltage. After

subtracting $v_{final}$ from both sides of Eq. 34, one obtains an expression of the form.

$$v_B - v_{final} = (v_{initial} - v_{final})e^{-t/R_2C}. \tag{35}$$

When the natural logarithm is applied to Eq. 35, one obtains an expression that is lin-

ear with respect to the unknown parameter $1/(R_2C)$. Linear least-squares estimation

is then used to obtain an initial value for the time constant.

The theory underlying the calculation of the time constant can be somewhat ap-

proximate. Note, for instance, that the load current might contain an initial transient

caused by either thermal or electromechanical phenomena. As long as these transients

are negligible before the battery's own homogeneous response has completed, then

the general form of Eq. 34 can still be used to estimate the time constant. One must
be careful, however, to apply the least-squares approach to the appropriate section of
the data.

The values obtained for $R_1$, $R_2$, and $C$ are ultimately combined to provide pre-
estimates for the composite parameters $\mu_1$, $\mu_2$, and $\mu_3$. It may ultimately be possible
to avoid a pre-estimation step by statistically tallying past data, but the process helps
to speed the estimation routine and thus reduce overall computational time.

### 4.2.3    Estimation

Final estimates for the parameter set $\mu$ are obtained using the nonlinear least-
squares method presented in [59]. That approach exploits residual structure to help
avoid local minima. To understand the method, one must begin by considering the
solution to Eq. 30. To obtain the minimum, the gradient of $\mathbf{r}^T\mathbf{r}$ must be zero. This
gradient can be written as

$$\mathbf{g}(\mu) = \mathbf{J}^T\mathbf{r}, \tag{36}$$

where $\mathbf{J}$ is the Jacobian matrix of the residuals with respect to the parameters. The
Gauss-Newton method can be applied to Eq. 36 to find a series of iterates $\mu^{(i)}$ that
can be evaluated by computer to solve for $\mathbf{g}(\mu^{(i)}) = 0$, i.e.

$$\mu^{(i+1)} = \mu^{(i)} - [\mathbf{J}^T\mathbf{J}]^{-1}\mathbf{J}^T\mathbf{r}, \tag{37}$$

where $\mathbf{J}$ and $\mathbf{r}$ are evaluated at $\mu^{(i)}$ [59].

Estimation problems are often difficult to solve because the gradient $\mathbf{g}(\mu)$ can
vanish at local minima corresponding to poor parameter estimates. This problem can

be overcome by performing minimization over telescoping intervals of data selected by analysis of the residuals. To see this, consider the nature of the residual vector, which is defined as

$$\mathbf{r} = \hat{\mathbf{v}}_\mathbf{B} - \mathbf{v}_\mathbf{B}. \tag{38}$$

In Eq. 38, $\mathbf{v}_\mathbf{B}$ is a series of measurements recorded at a rate $1/T$. $\hat{\mathbf{v}}_\mathbf{B}$, on the other hand, consists of estimates generated at the same time increments. The residual vector is thus a time series that can be written as $\mathbf{r}(t)$. Assuming that a Taylor series exists for the system model, and that the measurements can be described by a polynomial in $t$, the $k$-th element of the residual vector can be rewritten as

$$r_k = \hat{v}_B(0) + \frac{d}{dt}\hat{v}_B(0)t_k + \frac{d^2}{dt^2}\hat{v}_B(0)t_k^2 \cdots$$
$$-(a + bt_k + ct_k^2 + \cdots), \tag{39}$$

where $t_k = (k-1)T$. In this example, and in many other non-linear estimation problems, the parameters are simply embedded in the low-order coefficients of the series consisting of the initial output $\hat{v}_B(0)$ and the slope $(\frac{d}{dt})\hat{v}_B(0)$. These quantities are analytically accessible for differential equation models, such as Eq. 119. Minimization is performed over successively larger intervals, with each sub-problem selected so that the initial terms of the Taylor series are a reasonable approximation. By ensuring this, the likelihood of convergence to the global minimum is greatly improved [59].

For example, suppose for the identification problem at hand with the residual vector of Eq. 38, let the set of target parameters be $\mu = [\lambda_1; \lambda_2; \lambda_3]$ and the defined set of parameters be $\mu = [\mu_1 = \frac{1}{C}; \mu_2 = \frac{1}{R_2C}; \mu_3 = R_1]$. Then the $\mathbf{v}_\mathbf{B}$ and $\hat{\mathbf{v}}_\mathbf{B}$ in Eq. 38 are

defined as

$$\mathbf{v_B} = v_B(0) - \mathbf{i_B}\lambda_3 - \mathbf{i_B}\frac{\lambda_1}{\lambda_2}(1 - e^{-\lambda_2 \mathbf{t}}), \quad \text{and}$$

$$\hat{\mathbf{v}}_\mathbf{B} = \hat{v}_B(0) - \mathbf{i_B}\mu_3 - \mathbf{i_B}\frac{\mu_1}{\mu_2}(1 - e^{-\mu_2 \mathbf{t}})$$

(40)

where $\mu_1 = \frac{1}{C}; \mu_2 = \frac{1}{R_2 C}$ yields $R_2 = \frac{\mu_1}{\mu_2}$. Then the identification problem of Eq. 38 can be expanded as

$$\mathbf{r_k} = \hat{v}_B(0) - \mathbf{i_B}\mu_3 - \mathbf{i_B}\frac{\mu_1}{\mu_2}(1 - e^{-\mu_2 \mathbf{t}}) - \{v_B(0) - \mathbf{i_B}\lambda_3 - \mathbf{i_B}\frac{\lambda_1}{\lambda_2}(1 - e^{-\lambda_2 \mathbf{t}})\}. \quad (41)$$

Since $e^{ax} = \{1 - ax + \frac{a^2 x^2}{2} - \cdots\}$, Eq. 41 is further expanded as

$$\mathbf{r_k} = \hat{v}_B(0) - \mathbf{i_B}\mu_3 - \mathbf{i_B}\frac{\mu_1}{\mu_2}\{\mu_2 \mathbf{t}\} - \{v_B(0) - \mathbf{i_B}\lambda_3 - \mathbf{i_B}\frac{\lambda_1}{\lambda_2}\{\lambda_2 \mathbf{t}\}\} \quad (42)$$

where higher order terms in the exponential series are neglected. Then Eq. 42 can be further simplified as

$$\mathbf{r_k} = \{\hat{v}_B(0) - \mathbf{i_B}\mu_3 - \mathbf{i_B}\mu_1 \mathbf{t}\} - \{v_B(0) - \mathbf{i_B}\lambda_3 - \mathbf{i_B}\lambda_1 \mathbf{t}\}. \quad (43)$$

The unconstrained loss function for this problem from Eq. 13 can be defined as

$$\mathbf{V}(\mu) = \frac{1}{2}\sum_{k=1}^{K^{(1)}}\{(\hat{v}_B(0) - v_B(0)) - (\mu_3 - \lambda_3)\mathbf{i_B} - (\mu_1 - \lambda_1)\mathbf{i_B}\mathbf{t}\}^2. \quad (44)$$

The gradient vector for the loss function in Eq. 44 will be

$$\mathbf{g}(\mu) = \sum_{k=1}^{K^{(1)}}\begin{pmatrix} \{(\hat{v}_B(0) - v_B(0)) - (\mu_3 - \lambda_3)\mathbf{i_B} - (\mu_1 - \lambda_1)\mathbf{i_B}\mathbf{t}\}.\{\mathbf{i_B}\mathbf{t}\} \\ 0 \\ \{(\hat{v}_B(0) - v_B(0)) - (\mu_3 - \lambda_3)\mathbf{i_B} - (\mu_1 - \lambda_1)\mathbf{i_B}\mathbf{t}\}.\{-\mathbf{i_B}\} \end{pmatrix}. \quad (45)$$

In the initial step during the minimization process, the gradient $\mathbf{g}(\mu)$ in Eq. 45 only

tends to zero for $\mu_1 = \lambda_1$ and $\mu_3 = \lambda_3$. This forces the convergence for $\mu_1$ and $\mu_3$.

Note that this step does not influence the remaining parameter $\mu_2$. After the initial

minimization step, the method will find $K^{(2)}$ so that the residual from $K^{(1)}$ to $K^{(2)}$

grows linearly. For the second interval, the linear coefficients of the power series can

be found by taking the gradient with respect to interval, which is

$$\frac{\partial \mathbf{r_k}}{\partial \mathbf{t}} = \frac{\partial(\hat{\mathbf{v}}_\mathbf{B} - \mathbf{v_B})}{\partial \mathbf{t}},$$

$$= \frac{\partial}{\partial \mathbf{t}}[\{\hat{v}_B(0) - \mathbf{i_B}\mu_3 - \mathbf{i_B}\frac{\mu_1}{\mu_2}(1 - e^{-\mu_2 \mathbf{t}})\} - \{v_B(0) - \mathbf{i_B}\lambda_3 - \mathbf{i_B}\frac{\lambda_1}{\lambda_2}(1 - e^{-\lambda_2 \mathbf{t}})\}],$$

$$= -\mathbf{i_B}\frac{\mu_1}{\mu_2}\mu_2 e^{-\mu_2 \mathbf{t}} + \mathbf{i_B}\frac{\lambda_1}{\lambda_2}\lambda_2 e^{-\lambda_2 \mathbf{t}},$$

$$= \{\lambda_1 e^{-\lambda_2 \mathbf{t}} - \mu_1 e^{-\mu_2 \mathbf{t}}\}\mathbf{i_B} \qquad . \tag{46}$$

The gradient in Eq. 46 will only be zero for $\mu_2 = \lambda_2$ forcing the convergence of $\mu_2$ in

the second stage. Thus the minimization process over the $k = 1 \cdots K^{(2)}$ effectively

constraints $\mu_1$ and $\mu_3$ over the first $K^{(1)}$ points and $\mu_2$ from $K^{(1)}$ to $K^{(2)}$ points. This

process repeats until the minimization is applied to the entire data set.

### 4.3    Simulation Result

The nonlinear least square estimation with structured residual method is used on

the simulated battery data so that the effectiveness of this method can be checked.

A laboratory generated current is sent to a 12 Volt lead-acid battery and the ter-

minal voltage out of the battery is plotted by the use of known parameters val-

ues.  Subsequently, the generated terminal voltage and current are sent back to

the nonlinear algorithm and the final parameters are estimated.  As expected, it

gives same parameter values within the allowed tolerance.  For the battery model

of Fig. 4, a sample unit current with transient dynamics as shown in the Fig. 15
is used in the algorithm. Assuming the parameter set for the battery model as
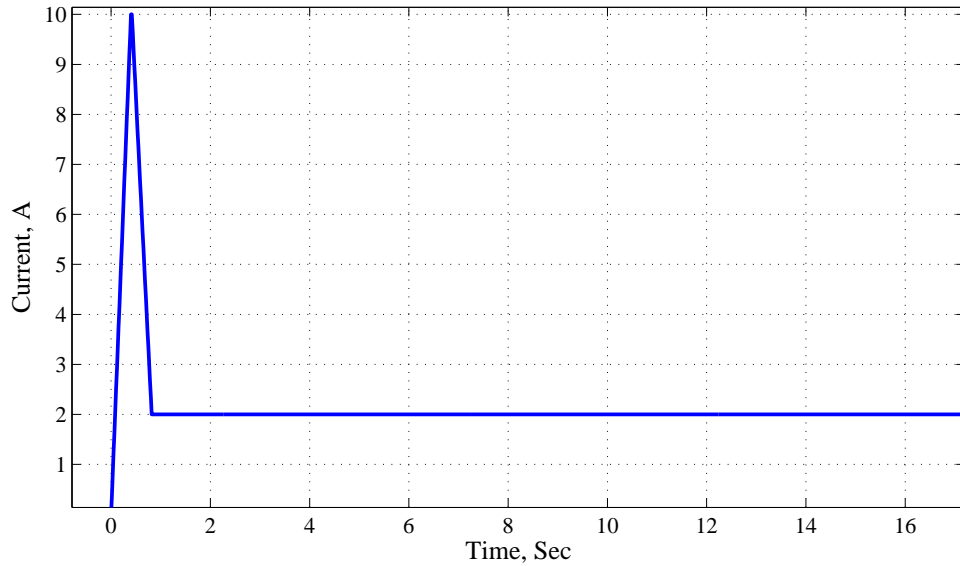


Figure 15: Sample current used in simulation for the nonlinear least square with linearization approach.

$\mu = \{C = 40; R_1 = 0.01; R_2 = 0.025\}$ and the battery open-circuit voltage at 12.6 V
, the terminal voltage is plotted. Taking this terminal voltage and sample current of
Fig. 15, data are sent to the nonlinear least squares with structural residual method
algorithm. When the set of estimated parameters is obtained, the battery terminal
voltage is re-plotted and the voltages are compared as shown in Fig. 16. Starting
with any kind of initial guesses gives the same final set of parameters, and the fitted
voltage completely follows the voltage from the battery.

## 4.4    Sample Result

The parameter estimation routine has been validated using the experimental setup
shown in Fig. 17. A picture of the real experiment at NC Laboratory for Energy

Efficient System at the UNC Charlotte is shown in Fig. 18

The loads are connected to the battery using a solid-state relay. Both the terminal voltage and current are sensed using Hall-effect transducers produced by LEM, and the ambient temperature is measured using an LM35 temperature sensor. To resolve small changes in the terminal voltage, a differential amplifier removes the offset and amplifies the difference. All of the data streams are sampled at 100Hz using a PCI-1710 data-acquisition card. For consistency, all tests are performed at approximately 24°C. Several different loads have been used to excite the test battery. Each was selected so that it provides what is effectively a "small-signal" excitation. Recall that
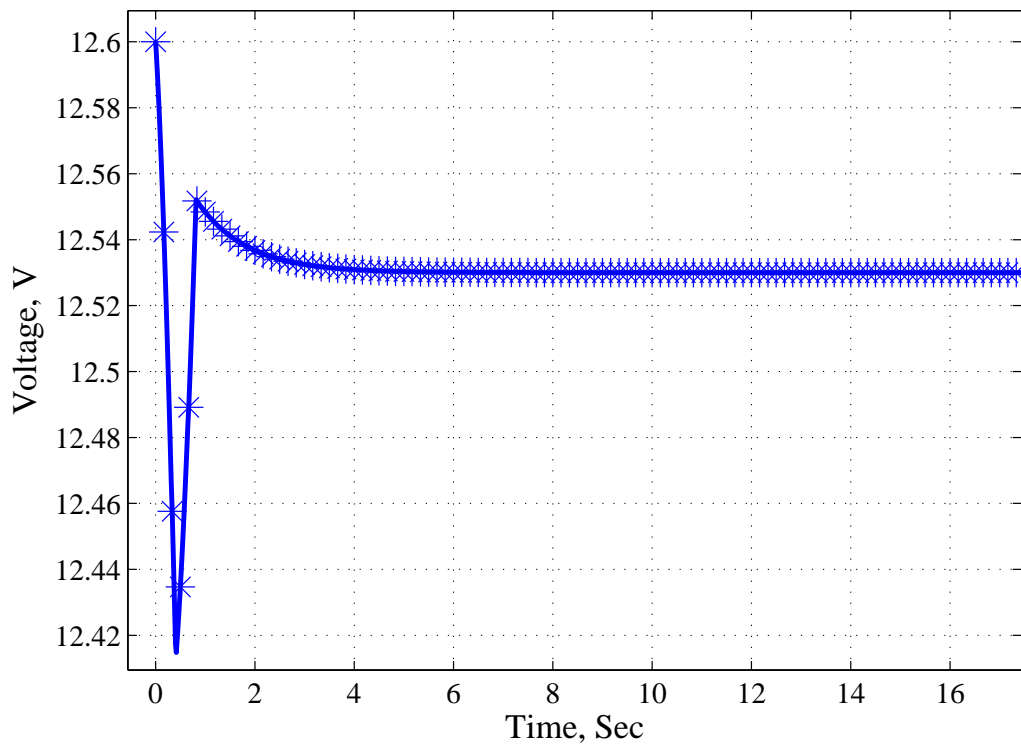


Figure 16: The input and output voltage comparison by nonlinear least squares with linearization approach method for parameter set of $\mu = \{C = 40; R_1 = 0.01; R_2 = 0.025\}$. In the figure, the solid line is input voltage, and the asterisks are the the output voltage.

this constraint was imposed so that the internal source $V_{INT}$ would remain effectively constant throughout the measurement interval. The use of small automotive loads such as head lamps and resistive heaters has ensured that this condition is met.

Fig. 19 shows the response immediately following the connection of a standard halogen head lamp. Note that the bulb has an initial thermally-induced transient that decays within one second. The long-tailed transient in the terminal voltage is primarily caused by the battery's own homogeneous response.

The estimation procedure from above section is applied to data sets such as the one shown in Fig. 19. Fig. 20 presents typical results. Note the close fit between the measured data and the model estimates. Table. 1 shows the values of parameters at different voltage levels from a NAPA-brand lead-acid batteries.
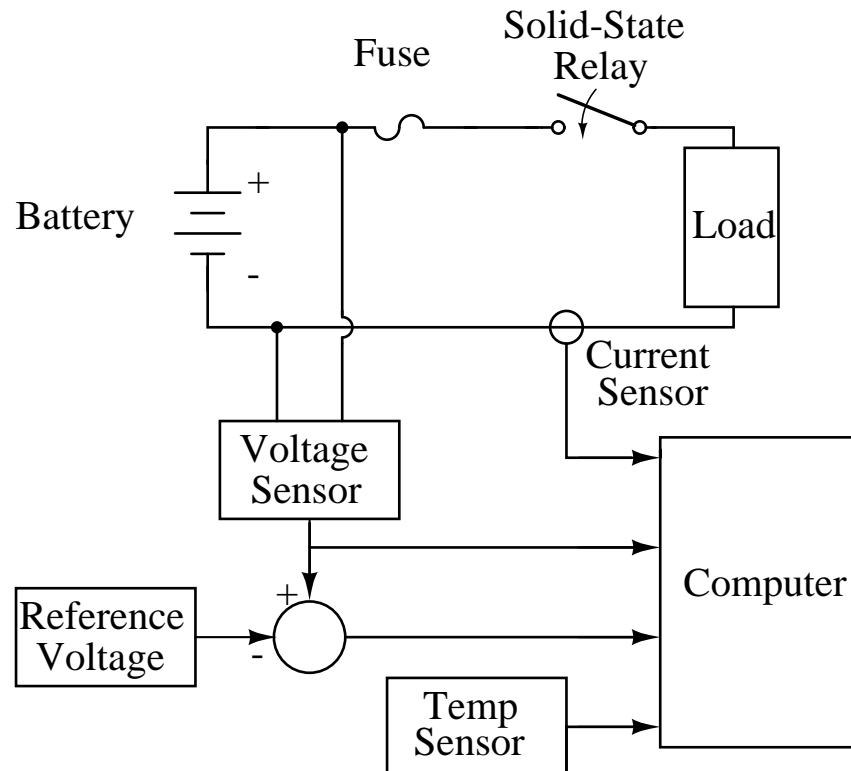


Figure 17: Block diagram of the measurement system.

Table 1: Various Parameter Values for a NAPA 12 Volt Lead-Acid Battery

| $V_{INT}$ (V) | $R_1(\Omega)$ | $R_2(\Omega)$ | $C$ (F) | $R_2C$ (Sec) |
|---|---|---|---|---|
| 12.79 | 0.0147 | 0.0771 | 362.3 | 27.93 |
| 12.69 | 0.0150 | 0.0635 | 364.00 | 23.13 |
| 12.60 | 0.0151 | 0.0527 | 323.00 | 17.02 |
| 12.49 | 0.0171 | 0.0483 | 288.29 | 13.93 |
| 12.39 | 0.0201 | 0.0436 | 259.83 | 11.32 |
| 12.30 | 0.0250 | 0.0465 | 228.26 | 10.62 |

## 4.5    Summary

This estimation technique has demonstrated the effectiveness of the proposed non-linear least square parameter extraction process. It exploits the structure in its residual. Starting with a small interval and continuing with bigger intervals, it makes sure
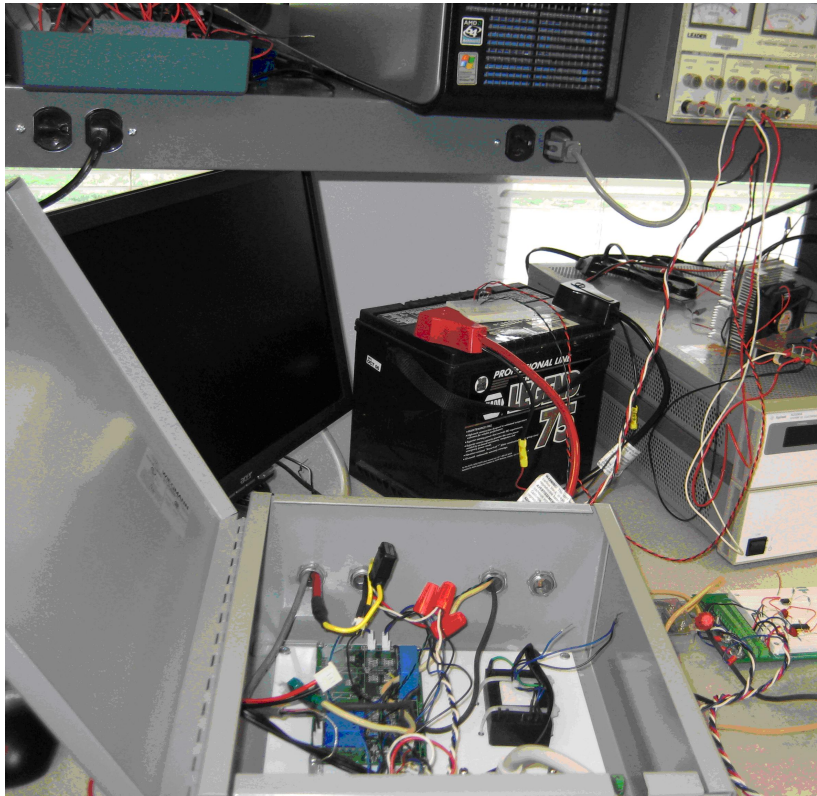


Figure 18: A picture of the experimental setup at the NC Laboratory for Energy Efficient Systems at the UNC Charlotte.

that it converges to the global minimum.
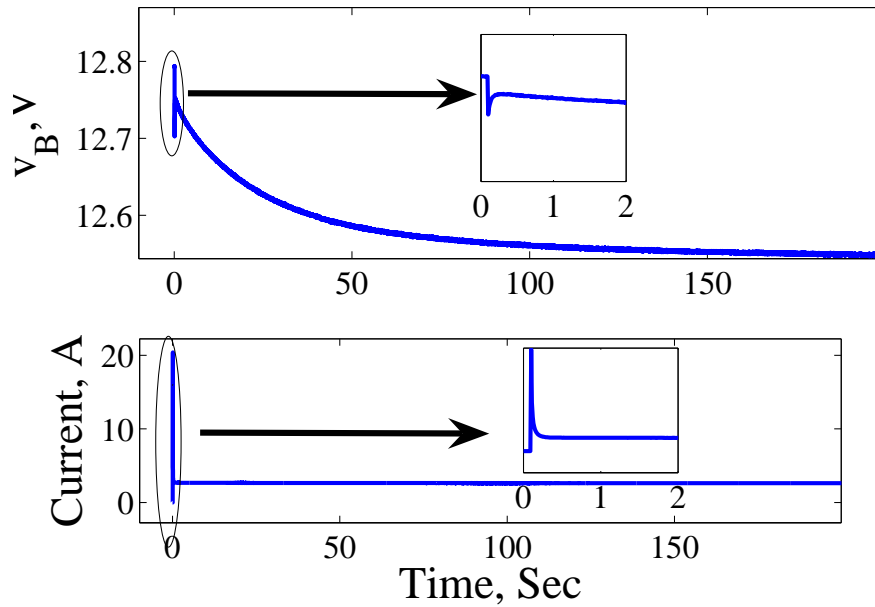


Figure 19: Top trace: The measured terminal voltage following the connection of a halogen head lamp. Bottom trace: The current drawn by the lamp. Initial transient details are presented in the inset plots.
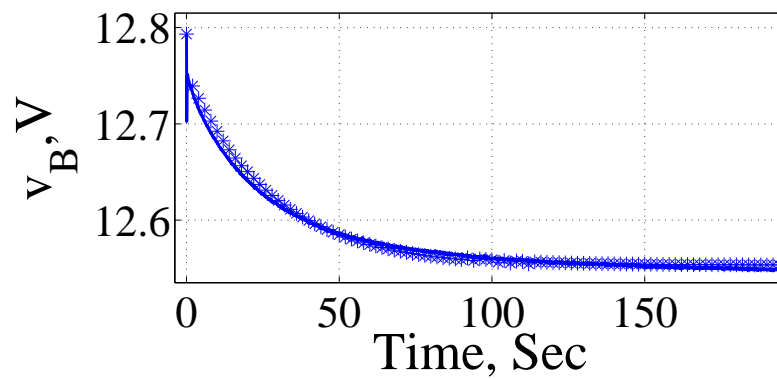


Figure 20: Experimental results. Solid line: Measured terminal voltage. Asterisks: Estimated terminal voltage.

CHAPTER 5: STATE ESTIMATION BY H$_\infty$ FILTER

Popular methods of state estimation are Kalman Filter, and Extended Kalman Filter etc. However, the performance of these methods in estimating state variable within given constraints of measurements and models for different problems are debated. Depending upon the availability of accurate system model, and measurement of discrete noise, the accuracy of predicting state variable may vary. In the presence of non-linearity within the real-time system model and the non-linear characteristic of states, such methods may have limited uses in certain applications. A few of these limitations are briefly discussed below.

- Kalman Filter

    1.) It estimates a state variable with known measurement and system noise.

    2.) It requires a finite model exhibiting all dynamics of the system.

    3.) It is not very efficient if the system characteristics are nonlinear.

    4.) The finite model for a dynamic system like a battery is difficult to obtain as explained in Chapter 3 and it is hard to quantize uncertainty and non-linearity associated with the battery characteristics.

- Extended Kalman Filter

    1.) It is a modified Kalman Filter method of the state estimation for a nonlinear system.

2.) During estimation process, the state variable is linearized.

3.) It may not be the optimal estimator without detailed model of a system.

Hence it may not estimate the open-circuit voltage of the battery in the diverse applications.

Researchers have used Kalman filters to estimate parameters and open-circuit voltage of a battery [60, 33, 61, 62, 63]. A detailed investigation can be found in Chapter 2. In a more generalized state-space models of [61, 64, 65], SOC is modeled as a state variable which requires an initial value, and poses an issue especially when SOC is not unity. This may limit the efficiency of this method as it poses a challenge to initialize SOC value. Using equivalent circuit models of [33, 29], the method seems to have reasonable predictions of SOC although it takes a long time to converge. Similarly, electrochemical models comprising of various parameters are presented in [66]. However, such method could be computationally expensive and difficult to keep track of all the parameters. All these works have shown the limitations of using Kalman filter for state estimation of a battery model.

Extending their work, the state estimation by $H_\infty$ filter method is presented for state estimation for a dynamic system like battery in this chapter. The proposed method is still a modified Kalman filter tool, but one which gives the robust estimation of state variable when the non-linearity and noise in the system can not be quantized definitely. Some of the features of this method are given below.

- Proposed H-infinity filter method

    1.) It takes into account the unknown noise in the system and measurement

process. The non-linearity associated with battery would be analogous to noise.

2.) It compensates for the uncertainty in model itself, which may be the case for a dynamic system like a battery.

3.) It provides the optimal estimation of open-circuit voltage along with the use of other parameters of the battery model. In other words, it gives the settled value of open-circuit voltage by using the measured terminal voltage for the improved estimation of SOC.

Using $H_\infty$ filter algorithm along with the estimated parameters as explained in Chapter 4, the open-circuit voltage of battery model would be estimated. To do so, first the background on $H_\infty$ filter is presented [38, 67].

## 5.1    Constrained Optimization

The background of constrained optimization is required to develop the $H_\infty$ filter fully. How to use Lagrange multiplier to a problem of static variables, inequality constraints and dynamic variables are shown in this section [38].

Suppose a discrete-time dynamic system given by

$$x_{k+1} = F_k x_k + \omega_k (k = 0, \cdots, N-1) \tag{47}$$

where $x_k$ is an $n$-dimensional state vector.

Let's assume the objective is to minimize some scaler function $J(x, \omega)$ with respect to $x$ and $\omega$ where $x$ is an $n$-dimensional vector and a dependant variable and $\omega$ is a $m$-dimensional vector and the independent variable. Suppose the constraint vector is given as $f(x, \omega) = 0$ and is the same dimension of $x$. Then the problem can be

defined as

$$\min_{x,\omega} J(x,\omega) \text{ such that } f(x,\omega) = 0. \tag{48}$$

Assume the solution of the constrained minimum of $J(x,\omega)$ occurs at $x = x^*$ and $\omega = \omega^*$. This is called the stationary point of $J(x,\omega)$. Let's choose the values of $x$ and $\omega$ such that $x$ is close to $x^*$ and $\omega$ is close to $\omega^*$ when the condition still holds true for $f(x,\omega) = 0$. Expanding $J(x,\omega)$ and $f(x,\omega)$ in a Taylor series around $x^*$ and $\omega^*$ gives

$$
\begin{aligned}
J(x,\omega) &= J(x^*,\omega^*) + \frac{\partial J}{\partial x}\Big|_{x^*,\omega^*} \triangle x + \frac{\partial J}{\partial \omega}\Big|_{x^*,\omega^*} \triangle \omega \\
f(x,\omega) &= f(x^*,\omega^*) + \frac{\partial f}{\partial x}\Big|_{x^*,\omega^*} \triangle x + \frac{\partial f}{\partial \omega}\Big|_{x^*,\omega^*} \triangle \omega
\end{aligned}
\tag{49}
$$

where higher-order terms of the series have been neglected with the assumption that $x$ is close to $x^*$ and $\omega$ is close to $\omega^*$, $\triangle x = x - x^*$ and $\triangle \omega = \omega - \omega^*$. Then Eq. 49 can be further simplified by Eq. 50 which is

$$
\begin{aligned}
\triangle J(x,\omega) &= J(x,\omega) - J(x^*,\omega^*) \\
&= \frac{\partial J}{\partial x}\Big|_{x^*,\omega^*} \triangle x + \frac{\partial J}{\partial \omega}\Big|_{x^*,\omega^*} \triangle \omega \\
\triangle f(x,\omega) &= f(x,\omega) - f(x^*,\omega^*) \\
&= \frac{\partial f}{\partial x}\Big|_{x^*,\omega^*} \triangle x + \frac{\partial f}{\partial \omega}\Big|_{x^*,\omega^*} \triangle \omega
\end{aligned}
\tag{50}
$$

Since the values of $x$ and $\omega$ are close to $x^*$ and $\omega^*$, it can be deduced that $\triangle J(x,\omega) = 0$. This is because the partial derivatives on the right side of the $\triangle J(x,\omega)$ are zero at the stationary point $J(x,\omega)$. Furthermore, $\triangle f(x,\omega) = 0$ are at the stationary point of $J(x,\omega)$ because $f(x^*,\omega^*) = 0$ at the constrained stationary point of $J(x,\omega)$ and $x$ and $\omega$ are also chosen such that $f(x,\omega) = 0$. Hence the Eq. 50 can

be rewritten as

$$\frac{\partial J}{\partial x}\big|_{x^*,\omega^*}\triangle x + \frac{\partial J}{\partial \omega}\big|_{x^*,\omega^*}\triangle \omega = 0,$$
$$\frac{\partial f}{\partial x}\big|_{x^*,\omega^*}\triangle x + \frac{\partial f}{\partial \omega}\big|_{x^*,\omega^*}\triangle \omega = 0. \tag{51}$$

These equations are true for arbitrary $x$ and $\omega$ that are close to $x^*$ and $\omega^*$ and that

satisfy the constraint $f(x,\omega) = 0$. Eq. 51 can be solved for $\triangle x$ as

$$\triangle x = -\left(\frac{\partial f}{\partial x}\big|_{x^*,\omega^*}\right)^{-1}\frac{\partial f}{\partial \omega}\big|_{x^*,\omega^*}\triangle \omega \tag{52}$$

Substituting Eq. 52 into Eq. 51 gives

$$\frac{\partial J}{\partial \omega}\big|_{x^*,\omega^*} - \frac{\partial J}{\partial x}\big|_{x^*,\omega^*}\left(\frac{\partial f}{\partial x}\big|_{x^*,\omega^*}\right)^{-1}\frac{\partial f}{\partial \omega}\big|_{x^*,\omega^*} = 0. \tag{53}$$

Eq. 53, combined with the constraint $f(x,\omega) = 0$, gives $(m+n)$ equations that can

be solved for the vectors $\omega$ and $x$ to find the constrained stationary point $j(x,\omega)$.

Now consider an augmented cost function

$$J_a = J + \lambda^T f \tag{54}$$

where $\lambda$ is an $n$-element unknown constant vector called a Lagrange multiplier. Note

that

$$\frac{\partial J_a}{\partial x} = \frac{\partial J}{\partial x} + \lambda^T\frac{\partial f}{\partial x},$$
$$\frac{\partial J_a}{\partial \omega} = \frac{\partial J}{\partial \omega} + \lambda^T\frac{\partial f}{\partial \omega}, \tag{55}$$
$$\frac{\partial J_a}{\partial \lambda} = f.$$

If all the three equations in Eq. 55 are set to zero, it results into

$$\lambda^T = -\frac{\partial J}{\partial x}\left(\frac{\partial f}{\partial x}\right)^{-1},$$
$$\frac{\partial J}{\partial \omega} - \frac{\partial J}{\partial x}\left(\frac{\partial f}{\partial x}\right)^{-1}\frac{\partial f}{\partial \omega} = 0, \tag{56}$$
$$f = 0.$$

The first part in Eq. 56 gives the value of the Lagrange multiplier, the second equation is identical to Eq. 53, and the third equation forces the constraint to be satisfied. Hence the original constrained problem can be solved by creating an augmented cost function $j_a$, taking the partial derivatives with respect to $x, \omega$ and $\lambda$, setting them equal to zero, and solving for $x, \omega$ and $\lambda$. The partial derivatives equations gives $(2n + m)$ equations to solve for the $n$-element vector $x$, the $m$-element vector $\omega$ and the $n$-element vector $\lambda$. Although the dimension of the original problem is increased by introducing a Lagrange multiplier, the constrained optimization problem is transformed into an unconstrained optimization problem, which can simplify the problem considerably.

## 5.2    Dynamic Constrained Optimization

Extending the Lagrange multiplier method of constrained optimization to the optimization of dynamic systems, suppose we want to minimize the scaler function

$$J = \psi(x_0) + \sum_{k=0}^{N-1} \mathcal{L}_k \tag{57}$$

where $\psi(x_0)$ is a known function of $x_0$ and $\mathcal{L}_k$ is a known function of $x_k$ and $\omega_k$. This is a common example of kind of constrained optimization problem that arises in a dynamic system. Now we can solve this problem by introducing a Lagrange multiplier

$\lambda$, creating an augmented cost function $J_a$, and then setting the partial derivatives of $J_a$ with respect to $x_k$, $\omega_k$ and $\lambda$ equal to zero. For the $N$ constraints of Eq. 47, $N$ Lagrange multipliers $\lambda_1, \cdots, \lambda_N$ have to be introduced. Hence the augmented cost function can be written as

$$J_a = \psi(x_0) + \sum_{k=0}^{N-1} [\mathcal{L}_k + \lambda_{k+1}^T(F_k x_k + \omega_k - x_{k+1})] \tag{58}$$

Eq. 58 can be further written as

$$
\begin{aligned}
J_a &= \psi(x_0) + \sum_{k=0}^{N-1} [\mathcal{L}_k + \lambda_{k+1}^T(F_k x_k + \omega_k)] - \sum_{k=0}^{N-1} \lambda_{k+1}^T x_{k+1} \\
&= \psi(x_0) + \sum_{k=0}^{N-1} [\mathcal{L}_k + \lambda_{k+1}^T(F_k x_k + \omega_k)] - \sum_{k=0}^{N-1} \lambda_k^T x_k + \lambda_0^T x_0
\end{aligned} \tag{59}
$$

where $\lambda_0$ is an additional term in the Lagrange multiplier sequence. Now let's define the Hamiltonian $\mathcal{H}_k$ as

$$\mathcal{H}_k = \mathcal{L}_k + \lambda_{k+1}^T(F_k x_k + \omega_k) \tag{60}$$

Substituting the definition of $\mathcal{H}_k$ in Eq. 59 gives

$$
\begin{aligned}
J_a &= \psi(x_0) + \sum_{k=0}^{N-1} \mathcal{H}_k - \sum_{k=0}^{N} \lambda_k^T x_k + \lambda_0^T x_0 \\
&= \psi(x_0) + \sum_{k=0}^{N-1} \mathcal{H}_k - \sum_{k=0}^{N-1} \lambda_k^T x_k(F_k x_k - \lambda_N^T x_N + \lambda_0^T x_0 \\
&= \psi(x_0) + \sum_{k=0}^{N-1} (\mathcal{H}_k - \lambda_k^T x_k) - \lambda_N^T x_N + \lambda_0^T x_0.
\end{aligned} \tag{61}
$$

The conditions that are required for a constrained stationary point are

$$\frac{\partial J_a}{\partial x_k} = 0 \quad (k = 0, \cdots, N),$$

$$\frac{\partial J_a}{\partial \omega_k} = 0 \quad (k = 0, \cdots, N - 1), \tag{62}$$

$$\frac{\partial J_a}{\partial \lambda_k} = 0 \quad (k = 0, \cdots, N).$$

The Eq. 62 can also be written as

$$\frac{\partial J_a}{\partial x_0} = 0,$$

$$\frac{\partial J_a}{\partial x_N} = 0,$$

$$\frac{\partial J_a}{\partial x_k} = 0 \quad (k = 0, \cdots, N - 1), \tag{63}$$

$$\frac{\partial J_a}{\partial \omega_k} = 0 \quad (k = 0, \cdots, N - 1),$$

$$\frac{\partial J_a}{\partial \lambda_k} = 0 \quad (k = 0, \cdots, N).$$

The fifth condition in Eq. 63 ensures that the constraints $x_{k+1} = F_k x_k + \omega_k$ is satisfied. Based on the expression for $J_a$ in Eq. 61, the first four conditions in Eq. 63 can be written as

$$\lambda_0^T + \frac{\partial \psi(x_0)}{\partial x_0} = 0,$$

$$-\lambda_N^T = 0,$$

$$\lambda_k^T = \frac{\partial \mathcal{H}_k}{\partial x_k} \quad (k = 1, \cdots, N - 1), \tag{64}$$

$$\frac{\partial \mathcal{H}_k}{\partial \omega_k} = 0 \quad (k = 1, \cdots, N - 1).$$

The result in Eq. 64 gives the necessary conditions for a constrained stationary point for the dynamic optimization problem of Eq. 47.

## 5.3    H$_\infty$ Filter Estimation

Using the above described concepts of constrained and dynamic constrained optimization will be used to derive H$_\infty$ filter estimation technique [38].

### 5.3.1    Definition

For the standard linear discrete-time system of Eq. 47, the H$_\infty$ filter objective is to estimate a state variable $z_k$ such as

$$z_k = L_k x_k \tag{65}$$

where $L_k$ is a user-defined matrix of full rank. For other standard linear estimator like Kalman filter, $L_k = I$ would be the case, but it could be any linear combination of the states. The cost function for the given problem is defined by

$$J_1 = \frac{\sum_{k=0}^{N-1} \|z_k - \hat{z}_k\|_{S_k}^2}{\|x_0 - \hat{x}_0\|_{P_0^{-1}}^2 + \sum_{k=0}^{N-1}(\|\omega_k\|_{Q_k^{-1}}^2 + \|v_k\|_{R_k^{-1}}^2)} \tag{66}$$

in which the goal is to find an estimate $\hat{z}_k$ that minimizes $J_1$. The estimate of $z_k$ is to be found from measurements up to and including time $(N-1)$ and $x_0$ is the initial state of the state variable. Moreover, $P_0, Q_k, R_k$ and $S_k$ in above equation are symmetric positive definite matrices chosen for the problem at hand. For example, if the objective is to estimate the third element of $z_k$ accurately, then the element $S_k(3,3)$ should be chosen to be larger relative to the other elements of $S_k$. Similarly, if the user knows *a priori* that the second element of $\omega_k$ disturbance is small, then $Q_k(2,2)$ is chosen smaller in comparison of other elements of $Q_k$.

Since the direct minimization of $J_1$ is not tractable, it is obtained within user

specified bound $\theta$ by satisfying the estimating strategy of Eq. 67 [38].

$$J_1 < \frac{1}{\theta}. \tag{67}$$

Rearranging Eq. 67 results into

$$J_1 = \frac{-1}{\theta}\|x_0 - \hat{x}_0\|_{P_0^{-1}}^2 + \sum_{k=0}^{N-1}[\|z_k - \hat{z}_k\|_{S_k}^2 - \frac{1}{\theta}(\|\omega_k\|_{Q_k^{-1}}^2 + \|v_k\|_{R_k^{-1}}^2)] < 1. \tag{68}$$

The H$_\infty$ filter problem is given by

$$J^* = \min_{\hat{x}_k} \max_{\omega_k, v_k, x_0} J. \tag{69}$$

Since $x_0, \omega_k, v_k$ completely determine the observation matrix $y_k$, the $v_k$ in Eq. 69 can be substituted by $y_k$, which gives

$$J^* = \min_{\hat{x}_k} \max_{\omega_k, y_k, x_0} J. \tag{70}$$

Since $y_k = H_k x_k + v_k$, it follows that

$$\|v_k\|_{R_k^{-1}}^2 = \|y_k - H_k x_k\|_{R_k^{-1}}^2. \tag{71}$$

Since $z_k = L_k x_k$ and $\hat{z}_k = L_k \hat{x}_k$, we also have

$$\|z_k - \hat{z}_k\|_{S_k}^2 = (z_k - \hat{z}_k)^T(z_k - \hat{z}_k),$$
$$= (x_k - \hat{x}_k)^T L_k^T S_k L_k (x_k - \hat{x}_k), \tag{72}$$
$$= \|x_k - \hat{x}_k\|_{\bar{S}_k}^2$$

where $\bar{S}_k = L_k^T S_k L_k$. Substituting the values of Eq. 72, 71 in Eq. 68 yields

$$J_1 = \frac{-1}{\theta}\|x_0 - \hat{x}_0\|_{P_0^{-1}}^2 + \sum_{k=0}^{N-1}[\|z_k - \hat{z}_k\|_{\bar{S}_k}^2 - \frac{1}{\theta}(\|\omega_k\|_{Q_k^{-1}}^2 + \|y_k - H_k x_k\|_{R_k^{-1}}^2)],$$

$$= \psi(x_0) + \sum_{k=0}^{N-1}\mathcal{L}_k \tag{73}$$

where $\psi(x_0) =$ and $\mathcal{L}_k$ represents the full equation. Then the H$_\infty$ filter solution for the problem in Eq. 47 is given by finding a stationary point of $J$ with respect to $x_0$ and $\omega_k$ and then finding a stationary point of $J$ with respect to $\hat{x}_k$ and $y_K$.

### 5.3.2    Stationarity with Respect to $x_0$ and $\omega_k$

To find the stationary point of $J$ with respect to $\hat{x}_k$ and $y_K$ of Eq. 73, let the Hamiltonian for this problem is defined as

$$\mathcal{H}_k = \mathcal{L}_k + \frac{2\lambda_{k+1}^T}{\theta}(F_k x_k + \omega_k) \tag{74}$$

where $\frac{2\lambda_{k+1}^T}{\theta}$ is the time-varying Lagrange multiplier that must be computed for ($k = 0, \cdots, N-1$). Note that the Lagrange multiplier is multiplied by 2 here which does not change the solution of the problem. It simply scales the Lagrange multiplier by a constant to simplify the calculation. As derived in Eq. 64, the constrained stationary point of $J$ with respect to $\hat{x}_k$ and $y_K$ is solved by

$$\frac{2\lambda_0^T}{\theta} + \frac{\partial\psi(x_0)}{\partial x_0} = 0,$$

$$\frac{2\lambda_N^T}{\theta} = 0,$$

$$\frac{\partial\mathcal{H}_k}{\partial\omega_k} = 0, \tag{75}$$

$$\frac{2\lambda_k^T}{\theta} = \frac{\partial\mathcal{H}_k}{\partial\omega_k}.$$

From the first expression in Eq. 75, it follows

$$\frac{2\lambda_0^T}{\theta} + \frac{2}{\theta}P_0^{-1}(x_0 - \hat{x}_0) = 0,$$

$$P_0\lambda_0 - x_0 + \hat{x}_0 = 0, \tag{76}$$

$$x_0 = \hat{x}_0 + P_0\lambda_0.$$

Similarly, from the first expression in Eq. 75, it follows

$$\lambda_N = 0. \tag{77}$$

Similarly, from the first expression in Eq. 75, it follows

$$-\frac{2}{\theta}Q_k^{-1}\omega_k + \frac{2}{\theta}\lambda_{k+1} = 0,$$

$$\omega_k = Q_k\lambda_{k+1} \tag{78}$$

Substituting the expression of $\omega_k$ in Eq. 47 gives

$$x_{k+1} = F_k x_k + Q_k\lambda_{k+1}. \tag{79}$$

Similarly, from the first expression in Eq. 75, we get

$$\frac{2\lambda_k}{\theta} = 2\bar{S}_k(x_k - \hat{x}_k) + \frac{2}{\theta}H_k^T R_k^{-1}(y_k - H_k x_k) + \frac{2}{\theta}F_k^T \lambda_{k+1},$$

$$\lambda_k = F_k^T \lambda_{k+1} + \theta\bar{S}_k(x_k - \hat{x}_k) + H_k^T R_k^{-1}(y_k - H_k x_k). \tag{80}$$

From Eq. 76, we know that $x_0 = \hat{x}_0 + P_0\lambda_0$, so we make the assumption that

$$x_k = \mu_k + P_k\lambda_k \tag{81}$$

for all $k$, where $\mu_k$ and $P_k$ are some functions to be determined, with $P_0$ given, and the initial condition $\mu_0 = \hat{x}_0$. Substituting the value from Eq. 81 in Eq. 79 yields

$$\mu_{k+1} + P_{k+1}\lambda_{k+1} = F_k\mu_k + F_kP_k\lambda_k + Q_k\lambda_{k+1}. \tag{82}$$

Also substituting Eq. 81 in Eq. 80 gives

$$\lambda_k = F_k^T\lambda_{k+1} + \theta\bar{S}_k(\mu_k + P_k\lambda_k - \hat{x}_k) + H_k^T R_k^{-1}[y_k - H_k(\mu_k + P_k\lambda_k)]. \tag{83}$$

Rearranging Eq. 83 gives

$$\lambda_k - \theta\bar{S}_kP_k\lambda_k + H_k^T R_k^{-1}H_kP_k\lambda_k = F_k^T\lambda_{k+1}+ \tag{84}$$
$$\theta\bar{S}_k(\mu_k - \hat{x}_k) + H_k^T R_k^{-1}(y_k - H_k\mu_k).$$

Eq. 84 can be solved for $\lambda_k$ as

$$\lambda_k = [I - \theta\bar{S}_kP_k + H_k^T R_k^{-1}H_kP_k]^{-1} \times [F_k^T\lambda_{k+1}+ \tag{85}$$
$$\theta\bar{S}_k(\mu_k - \hat{x}_k) + H_k^T R_k^{-1}(y_k - H_k\mu_k)].$$

Substituting the expression of $\lambda_k$ into Eq. 82 gives

$$\mu_{k+1} + P_{k+1}\lambda_{k+1} = F_k\mu_k + F_kP_k[I - \theta\bar{S}_kP_k + H_k^T R_k^{-1}H_kP_k]^{-1}\times \tag{86}$$
$$[F_k^T\lambda_{k+1} + \theta\bar{S}_k(\mu_k - \hat{x}_k) + H_k^T R_k^{-1}(y_k - H_k\mu_k)] + Q_k\lambda_{k+1}.$$

The Eq. 86 can be rearranged as

$$\mu_{k+1} - F_k\mu_k - F_kP_k[I - \theta\bar{S}_kP_k + H_k^T R_k^{-1}H_kP_k]^{-1}\times$$
$$[\theta\bar{S}_k(\mu_k - \hat{x}_k) + H_k^T R_k^{-1}(y_k - H_k\mu_k)] = [-P_{k+1} + F_kP_k \tag{87}$$
$$[I - \theta\bar{S}_kP_k + H_k^T R_k^{-1}H_kP_k]^{-1}F_k^T + Q_k]\lambda_{k+1}.$$

Eq. 87 is satisfied if both sides are zero. Setting the left-side equal to zero gives

$$\mu_{k+1} = F_k \mu_k + F_k P_k [I - \theta \bar{S}_k P_k + H_k^T R_k^{-1} H_k P_k]^{-1} \times$$
$$[\theta \bar{S}_k (\mu_k - \hat{x}_k) + H_k^T R_k^{-1} (y_k - H_k \mu_k)] \tag{88}$$

with the initial condition $\mu_0 = \hat{x}_0$. Similarly, setting the right hand side in Eq. 87 equal to zero gives

$$P_{k+1} = F_k P_k [I - \theta \bar{S}_k P_k + H_k^T R_k^{-1} H_k P_k]^{-1} F_k^T + Q_k$$
$$= F_k \tilde{P}_k F_k^T + Q_k \tag{89}$$

where $\tilde{P}_k$ is substituted as a new term in the above equation. That is,

$$\tilde{P}_k = P_k [I - \theta \bar{S}_k P_k + H_k^T R_k^{-1} H_k P_k]^{-1},$$
$$= [P_k^{-1} - \theta \bar{S}_k P_k + H_k^T R_k^{-1} H_k]^{-1}. \tag{90}$$

From Eq. 90, it is clear that if $P_k$, $\bar{S}_k$ and $R_k$ are symmetric, then $\tilde{P}_k$ will be symmetric. We also notice from Eq. 89 that if $Q_k$ is symmetric, then $P_{k+1}$ will be symmetric. Hence if $P_0, R_k, Q_k$ and $S_k$ are symmetric for all $k$, then $\tilde{P}_k$ and $P_k$ will be symmetric for all $k$. The values of $x_0$ and $\omega_k$ that provide a stationary point of $J$ are summarized in

Eq. 91.

$$x_0 = \hat{x}_0 + P_0 \lambda_0$$

$$\omega_k = Q_k \lambda_{k+1}$$

$$\lambda_k = [I - \theta \bar{S}_k P_k + H_k^T R_k^{-1} H_k P_k]^{-1} \times [F_k^T \lambda_{k+1} +$$

$$\theta \bar{S}_k (\mu_k - \hat{x}_k) + H_k^T R_k^{-1}(y_k - H_k \mu_k)]$$

$$P_{k+1} = F_k P_k [I - \theta \bar{S}_k P_k + H_k^T R_k^{-1} H_k P_k]^{-1} F_k^T + Q_k \qquad (91)$$

$$\mu_0 = \hat{x}_0$$

$$\mu_{k+1} = F_k \mu_k + F_k P_k [I - \theta \bar{S}_k P_k + H_k^T R_k^{-1} H_k P_k]^{-1} \times$$

$$[\theta \bar{S}_k (\mu_k - \hat{x}_k) + H_k^T R_k^{-1}(y_k - H_k \mu_k)]$$

Eq. 91 provides the stationary point of $J$ with respect to $x_0$ and $\omega_k$.

### 5.3.3    Stationarity with Respect to $\hat{x}$ and $y$

The next step is to find a stationary point with respect to $x_k$ and $y_k$ for the cost function of Eq. 73 subject to the constraints of Eq. 47. From Eq. 81 and $x_0 = \mu_0$, we get

$$\lambda_k = P_k^{-1}(x_k - \hat{\mu}_k),$$
$$\lambda_0 = P_0^{-1}(x_0 - \hat{x}_0). \qquad (92)$$

Hence it gives us

$$\|\lambda_0\|_{P_0}^2 = \lambda_0^T P_0 \lambda_0,$$

$$= (x_0 - \hat{x}_0)^T P_0^{-T} P_0 P_0^{-1}(x_0 - \hat{x}_0), \qquad (93)$$

$$= (x_0 - \hat{x}_0)^T P_0^{-1}(x_0 - \hat{x}_0).$$

Therefore, Eq. 73 becomes

$$J = \frac{-1}{\theta}\|\lambda_0\|_{P_0}^2 + \sum_{k=0}^{N-1}[\|x_k - \hat{x}_k\|_{\bar{S}_k}^2 - \frac{1}{\theta}(\|\omega_k\|_{Q_k^{-1}}^2 + \|y_k - H_k x_k\|_{R_k^{-1}}^2)]. \tag{94}$$

Substituting for $x_k$ from Eq. 81 becomes

$$J = \frac{-1}{\theta}\|\lambda_0\|_{P_0}^2 + \sum_{k=0}^{N-1}[\|\mu_k + P_k\lambda_k - \hat{x}_k\|_{\bar{S}_k}^2$$

$$-\frac{1}{\theta}(\|\omega_k\|_{Q_k^{-1}}^2 + \|y_k - H_k(\mu_k + P_k\lambda_k)\|_{R_k^{-1}}^2)]. \tag{95}$$

Considering the term $\omega_k^T Q_k^{-1}\omega_k$ in Eq. 95 and substituting for $\omega_k$ from Eq. 78 gives

$$\omega_k^T Q_k^{-1}\omega_k = \lambda_{k+1}^T Q_k^T Q_k^{-1} Q_k \lambda_{k+1}$$

$$= \lambda_{k+1}^T Q_k \lambda_{k+1} \tag{96}$$

where $Q_k$ is taken as symmetric matrix. Hence Eq. 95 can be written as

$$J = \frac{-1}{\theta}\|\lambda_0\|_{P_0}^2 + \sum_{k=0}^{N-1}[\|\mu_k + P_k\lambda_k - \hat{x}_k\|_{\bar{S}_k}^2$$

$$-\frac{1}{\theta}\|y_k - H_k(\mu_k + P_k\lambda_k)\|_{R_k^{-1}}^2)] - \frac{1}{\theta}\sum_{k=0}^{N-1}\|\lambda_{k+1}\|_{Q_k}^2. \tag{97}$$

Note that $(\sum_{k=0}^{N}\lambda_k^T P_k\lambda_k - \sum_{k=0}^{N-1}\lambda_k^T P_k\lambda_k) = 0$ because $\lambda_N = 0$ from Eq. 77. Therefore, the last term in the first summation is equal to zero and the two summations are equal in Eq. 97. Hence Eq. 97 can be written as

$$0 = \lambda_0^T P_0\lambda_0 + \sum_{k=0}^{N}\lambda_k^T P_k\lambda_k - \sum_{k=0}^{N-1}\lambda_k^T P_k\lambda_k,$$

$$= \lambda_0^T P_0\lambda_0 + \sum_{k=0}^{N-1}\lambda_{k+1}^T P_{k+1}\lambda_{k+1} - \sum_{k=0}^{N-1}\lambda_k^T P_k\lambda_k, \tag{98}$$

$$\frac{-1}{\theta}\|\lambda_0\|_{P_0}^2 - \frac{-1}{\theta}\sum_{k=0}^{N-1}(\lambda_{k+1}^T P_{k+1}\lambda_{k+1} - \lambda_k^T P_k\lambda_k).$$

Subtracting the Eq. 98 from the cost function of Eq. 97 gives,

$$
J = \sum_{k=0}^{N-1} [\|\mu_k + P_k\lambda_k - \hat{x}_k\|_{\bar{S}_k}^2 - \frac{1}{\theta}\|\lambda_{k+1}\|_{Q_k}^2 -
$$

$$
\frac{1}{\theta}\sum_{k=0}^{N-1}(\lambda_{k+1}^T P_{k+1}\lambda_{k+1} - \lambda_k^T P_k\lambda_k) - \frac{1}{\theta}\|y_k - H_k(\mu_k + P_k\lambda_k)\|_{R_k^{-1}}^2],
$$

$$
= \sum_{k=0}^{N-1} [(\mu_k - \hat{x}_k)^T \bar{S}_k(\mu_k - \hat{x}_k) + 2(\mu_k - \hat{x}_k)^T \bar{S}_k P_k\lambda_k + \lambda_k^T P_k \bar{S}_k P_k\lambda_k +
$$

$$
\frac{1}{\theta}\lambda_{k+1}^T(P_{k+1} - Q_k)\lambda_{k+1} - \frac{1}{\theta}\lambda_k^T P_k\lambda_k - \frac{1}{\theta}(y_k - H_k\mu_k)^T R_k^{-1}(y_k - H_k\mu_k) +
$$

$$
\frac{2}{\theta}(y_k - H_k\mu_k)^T R_k^{-1} H_k P_k\lambda_k - \frac{1}{\theta}\lambda_k^T P_k R_k^{-1} H_k P_k\lambda_k].
$$

(99)

For the term $\lambda_{k+1}^T(P_{k+1} - Q_k)\lambda_{k+1}$ in Eq. 99, substituting for $P_{k+1}$ from Eq. 89 gives

$$
\lambda_{k+1}^T(P_{k+1} - Q_k)\lambda_{k+1} = \lambda_{k+1}^T(Q_k + F_k\tilde{P}_k F_k^T - Q_k)\lambda_{k+1},
$$

$$
= \lambda_{k+1}^T F_k\tilde{P}_k F_k^T \lambda_{k+1}.
$$

(100)

However, Eq. 82 gives

$$
F_k^T \lambda_{k+1} = \lambda_k - \theta\bar{S}_k(\mu_k + P_k\lambda_k - \hat{x}_k) - H_k^T R_k^{-1}[y_k - H_k(\mu_k + P_k\lambda_k)]. \qquad (101)
$$

Substituting the value of Eq. 101 in Eq. 100 yields

$$
\lambda_{k+1}^T(P_{k+1} - Q_k)\lambda_{k+1} = \{\lambda_k - \theta\bar{S}_k(\mu_k + P_k\lambda_k - \hat{x}_k) - H_k^T R_k^{-1}[y_k - H_k(\mu_k + P_k\lambda_k)]\}^T
$$

$$
\tilde{P}_k\{\lambda_k - \theta\bar{S}_k(\mu_k + P_k\lambda_k - \hat{x}_k) - H_k^T R_k^{-1}[y_k - H_k(\mu_k + P_k\lambda_k)]\},
$$

$$
= \{\lambda_k^T(I - \theta P_k\bar{S}_k + P_k H_k^T R_k^{-1} H_k) - \theta(\mu_k - \hat{x}_k)^T \bar{S}_k -
$$

$$
(y_k - H_k\mu_k)^T R_k^{-1} H_k\}\tilde{P}_k\{\lambda_k^T(I - \theta P_k\bar{S}_k + P_k H_k^T R_k^{-1} H_k) - \theta(\mu_k - \hat{x}_k)^T \bar{S}_k -
$$

$$
(y_k - H_k\mu_k)^T R_k^{-1} H_k\}^T
$$

(102)

Note from Eq. 90 that $[(I - \theta P_k\bar{S}_k + P_k H_k^T R_k^{-1} H_k) = P_k\tilde{P}_k^{-1}]$. Substituting this value

in Eq. 102 gives

$$\lambda_{k+1}^T(P_{k+1} - Q_k)\lambda_{k+1} = \{\lambda_k^T P_k \tilde{P}_k^{-1} - \theta(\mu_k - \hat{x}_k)^T \bar{S}_k - (y_k - H_k\mu_k)^T R_k^{-1} H_k\}$$

$$\tilde{P}_k\{\lambda_k^T P_k \tilde{P}_k^{-1} - \theta(\mu_k - \hat{x}_k)^T \bar{S}_k - (y_k - H_k\mu_k)^T R_k^{-1} H_k\}^T$$

$$= \lambda_k^T P_k \tilde{P}_k^{-1} P_k \lambda_k - \theta(\mu_k - \hat{x}_k)^T \bar{S}_k P_k \lambda_k - (y_k - H_k\mu_k)^T R_k^{-1} H_k P_k \lambda_k -$$

$$\theta\lambda_k P_k \bar{S}_k(\mu_k - \hat{x}_k) + \theta^2(\mu_k - \hat{x}_k)^T \bar{S}_k \tilde{P}_k \bar{S}_k(\mu_k - \hat{x}_k) + \quad (103)$$

$$\theta(y_k - H_k\mu_k)^T R_k^{-1} H_k \tilde{P}_k \bar{S}_k(\mu_k - \hat{x}_k) - \lambda_k^T P_k H_k^T R_k^{-1}(y_k - H_k\mu_k) +$$

$$\theta(\mu_k - \hat{x}_k)^T \bar{S}_k \tilde{P}_k H_k^T R_k^{-1}(y_k - H_k\mu_k) +$$

$$(y_k - H_k\mu_k)^T R_k^{-1} H_k \tilde{P}_k H_k^T R_k^{-1}(y_k - H_k\mu_k).$$

Since the expression in Eq. 103 is a scalar, it can also be written as

$$\lambda_{k+1}^T(P_{k+1} - Q_k)\lambda_{k+1} = \lambda_k^T P_k \tilde{P}_k^{-1} P_k \lambda_k - 2\theta(\mu_k - \hat{x}_k)^T \bar{S}_k P_k \lambda_k -$$

$$2(y_k - H_k\mu_k)^T R_k^{-1} H_k P_k \lambda_k + \theta^2(\mu_k - \hat{x}_k)^T \bar{S}_k \tilde{P}_k \bar{S}_k(\mu_k - \hat{x}_k) +$$

$$\quad (104)$$

$$2\theta(\mu_k - \hat{x}_k)^T \bar{S}_k \tilde{P}_k H_k^T R_k^{-1}(y_k - H_k\mu_k) +$$

$$(y_k - H_k\mu_k)^T R_k^{-1} H_k \tilde{P}_k H_k^T R_k^{-1}(y_k - H_k\mu_k).$$

Note that Eq. 90 also gives

$$\tilde{P}_k^{-1} = [I - \theta\bar{S}_k P_k + H_k^T R_k^{-1} H_k P_k]P_k^{-1}$$

$$= P_k^{-1}[P_k^{-1} - \theta\bar{S}_k + H_k^T R_k^{-1} H_k]P_k^{-1} \quad (105)$$

$$= P_k^{-1}[I - P_k\theta\bar{S}_k + P_k H_k^T R_k^{-1} H_k].$$

Hence we get the expression

$$\lambda_k^T P_k \tilde{P}_k^{-1} P_k \lambda_k = \lambda_k^T[I - \theta P_k \bar{S}_k + P_k H_k^T R_k^{-1} H_k]P_k \lambda_k,$$

$$\quad (106)$$

$$= \lambda_k^T P_k \lambda_k - \theta\lambda_k^T P_k \bar{S}_k P_k \lambda_k + \lambda_k^T P_k H_k^T R_k^{-1} H_k P_k \lambda_k.$$

Substituting the value of Eq. 106 in Eq. 104 gives

$$\lambda_{k+1}^T(P_{k+1} - Q_k)\lambda_{k+1} = \lambda_k^T P_k \lambda_k - \theta\lambda_k^T P_k \bar{S}_k P_k \lambda_k + \lambda_k^T P_k H_k^T R_k^{-1} H_k P_k \lambda_k -$$

$$2\theta(\mu_k - \hat{x}_k)^T \bar{S}_k P_k \lambda_k - 2(y_k - H_k\mu_k)^T R_k^{-1} H_k P_k \lambda_k +$$

$$\theta^2(\mu_k - \hat{x}_k)^T \bar{S}_k \tilde{P}_k \bar{S}_k(\mu_k - \hat{x}_k) + 2\theta(\mu_k - \hat{x}_k)^T \bar{S}_k \tilde{P}_k H_k^T R_k^{-1}(y_k - H_k\mu_k) +$$

$$(y_k - H_k\mu_k)^T R_k^{-1} H_k \tilde{P}_k H_k^T R_k^{-1}(y_k - H_k\mu_k). \tag{107}$$

Substituting the value of $\lambda_{k+1}^T(P_{k+1} - Q_k)\lambda_{k+1}$ from Eq. 107 in Eq. 99 gives the augmented cost function

$$J = \sum_{k=0}^{N-1}[(\mu_k - \hat{x}_k)^T \bar{S}_k(\mu_k - \hat{x}_k) - \frac{1}{\theta}(y_k - H_k\mu_k)^T R_k^{-1}(y_k - H_k\mu_k) +$$

$$\theta(\mu_k - \hat{x}_k)^T \bar{S}_k \tilde{P}_k \bar{S}_k(\mu_k - \hat{x}_k) + 2(\mu_k - \hat{x}_k)^T \bar{S}_k \tilde{P}_k H_k^T R_k^{-1}(y_k - H_k\mu_k) +$$

$$\frac{1}{\theta}(y_k - H_k\mu_k)^T R_k^{-1} H_k \tilde{P}_k H_k^T R_k^{-1}(y_k - H_k\mu_k)],$$

$$= \sum_{k=0}^{N-1}[(\mu_k - \hat{x}_k)^T(\bar{S}_k + \theta\bar{S}_k \tilde{P}_k \bar{S}_k)(\mu_k - \hat{x}_k) + \tag{108}$$

$$2(\mu_k - \hat{x}_k)^T \bar{S}_k \tilde{P}_k H_k^T R_k^{-1}(y_k - H_k\mu_k) +$$

$$\frac{1}{\theta}(y_k - H_k\mu_k)^T(R_k^{-1} H_k \tilde{P}_k H_k^T R_k^{-1} - R_k^{-1})(y_k - H_k\mu_k)].$$

To find the stationary point of $J$ with respect to $\hat{x}_k$ and $y_k$, we take the partial derivative of the expression in Eq. 108 and equate it to 0, which gives

$$\frac{\partial J}{\partial \hat{x}_k} = 2(\bar{S}_k + \theta\bar{S}_k \tilde{P}_k \bar{S}_k)(\hat{x}_k - \mu_k) + 2\bar{S}_k \tilde{P}_k H_k^T R_k^{-1}(H_k\mu_k - y_k) = 0,$$

$$\frac{\partial J}{\partial y_k} = \frac{2}{\theta}(R_k^{-1} H_k \tilde{P}_k H_k^T R_k^{-1} - R_k^{-1})(y_k - H_k\mu_k) + 2R_k^{-1} H_k \tilde{P}_k \bar{S}_k(\mu_k - \hat{x}_k) = 0. \tag{109}$$

The equations in Eq. 109 are satisfied for the values of $\hat{x}_k$ and $y_k$ as

$$\hat{x}_k = \mu_k,$$

$$y_k = H_k\mu_k. \tag{110}$$

The values of $\hat{x}_k$ and $y_k$ in Eq. 110 are the solutions for the cost function of Eq. 73. To find out whether these values constitute a local minima or maxima, the second derivative of $J$ with respect to $\hat{x}_k$ is computed as

$$\frac{\partial^2 J}{\partial \hat{x}_k^2} = 2(\bar{S}_k + \theta \bar{S}_k \tilde{P}_k \bar{S}_k) \tag{111}$$

which gives a minima if $(\bar{S}_k + \theta \bar{S}_k \tilde{P}_k \bar{S}_k)$ is positive definite. Note also from the definition of $\tilde{P}_k$ in Eq. 90, the condition required for $\hat{x}_k$ to minimize the cost function $J$ is that $(P_k^{-1} - \theta \bar{S}_k + H_k^T R_k^{-1} H_k)^{-1}$ is always positive definite. Similarly, we would like the value of $y_k$ to provide the maximizing value of $J$. The second derivative of $J$ with respect to $y_k$ is computed as

$$\begin{aligned} \frac{\partial^2 J}{\partial y_k^2} &= \frac{2}{\theta}(R_k^{-1} H_k \tilde{P}_k H_k^T R_k^{-1} - R_k^{-1}), \\ &= \frac{2}{\theta} R_k^{-1}(H_k \tilde{P}_k H_k^T - R_k)R_k^{-1} \end{aligned} \tag{112}$$

which requires $R_K$ to be positive definite to make the function $J$ negative definite and that would be maximizing value of $J$ with respect to $y_k$.

## 5.4    Battery Open-Circuit Voltage Estimation by H$_\infty$ Filter

State estimation of open-circuit voltage $V_{INT}$ is still an open question although it has been explored much in past. Most of the used methods are the popular state estimation tools such as Kalman Filter, and Extended Kalman Filter. However, the performances in predicting the subsequent SOC has not been satisfactory [60, 33, 61]. Because of the inherent non-linearity within the battery model and the hysteresis-like characteristic of open-circuit voltage, many methods have limited performances. Considering these limitations, H$_\infty$ filter method is introduced here which is still a

modified Kalman filter tool, but is robust in estimating a state variable when the non-linearity of a system is unpredictable and the measurement noise is difficult to quantify. Although modeling of battery kinetics has been done in details [68] and Fig. 4 is the most commonly used model, it may not necessarily represent all the changes that may happen inside the battery. In fact, how the battery dynamics change with respect to temperature, usage, and other state-based factors is a subject to debate. However, the use of Kalman filter is robust only when the system has accurate models [38]. For example, the Kalman filter estimates the state of a linear dynamic system defined by the equations

$$x_{k+1} = F_k x_k + \omega_k$$

$$y_k = H_k x + \upsilon_k$$

$$(113)$$

where $\omega_k$ and $\upsilon_k$ are stochastic processes with covariance $Q_k$ and $R_k$ respectively. Then the Kalman filter equations are given by Eq. 114 [38].

$$\hat{x}_{k+1}^- = F_k \hat{x}_k^- + F_k K_k (y_k - H_k \hat{x}_k^-)$$

$$K_k = P_k^- (I + H_k^T R_k^{-1} H_k P_k^-)^{-1} H_k^T R_k^{-1}$$

$$(114)$$

$$P_{k+1}^- = F_k P_k^- (I + H_k^T R_k^{-1} H_k P_k^-)^{-1} F_k^T + Q_k$$

The Kalman filter works well, but only under certain conditions.

- The mean and correlation of the noises $\{\omega_k\}$ and $\{\upsilon_k\}$ need to be known at each time step.

- The covariances $Q_k$ and $R_k$ of the noise processes are determined at each time step. The Kalman filter uses $Q_k$ and $R_k$ as design parameters.

- It is an estimator which yields the smallest possible standard deviation of the residual error. In other words, the Kalman filter is the minimum variance estimator if the noise is Gaussian, and it is the linear minimum variance estimator if the noise is not Gaussian. If it is required to minimize a cost function such as the worst-case estimation error, it may not be able to estimate the states optimally.

- The system model matrices $F_k$ and $H_k$ have to finite for all cases.

If the above assumptions about the Kalman filter do not hold true, it may not estimate state variable optimally. Even with the use of Extended Kalman filter (EFK), the state variable is approximated and linearized which compromises the performance [64]. For the problem of estimating the open-circuit voltage of battery, the non-linearity associated with it can be hard to measure. In such scenario, a new filter called $H_\infty$ filter or minimax filter may be an attractive option as it enjoys the following advantages [38, 67].

- It does not require the covariances $Q_k$ and $R_k$ of the noise processes at each time step.

- It compensates for the uncertainty in the model itself, which may be the case for the battery model.

- It is an estimator which minimizes a cost function in a worst-case estimation error, and hence may provide the optimal estimation.

## 5.4.1 Review of H$_\infty$ Filter

The detailed description has been provided early in this chapter. For the standard linear discrete-time system of Eq. 113, the H$_\infty$ filter objective is to estimate a state variable $z_k$ such as

$$z_k = L_k x_k \tag{115}$$

where $L_k$ is a user-defined matrix. The cost function to be optimized is given by Eq. 116

$$J_1 = \frac{\sum_{k=0}^{N-1} \|z_k - \hat{z}_k\|_{S_k}^2}{\|x_0 - \hat{x}_0\|_{P_0^{-1}}^2 + \sum_{k=0}^{N-1} (\|\omega_k\|_{Q_k^{-1}}^2 + \|\upsilon_k\|_{R_k^{-1}}^2)} \tag{116}$$

in which the goal is to find an estimate $\hat{z}_k$ that minimizes $J_1$. The estimate of $z_k$ is to be found from measurements up to and including time $(N-1)$ and $x_0$ is the initial state of the state variable. Moreover, $P_0, Q_k, R_k$ and $S_k$ in Eq. 116 are symmetric positive definite matrices chosen for the problem at hand.

Since the direct minimization of $J_1$ is not tractable, it is obtained within user specified bound $\theta$ by satisfying the estimating strategy of Eq. 118 [38].

$$
\begin{aligned}
\bar{S}_k &= L_k^T S_k L_k \\
K_k &= P_k [I - \theta \bar{S}_k P_k + H_k^T R_k^{-1} H_k P_k]^{-1} H_k^T R_k^{-1} \\
\hat{x}_{k+1} &= F_k \hat{x}_k^- + F_k K_k (y_k - H_k \hat{x}_k^-) \\
P_{k+1} &= F_k P_k [I - \theta \bar{S}_k P_k + H_k^T R_k^{-1} H_k P_k]^{-1} F_k^T + Q_k
\end{aligned}
\tag{117}
$$

At each step of estimation, the condition of Eq. 118 must hold true.

$$P_k^{-1} - \theta \bar{S}_k + H_k^T R_k^{-1} H_k > 0 \tag{118}$$

### 5.4.2    Formation of State Equations

The model for the battery circuit shown in Fig. 21 consists of the state equation
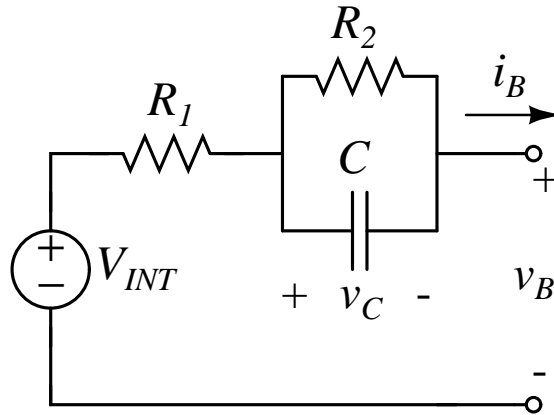


Figure 21: The simplified series-capacitor model of a battery.

$$\frac{dv_C}{dt} = \frac{i_B}{C} - \frac{v_C}{R_2 C} \tag{119}$$

and the output equation

$$v_B = V_{INT} - i_B R_1 - v_C. \tag{120}$$

For simplicity, the model is reformulated in terms of a vector of composite parameters, i.e.

$$\frac{dv_C}{dt} = \mu_1 i_B - \mu_2 v_C \tag{121}$$

and

$$v_B = V_{INT} - \mu_3 i_B - v_C, \tag{122}$$

where $\mu_1 = 1/C$, $\mu_2 = 1/(R_2 C)$, and $\mu_3 = R_1$.

Let the state variables be defined as $x_1 = v_C$ and $x_2 = V_{INT}$, and the observable output variable $y$ represents $v_B$. Then from the above equations, it follows that

$$\frac{dx_1}{dt} = \mu_1 i_B - \mu_2 x_1,$$
$$\frac{dx_2}{dt} = 0, \tag{123}$$
$$y = -x_1 + x_2 - i_B \mu_3$$

where the assumption is that the state variable $x_2 = V_{INT}$ does not change with respect to time $t$ during the short test interval.

Eq. 123 can also be represented in matrix form as

$$\begin{bmatrix} \frac{dx_1}{dt} \\ \frac{dx_2}{dt} \end{bmatrix} = \begin{bmatrix} -\mu_2 & 0 \\ 0 & 0 \end{bmatrix} \begin{bmatrix} x_1 \\ x_2 \end{bmatrix} + \begin{bmatrix} \mu_1 \\ 0 \end{bmatrix} i_B,$$

$$y = \begin{bmatrix} -1 & 1 \end{bmatrix} \begin{bmatrix} x_1 \\ x_2 \end{bmatrix} + \begin{bmatrix} -\mu_3 \end{bmatrix} i_B. \tag{124}$$

Substituting the terms as $\mathbf{F} = \begin{bmatrix} -\mu_2 & 0 \\ 0 & 0 \end{bmatrix}$, $\mathbf{B} = \begin{bmatrix} \mu_1 \\ 0 \end{bmatrix}$, $\mathbf{H} = \begin{bmatrix} -1 & 1 \end{bmatrix}$ and $\mathbf{D} = \begin{bmatrix} -\mu_3 \end{bmatrix}$ in Eq. 124 gives the continuous state equation of the form

$$\dot{\mathbf{x}} = \mathbf{F}\,\mathbf{x} + \mathbf{B}\,i_B$$
$$y = \mathbf{H}\,\mathbf{x} + \mathbf{D}\,i_B. \tag{125}$$

Applying the results from Appendix A, the continuous-time equations of Eq. 125 are converted to its equivalent discrete-time as ,

$$\mathbf{F_k} = e^{\mathbf{F}T}$$

$$= I + \mathbf{F_k}T + \frac{\mathbf{F_k}^2 T^2}{2} + \cdots$$

$$= \begin{bmatrix} 1 & 0 \\ 0 & 1 \end{bmatrix} + \begin{bmatrix} -\mu_2 T & 0 \\ 0 & 0 \end{bmatrix}$$

$$= \begin{bmatrix} 1 - \mu_2 T & 0 \\ 0 & 1 \end{bmatrix} \tag{126}$$

where higher order terms of the exponential series are neglected and

$$\mathbf{B_k} = \int_0^T e^{\mathbf{F}s} ds B$$

$$= \int_0^T \begin{bmatrix} 1 - \mu_2 s & 0 \\ 0 & 1 \end{bmatrix} \begin{bmatrix} \mu_1 \\ 0 \end{bmatrix} ds$$

$$= \int_0^T \begin{bmatrix} \mu_1 - \mu_1 \mu_2 s \\ 0 \end{bmatrix} ds \tag{127}$$

$$= \begin{bmatrix} \mu_1 T - \frac{\mu_1 \mu_2 T^2}{2} \\ 0 \end{bmatrix}$$

and $\mathbf{H_k} = \mathbf{H}$, $\mathbf{D_k} = \mathbf{D}$. Hence the discrete-time state equations for the battery model have the final form of

$$\mathbf{x_{k+1}} = \mathbf{F_k} \, \mathbf{x_k} + \mathbf{B_k} \, i_B + \omega_k$$

$$y_k = \mathbf{H_k} \, \mathbf{x} + \mathbf{D_k} \, i_B + \upsilon_k \tag{128}$$

where $\{\omega_k\}$ and $\{\upsilon_k\}$ are stochastic noise added to the system. These noise represents

the uncertainty associated with the parameters and open-circuit voltage of the battery and may account for varying characteristics due to temperature, discharge/charge rates, waiting periods, aging, and other structural and environmental based factors.

### 5.4.3 System Observability

For the battery state equation of Eq. 128, the observability matrix is

$$
\begin{aligned}
\mathbf{W_0} &= \begin{pmatrix} H_k \\ H_k F_k \end{pmatrix} \\
&= \begin{pmatrix} -1 & 1 \\ -1 + \mu_2 T & 1 \end{pmatrix}
\end{aligned}
\tag{129}
$$

Since the matrix of Eq. 129 has full rank for nonzero unique values of $\mu_2$, the system model is observable.

### 5.4.4 State Estimation

Using $H_\infty$ filter described above for the state equations of Eq. 128, the estimation proceeds as follows.

$$
\begin{aligned}
\bar{S}_k &= L_k^T S_k L_k \\
K_k &= P_k [I - \theta \bar{S}_k P_k + H_k^T R_k^{-1} H_k P_k]^{-1} H_k^T R_k^{-1} \\
\hat{x}_{k+1} &= F_k \hat{x}_k + B_k i_{B,k} + F_k K_k (y_k - H_k \hat{x}_k - D_k i_{B,k}) \\
P_{k+1} &= F_k P_k [I - \theta \bar{S}_k P_k + H_k^T R_k^{-1} H_k P_k]^{-1} F_k^T + Q_k
\end{aligned}
\tag{130}
$$

where $F_k = \begin{bmatrix} 1 - \mu_2 T & 0 \\ 0 & 1 \end{bmatrix}$, $B_k = \begin{bmatrix} \mu_1 T - \frac{\mu_1 \mu_2 T^2}{2} \\ 0 \end{bmatrix}$, $H_k = \begin{bmatrix} -1 & 1 \end{bmatrix}$ and $D_k =$

$\left[ -\mu_3 \right]$. At each step, the condition of Eq. 131 is made sure to hold true.

$$P_k^{-1} - \theta \bar{S}_k + H_k^T R_k^{-1} H_k > 0 \tag{131}$$

## 5.5    Simulation Result

A test data at $V_{INT} = 4$ Volt, $\mu = \{0.0005; 0.1; 0.020\}$ and a load current of $i_B = 0.2$ A is generated in which a test is initiated 30 seconds after the discharge has started and is shown in Fig. 22. Note that the open-circuit voltage has gone through change in its dynamics because of the load discharge. In absence of any external noise, the correct open-circuit voltage would still be 4V as no noise has been added to the data. However, the voltage level at which the test is triggered is different from the correct open-circuit voltage. The $H_\infty$ filter task is to estimate the correct open-circuit voltage which could subsequently form the basis for correct SOC estimation.

From the test data of Fig. 22, the voltage and current data are extracted for $H_\infty$ algorithm and is shown in Fig. 23 Using the $H_\infty$ filter algorithm of Eq. 131, $V_{INT}$ is correctly estimated to be 4.0V. The convergence of $H_\infty$ filter is shown in Fig. 24.

## 5.6    Sample Result

Fig. 25 shows a discharge curve from lithium-ion battery during which a test has been completed. Note that the test is started while the battery is under a stead-state condition and it triggers a change in voltage and current.

First, the nonlinear parameter estimation procedure of chapter IV is applied on the extracted test data of Fig. 26 and the estimation yields the set of parameter values as $\hat{\mu} = \{0.0017; 0.1227; 0.0273\}$. Fig. 27 shows the nonlinear fit of the voltage data. Note

the close fit between the measured data and the model estimates. For open-circuit voltage estimation by $H_\infty$ filter, the current and voltage data is separated as shown in Fig. 28.

The $H_\infty$ filter estimation of Eq. 131, $V_{INT}$ is found out to be 3.422 V whereas the measured open-circuit voltage is 3.4211 V, which yield the error of 0.01 %. Such a low error can be considered within excellent bound for such a non-linear problem. The convergence of $H_\infty$ filter is shown in Fig. 29.
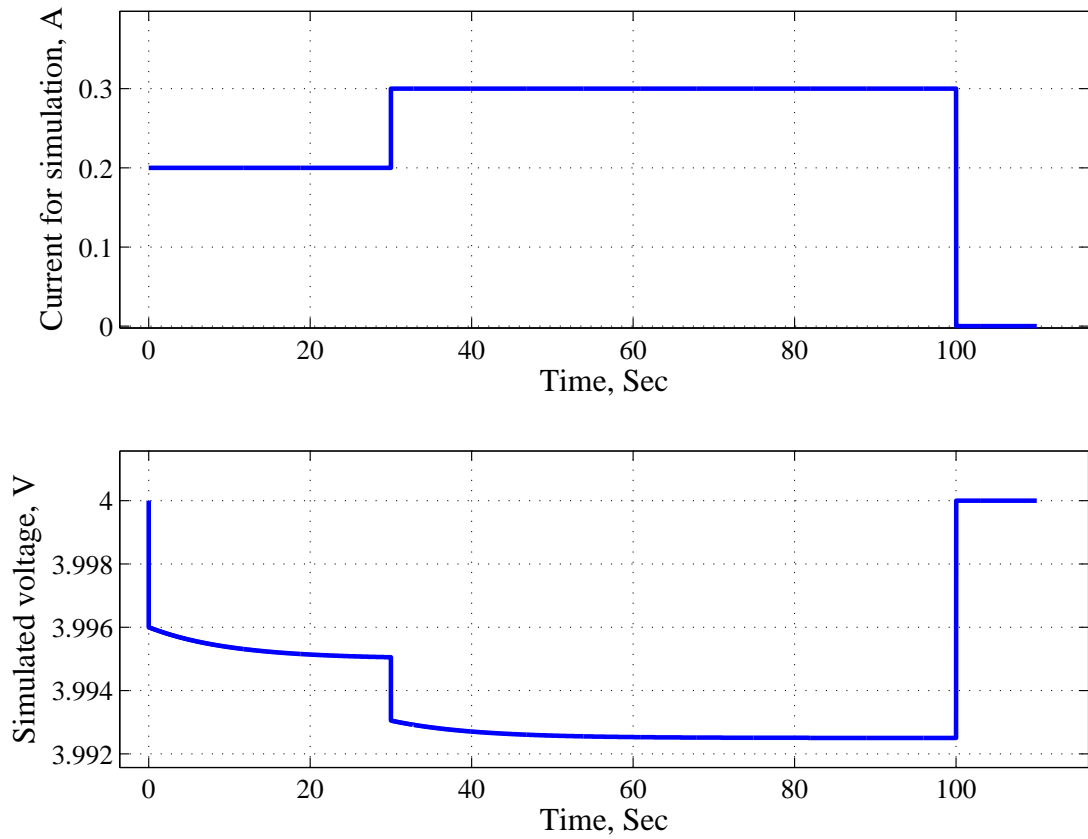


Figure 22: The generated test data for simulation in which a test is initiated 30 seconds after the discharge has begun. A parameter set of $\mu = \{0.0005; 0.1; 0.020\}$ is used in this test discharge. Top trace: The simulated current data. Bottom trace: The resulting voltage data for the simulated current data for the chosen set of parameters.

## 5.7    Summary

This chapter presents an effective means to estimate the state variable by $H_\infty$ filter especially when there is uncertainty in system model and noise in the measurement process. This method is especially suitable for the estimation of open-circuit voltage $V_{INT}$ of the battery, which is inaccessible for direct measurement and varies with respect to several factors. The method is supported by simulation and the experimental results.
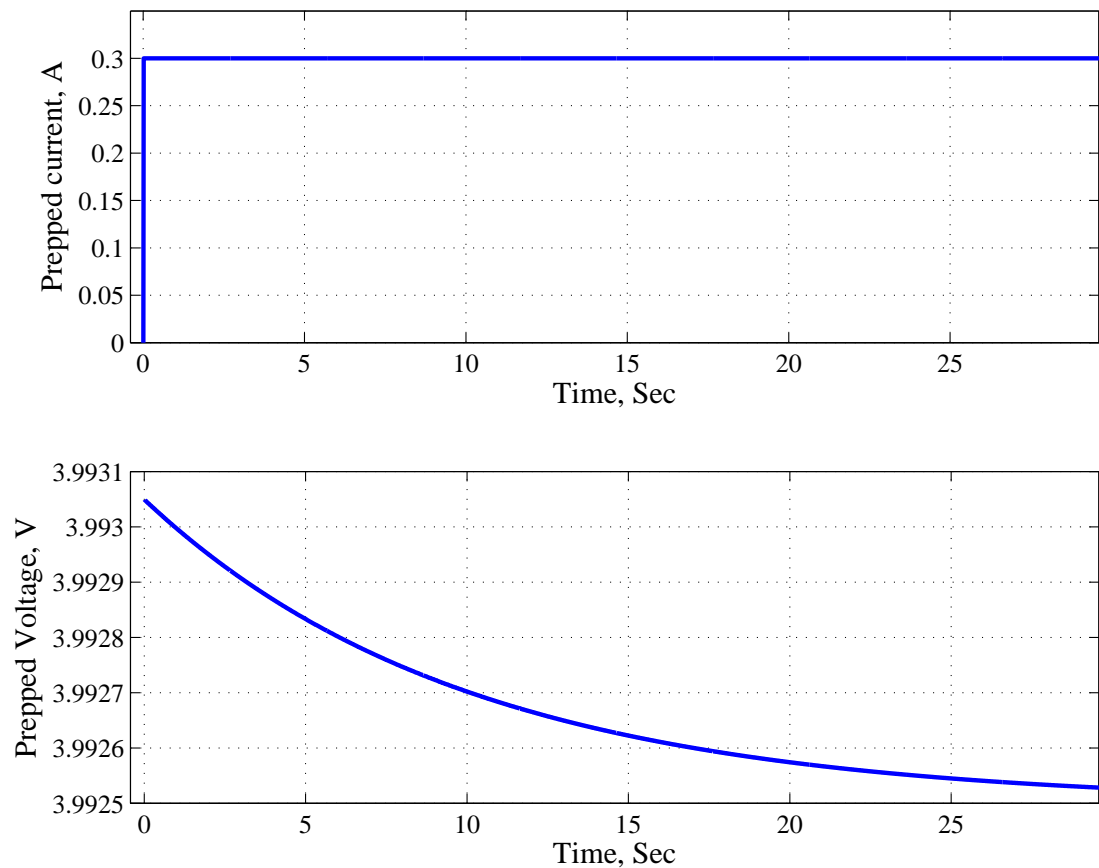


Figure 23: The test data extracted for the $H_\infty$ filter algorithm from Fig. 23. Upper trace: Total current drawn from the battery during the test. Bottom trace: The change in voltage triggered by the test.
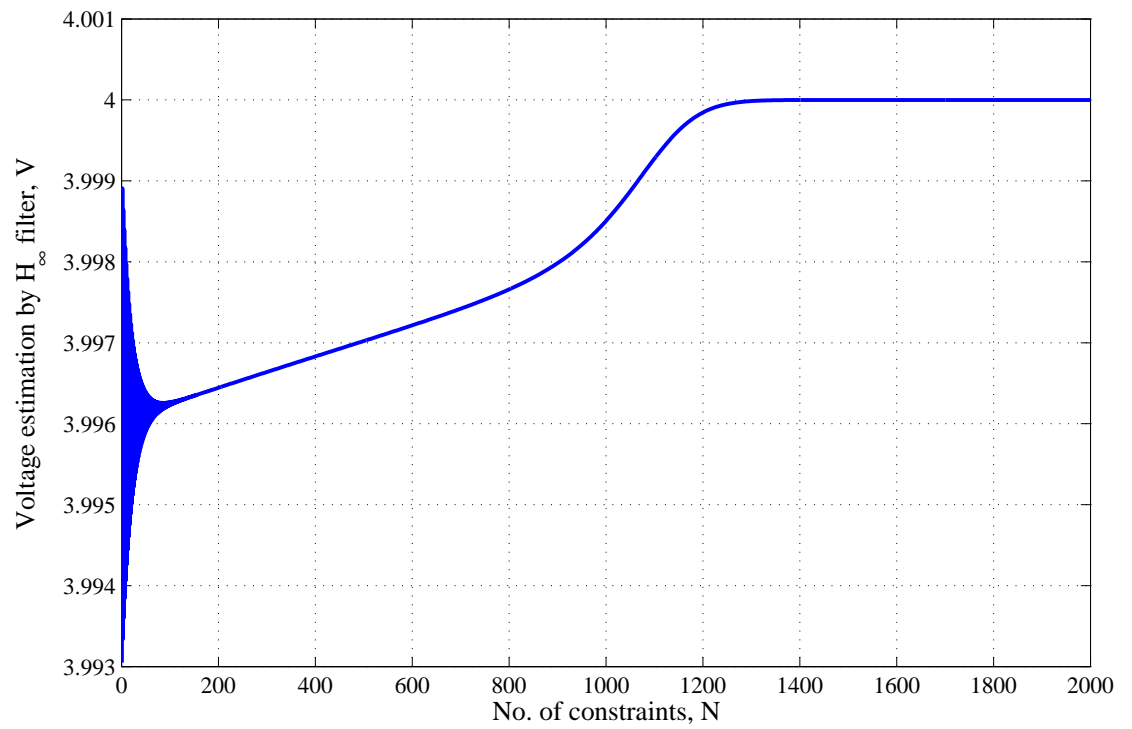
Figure 24: The $H_\infty$ filter convergence for simulated voltage data.
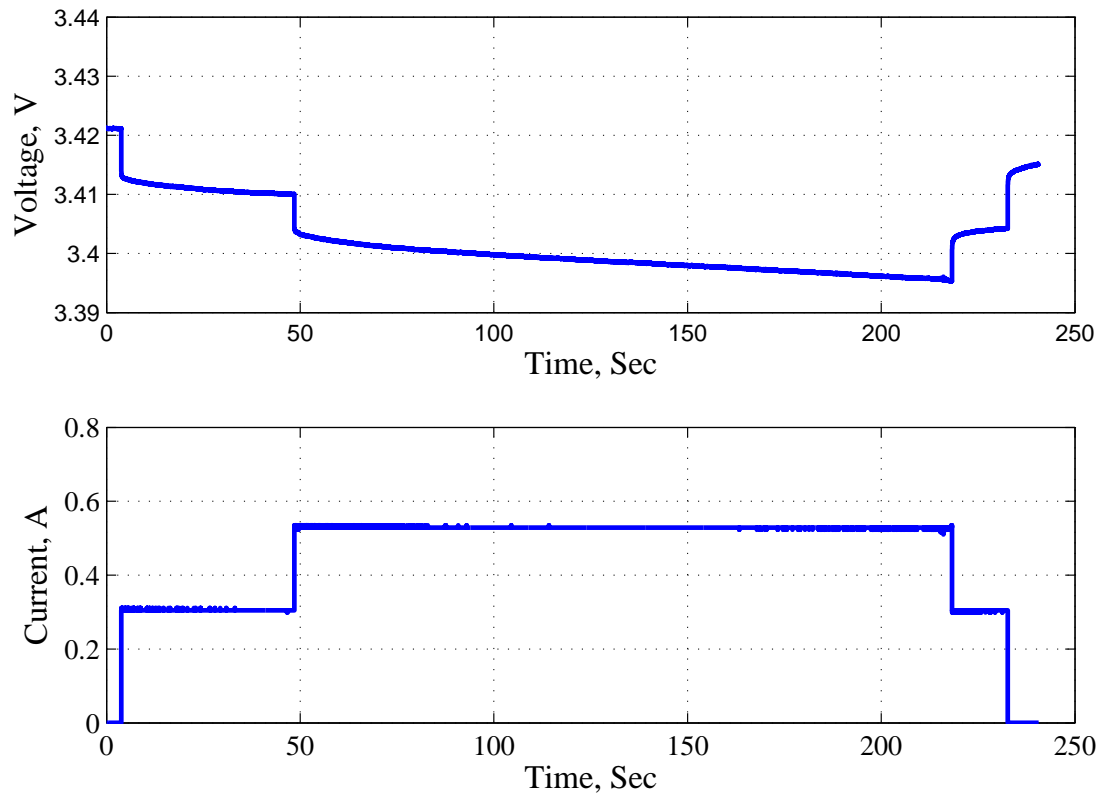
Figure 25: Top trace: The measured terminal voltage during a discharge from a 3.6 Volt nominal, 18650-type lithium-ion battery. Note the test starts at a chosen instant during the discharge. Bottom trace: The current drawn from the battery.
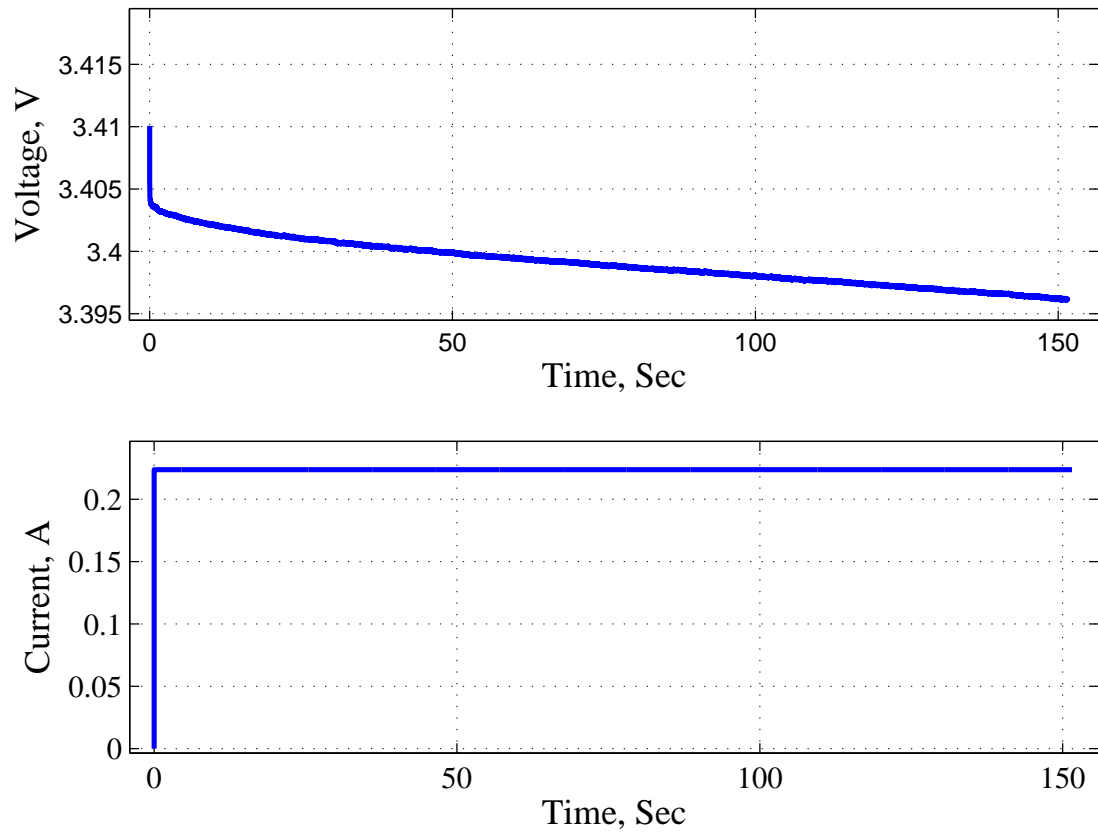
Figure 26: Top trace: The extracted voltage data for estimation. Bottom trace: The extracted current data.
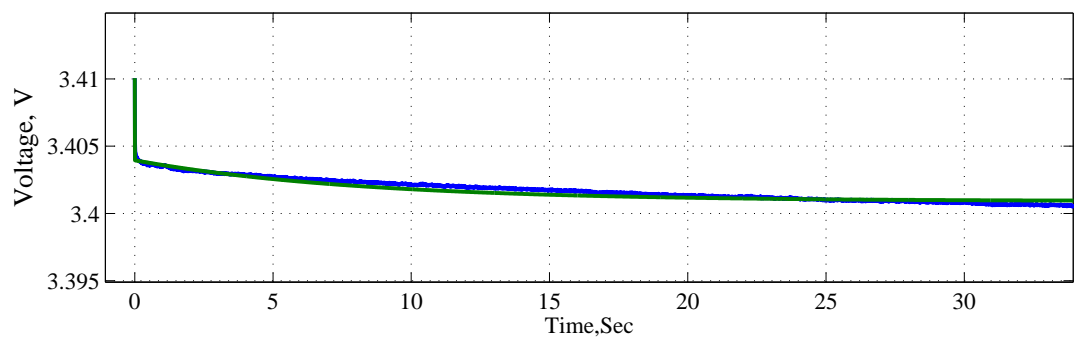


Figure 27: Nonlinear estimation result. Note the close fit between the measured data and the model estimate.
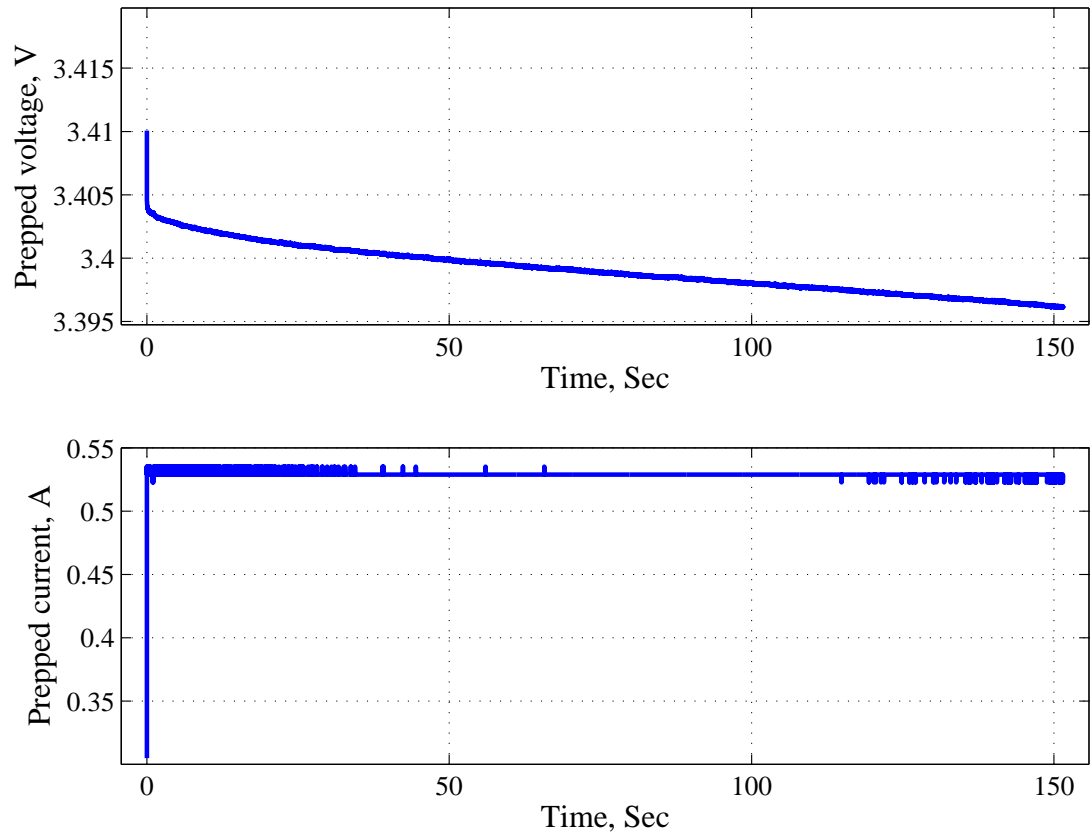
Figure 28: Top trace: The extracted voltage data for estimation. Bottom trace: The extracted total current data.
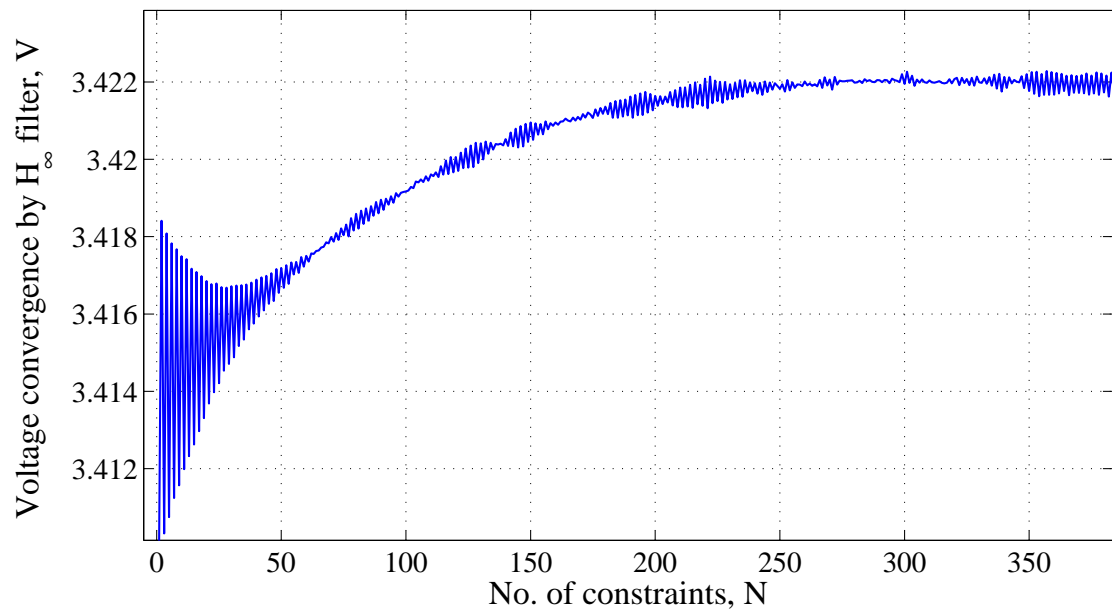
Figure 29: H-infinity convergence of the experimental data.

CHAPTER 6: EXPERIMENTAL RESULTS

This chapter presents the experimental setup, measurement, and tabulations of results. It combines together the nonlinear least square estimation methodology of Chapter IV and the $H_\infty$ filter of the state estimation methodology of Chapter V to form a streamlined test procedure for the SOC and SOH analysis of a battery. It also presents validation tests to support the proposed methodology and results.

## 6.1  Test Procedure

The general procedure to conduct a test is shown in Fig. 30.
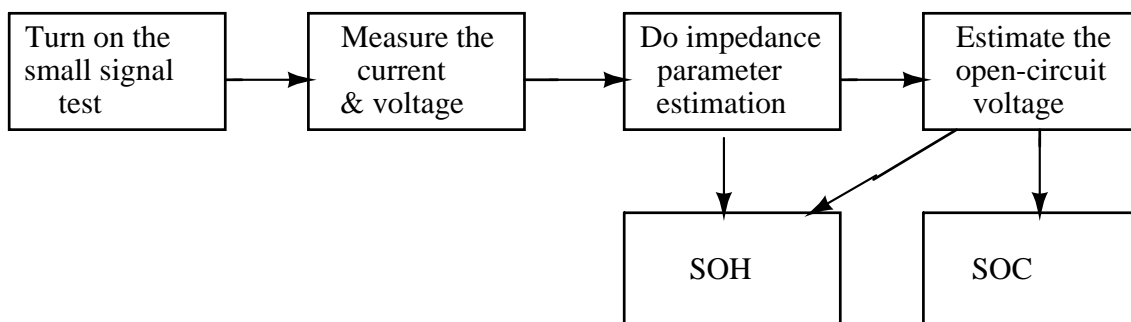


Figure 30: The combined procedural steps to estimate impedance parameters and open-circuit voltage forming the basis for SOC and SOH analysis.

As the figure shows, a small test signal is sent to a battery load, which would trigger transient dynamics inside the battery. The resulting voltage and current are measured. First, impedance parameter estimation is performed to find out the parameters of the battery model. Second, the open-circuit voltage is estimated with the use of impedance parameters and test data. The combination of parameters and

open-circuit voltage forms the basis for SOC and SOH analysis.

## 6.2    Experimental Results

The estimation routine has been validated using the experimental setup shown in Fig. 31. The battery used is 18650-type lithium-ion cell, and loads are connected to it using a solid-state relay. Both the terminal voltage and current are sensed using Hall-effect transducers produced by LEM, and the ambient temperature is measured using an LM35 temperature sensor. To resolve small changes in the terminal voltage, a differential amplifier removes the offset and amplifies the difference. All of the data streams are sampled at 100Hz using a PCI-1710 data-acquisition card. For consistency, all tests are performed at approximately 24°C.
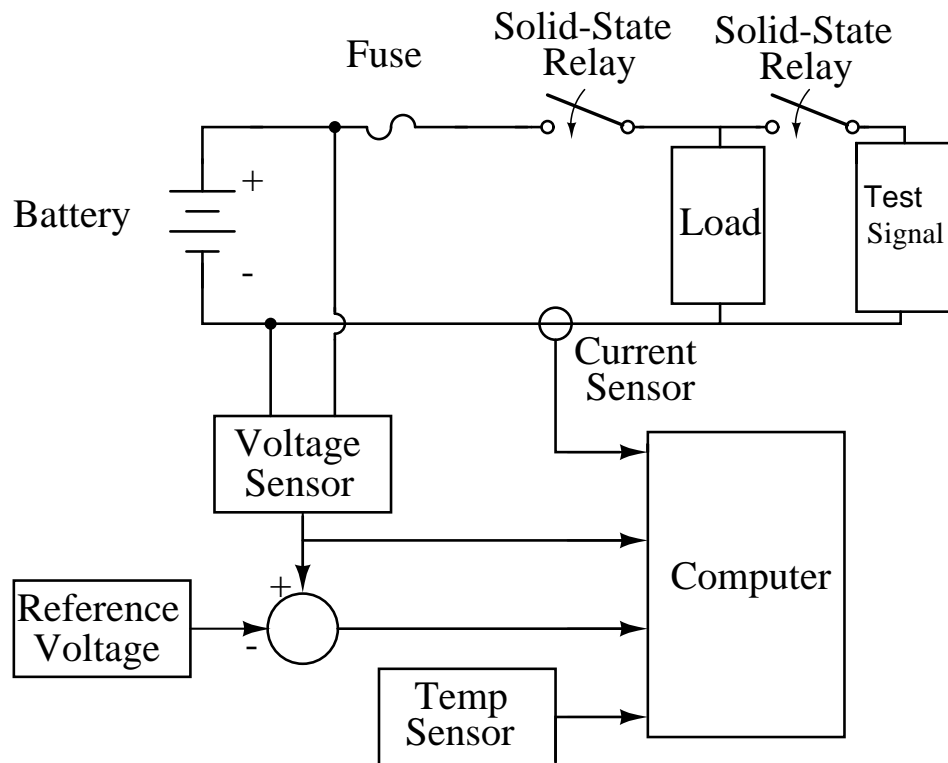


Figure 31: Block diagram of the measurement system.

Several different loads have been used to excite the test battery. Each was selected

so that it provides what is effectively a "small-signal" excitation. Recall that this constraint was imposed so that the internal source $V_{INT}$ would remain effectively constant throughout the measurement interval. The use of small loads such as power resistors are used for the experiments.

Fig. 32 shows a discharge curve during which a test has been completed. Note that the test is started while the battery is under a stead-state condition and it triggers a change in voltage and current.
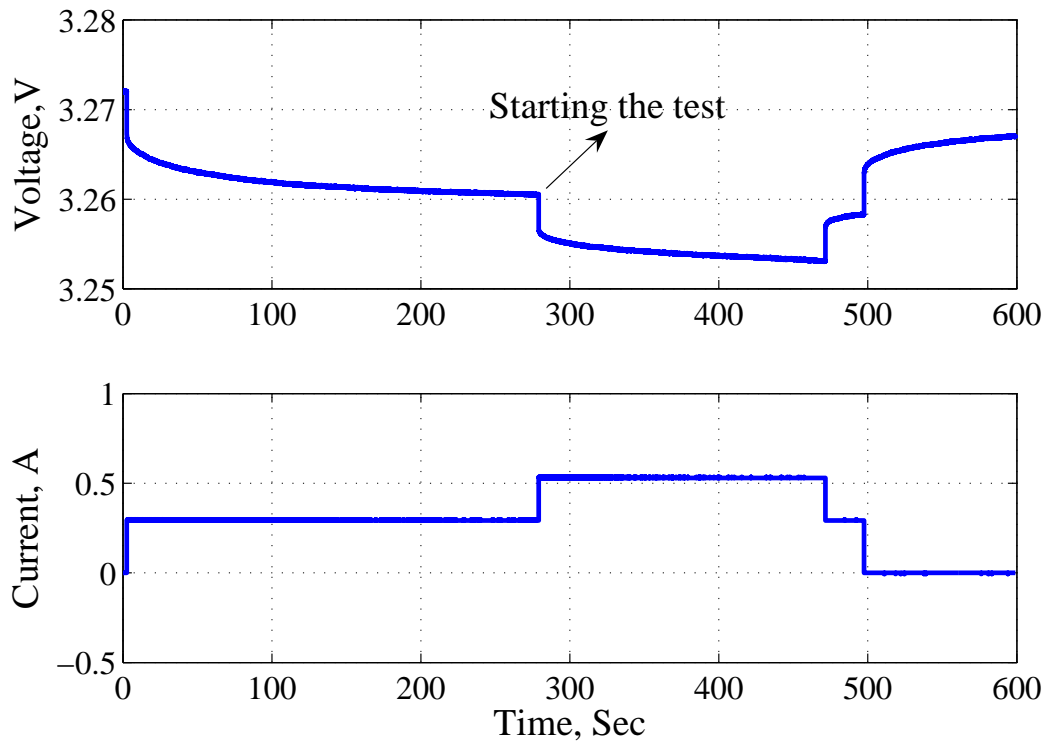


Figure 32: Top trace: The measured terminal voltage during a discharge from a 18650-type lithium-ion battery. Note the test starts at a chosen moment during the discharge. Bottom trace: The current drawn from the battery.

Once the data of Fig. 32 is recorded, the required voltage and current data for the estimation of parameters are extracted as shown in Fig. 33.

The estimation procedure from chapter IV is applied to data sets such as the one

shown in Fig. 33. Fig. 34 presents typical results. Note the close fit between the measured data and the model estimates.

After parameters are estimated through the non-linear least square estimation, the obtained parameters, voltage and current data are sent to $H_\infty$ filter module for the estimation of open-circuit voltage $\hat{V}_{INT}$.

Experiments and estimations have been performed at various SOC levels, and the results have been compared to expectations. Parameters have been correlated with
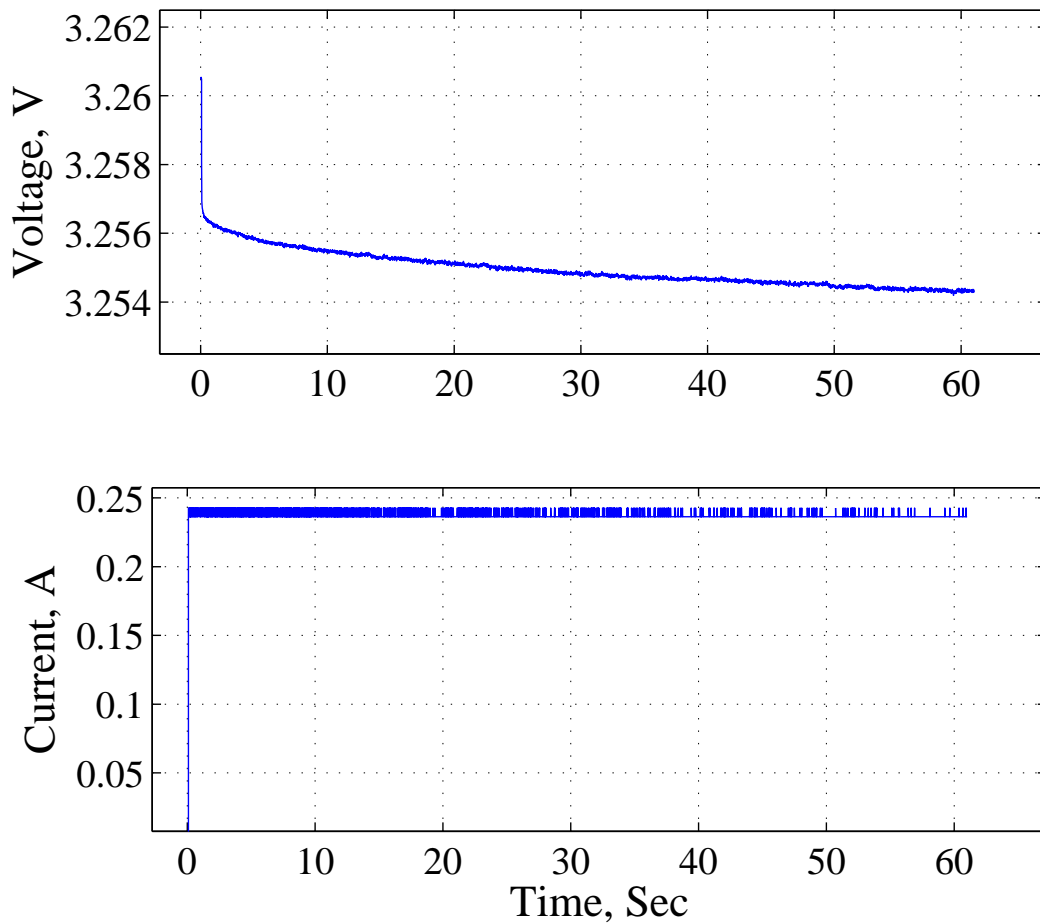


Figure 33: Top trace: The extracted voltage data for estimation. Bottom trace: The extracted current data for estimation.

SOC using a two-step process. First, an initial experiment is performed in which SOC is related to open-circuit voltage. The 3.6 V nominal LG brand lithium-ion battery is discharge at a rate of $\frac{C}{55}$ so that the open-circuit voltage does not show any memory effect. The open-circuit voltage generated at such a slow discharge should correlate with SOC directly. Fig. 35 shows a full discharge of a freshly charged battery until the voltage is cut-off at 3 V. Fig. 36 shows the estimated open-circuit voltage $V_{INT}$ versus SOC. The results match closely to published expectations for 18650 cells [69], with an approximately linear relationship over most of the useable range of the cell [70, 33, 69].

In subsequent tests, the parameter values were obtained and the open-circuit voltage was estimated to determine the corresponding state-of-charge. Table 2 summa-
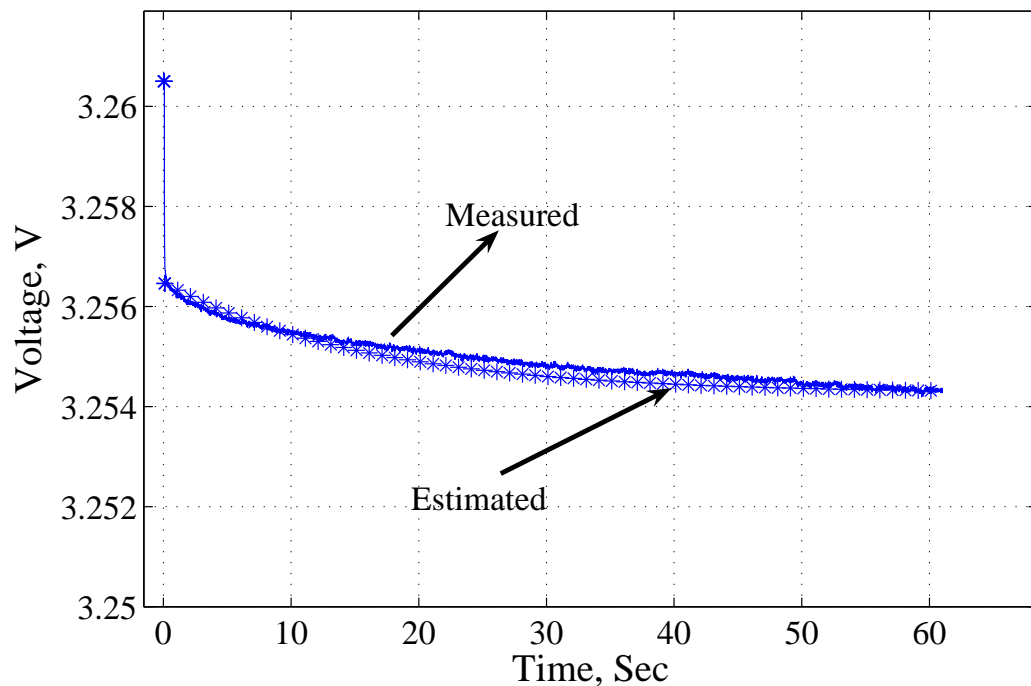


Figure 34: Experimental results. Solid line: Measured terminal voltage. Asterisks: Estimated terminal voltage.
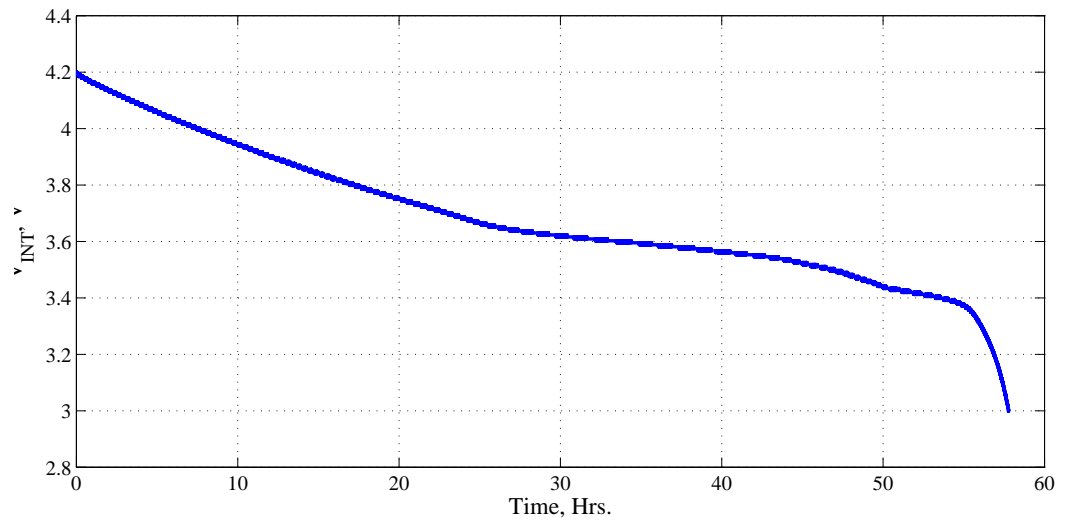
Figure 35: The full discharge of a freshly charged 3.6 V nominal LG lithium-ion battery at $\frac{C}{55}$ rate. The open-circuit voltage relates directly with the SOC, and it has almost negligible memory effect at such a low discharge rate.
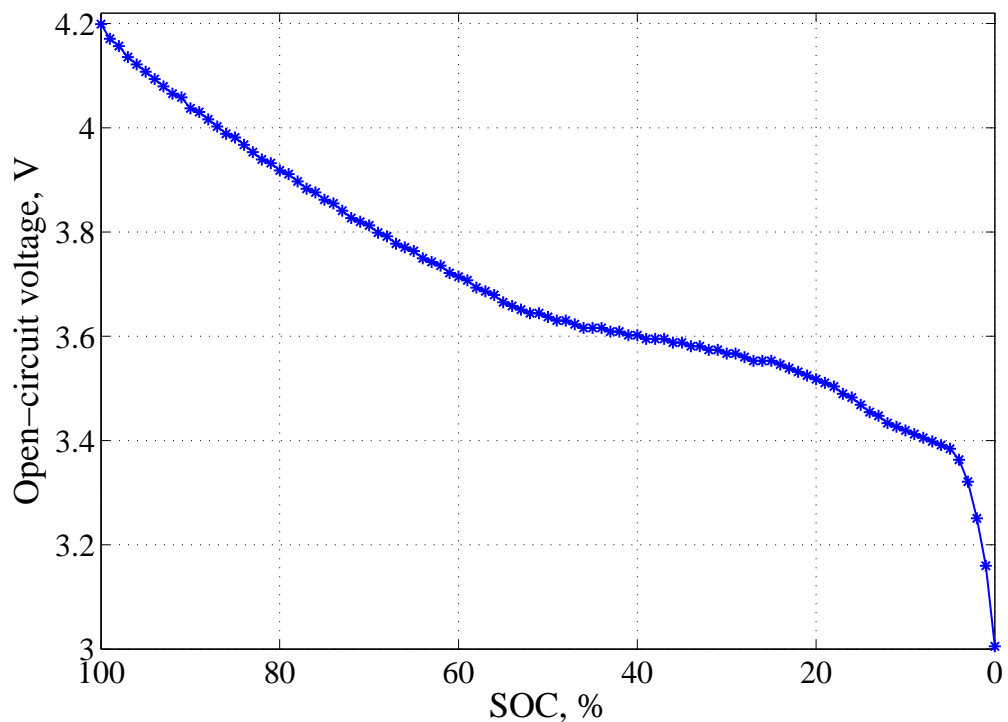


Figure 36: The relationship between SOC and the open-circuit voltage. Note that the open-circuit voltage is equivalent to the internal source $V_{INT}$.

rizes the results of several different tests. $v_B(0)$ in Table 2 is the starting steady-state voltage under battery load when the test is initiated. Note the clear relationships between SOC and the parameters. In addition, one should be aware that each test was performed following a pre-determined waiting period at a fixed temperature.

Table 2: Test Results Showing Estimates of Parameters and SOCs

| Test No. | $v_B(0)$ (V) | $\hat{R}_1(\Omega)$ | $\hat{R}_1 + \hat{R}_2(\Omega)$ | $\widehat{R_2C}$ (Sec) | $\hat{V}_{INT}$ (V) | $\widehat{SOC}$ (%) |
|---|---|---|---|---|---|---|
| Test I | 3.5947 | 0.0189 | 0.0249 | 12.71 | 3.600 | 40 |
| Test II | 3.5436 | 0.0215 | 0.0287 | 10.96 | 3.5498 | 24.5 |
| Test III | 3.4801 | 0.0221 | 0.0316 | 9.52 | 3.4879 | 17 |
| Test IV | 3.4101 | 0.0273 | 0.0409 | 8.15 | 3.4207 | 10 |
| Test V | 3.1948 | 0.0433 | 0.0868 | 5.78 | 3.3146 | 2.75 |

Particular emphasis has been given to the relationships between SOC and the resistance $R_1$ and the time constant $R_2C$. Fig. 37, for instance, shows that $R_1$ increases as SOC decreases. This result is consistent other published findings [9, 21]. Fig. 38 shows the relationship between SOC and the time constant $R_2C$. Note that this result is also consistent with the literature [9, 19].

## 6.3 Validation Tests

Tests are performed to check the effectiveness of the proposed methodology in dynamic operations of battery. The impedance parameter estimation would form the basis for SOH analysis whereas the estimation of open-circuit voltage would form the basis for SOC estimation. Comparing the results obtained from this methodology with known value of SOC, the effectiveness of the proposed methodology is found.

### 6.3.1    Continuous On-Off Discharge Operations

First, validation of the proposed methodology is done for applications in which the battery goes in continuous on-off conditions. During a discharge, a test is performed and immediately the battery is turned off so that it settles to its correct open-circuit voltage. For the battery to settle down to its correct value, sufficient rest-time is given. It is helpful to know the correct value of open-circuit voltage so that it can be compared with the estimated open-circuit voltage by the proposed methodology.

Fig. 39 shows one of such experiments in which several tests are performed at increasing time during on-off operations. The instants that the tests are performed are marked, and it also allows the open-circuit voltage to settle to its correct values by resting it for sufficiently long time. For the tests of Fig. 39, the current drawn from the battery is shown in Fig. 40. Note the steady-state current during discharge, a step-
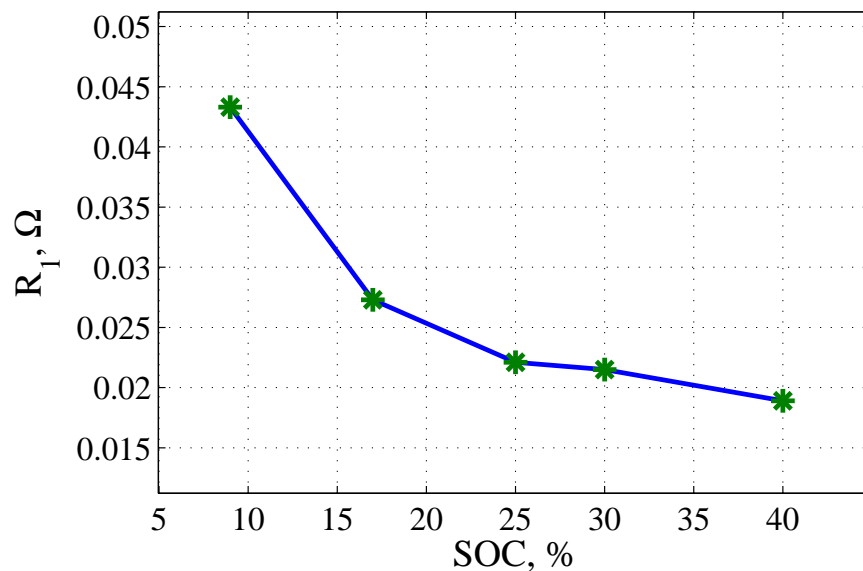


Figure 37: The relationship between $R_1$ and SOC.
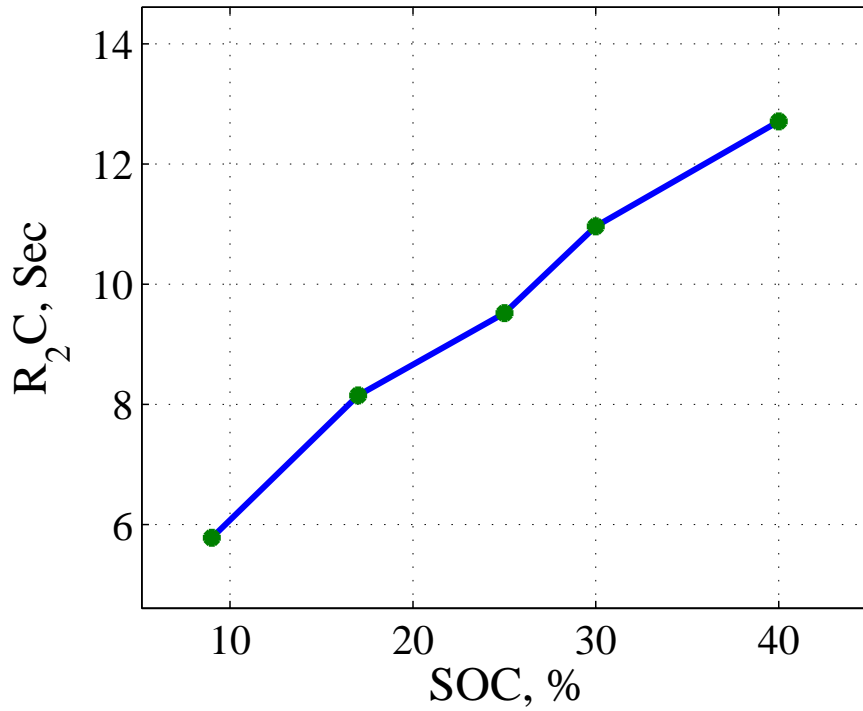
Figure 38: The relationship between $R_2C$ and SOC.

like test signal during the test period, and zero current during off periods. By using the proposed methodology, the open-circuit voltages for different tests are estimated and shown in Table 3. Note the small errors in estimating the open-circuit voltage which should be within the allowed tolerance for most of the battery applications.

Table 3: Validation Tests during Continuous On-Off Operations

| Test No. | $(v_B(0))$ | $\hat{V}_{INT}$ | $V_{settled}$ | (%) Error | SOC |
|---|---|---|---|---|---|
| Test I | 4.1102 V | 4.1457 V | 4.1538 V | 0.19 % | 97.5 % |
| Test II | 4.0682 V | 4.1026 V | 4.1123 V | 0.23 % | 95 % |
| Test III | 4.0171 V | 4.0727 V | 4.0641 V | 0.21 % | 93 % |
| Test IV | 3.9645 V | 4.056 V | 4.0612 V | 0.13 % | 91 % |
| Test V | 3.9092 V | 3.9562 V | 3.9663 V | 0.25 % | 83 % |
| Test VI | 3.8603 V | 3.9250 V | 3.9189 V | 0.15 % | 80.5 % |
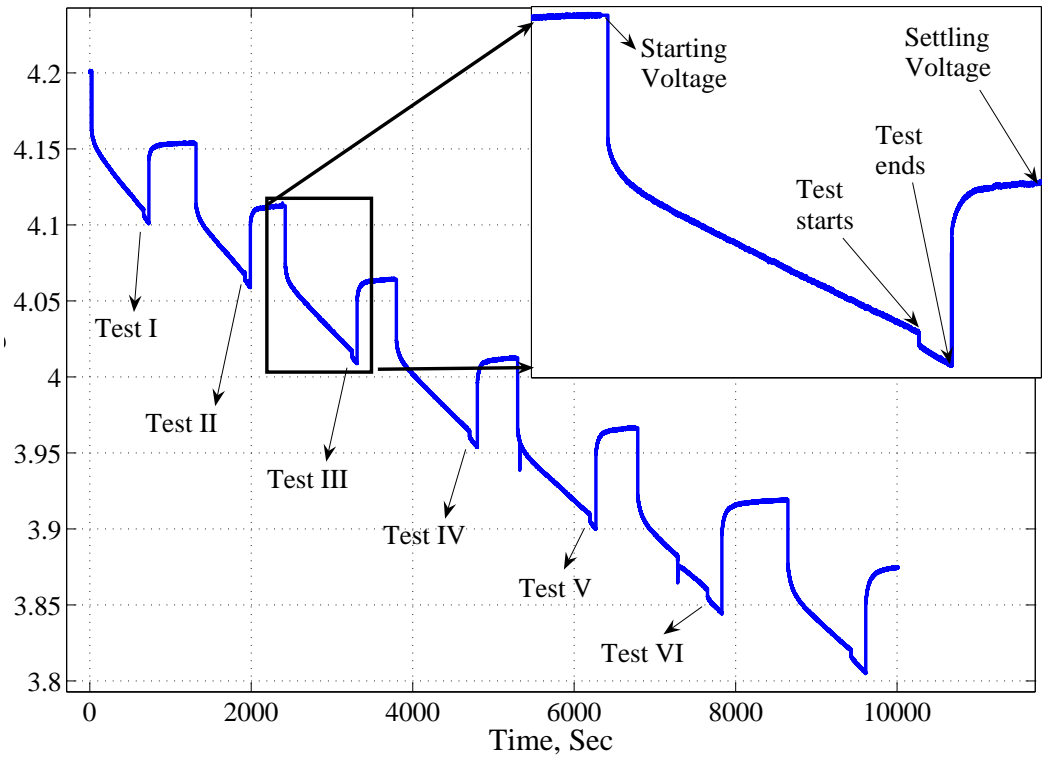
Figure 39: Various tests performed during on-off operations from a battery. The inset shows the starting, ending and settling value of the battery voltage.

### 6.3.2    UDDS Cycle Test

Second, how effectively the proposed methodology would be able to estimate SOC in a dynamic operation such as during urban dynamometer driving schedule (UDDS) cycle is studied. One cycle of UDDS is taken as the sample driving speed from supposedly an electric vehicle for urban driving conditions [71]. Performing simulation on an electric vehicle model presented in [72], the simulated power drawn by the battery pack is shown in Fig. 41.

Approximating the continuous change in the current profile from the Fig. 41 and neglecting the negative current, an equivalent dynamic current profile is generated
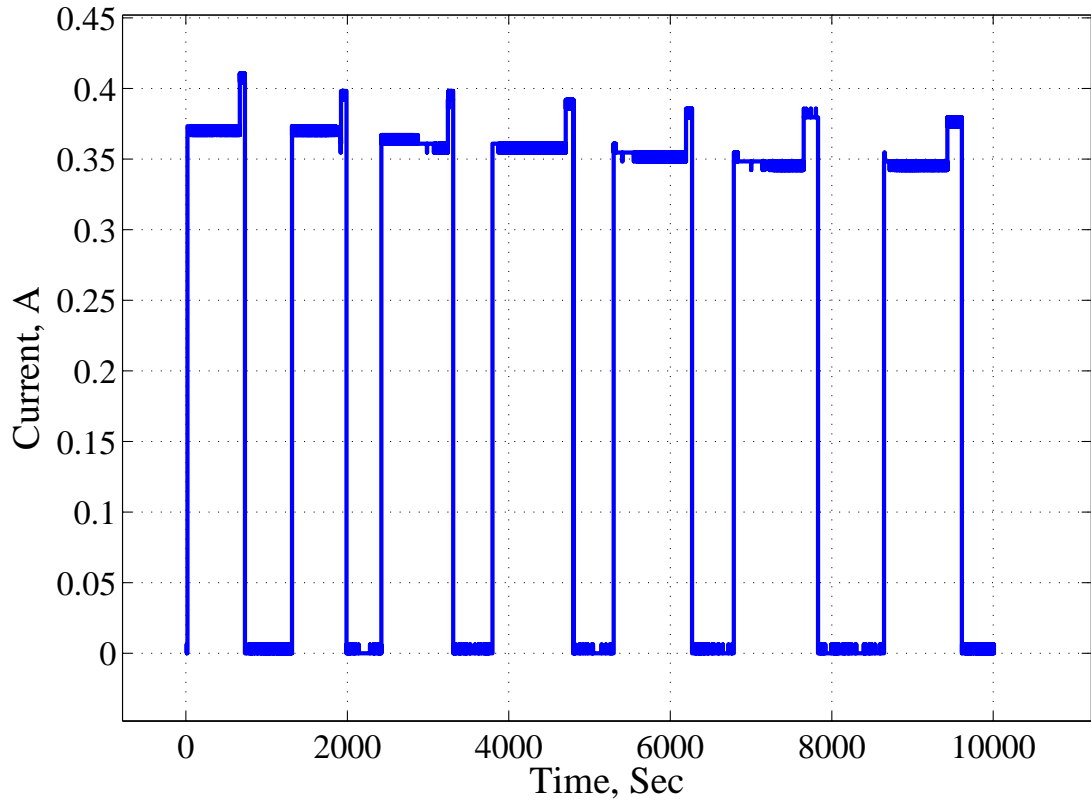
Figure 40: The current discharge profiles for the validation tests in Fig. 39.

as shown in Fig. 42. The profile is an approximation of the current discharge that may occur during UDDS cycle, and is not the exact result from a live test. Using the sample current profile from the Fig. 42, a discharged is performed from a nominal 3.6 V Li-ion cell during which several tests are performed as shown in Fig. 43. After extracting voltage and current data for each test, a nonlinear least square estimation is performed to extract the parameters and subsequently open-circuit voltages are estimated. The results are shown in Table 4 in which the estimated voltage and SOC is compared with the calculated SOC and its corresponding open-circuit voltage by the current integration method. The close matches in the open-circuit voltages show the effectiveness of the proposed methodology.
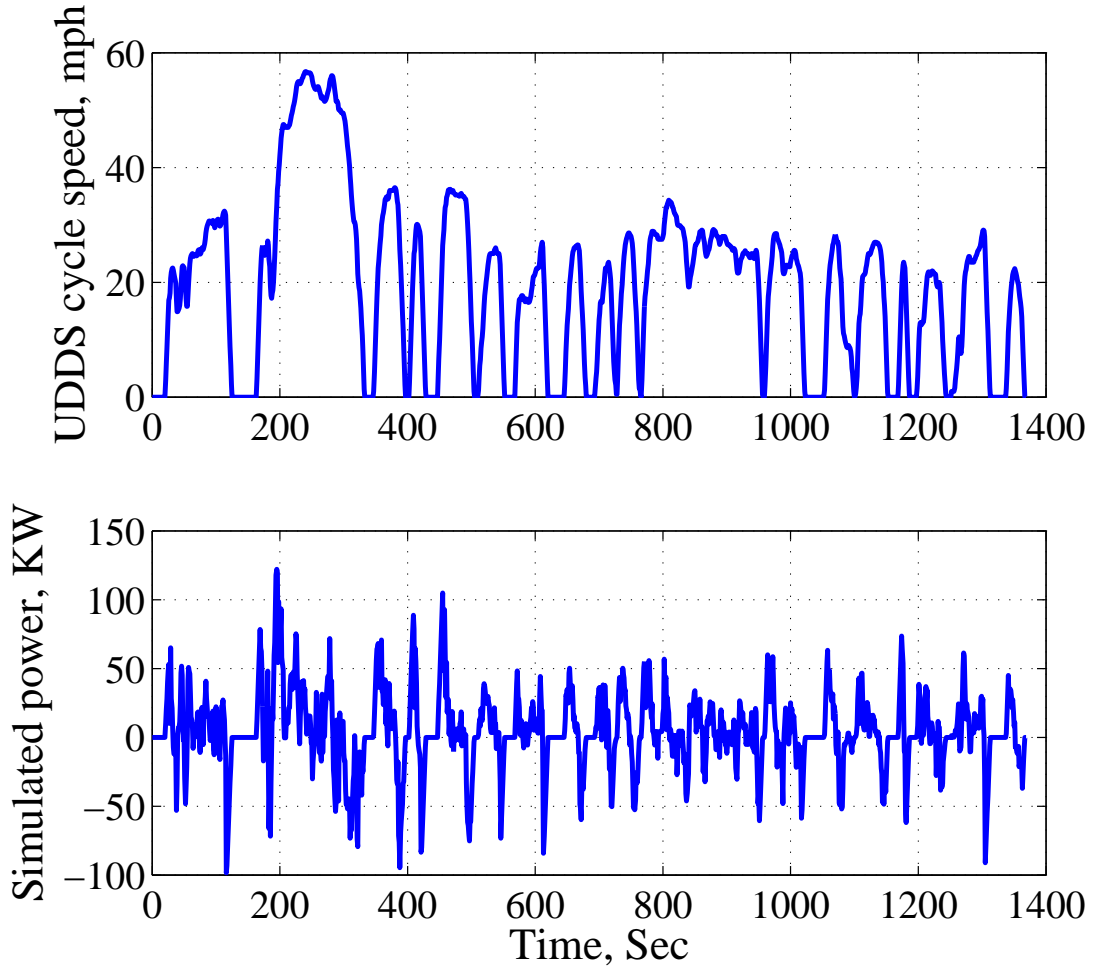
Figure 41: The speed vs. power profile for UDDS cycle. Top trace: The speed from a UDDS cycle driving. Bottom trace: The simulated power drawn from a battery pack for an electric vehicle model.

Table 4: Validation Tests for the Simulated Current Profile for a UDDS Cycle

| Test No. | $v_B(0)$ | $\hat{V}_{INT}$ | $\hat{SOC}$ | $SOC_{Calculated}$ | Error |
|----------|----------|-----------------|-------------|--------------------|-------|
| Test I | 4.0101 V | 4.0147 V | 87.8 % | 88.19 % | 0.34 % |
| Test II | 4.0091 V | 4.0131 V | 87.7 % | 88.06 % | 0.41 % |
| Test III | 4.0078 V | 4.0101 V | 87.5 % | 87.96 % | 0.52 % |
| Test IV | 4.0000 V | 4.0061 V | 87.2 % | 87.6 % | 0.46 % |
| Test V | 3.9992 V | 4.0042 V | 87.0 % | 87.46 % | 0.45 % |

### 6.3.3    Analysis of SOC Estimation Based on Temperature

Experiments are performed upon the same lithium-ion battery at two different tem-

peratures of 22°C and 40°C to observe the effectiveness of the proposed methodology
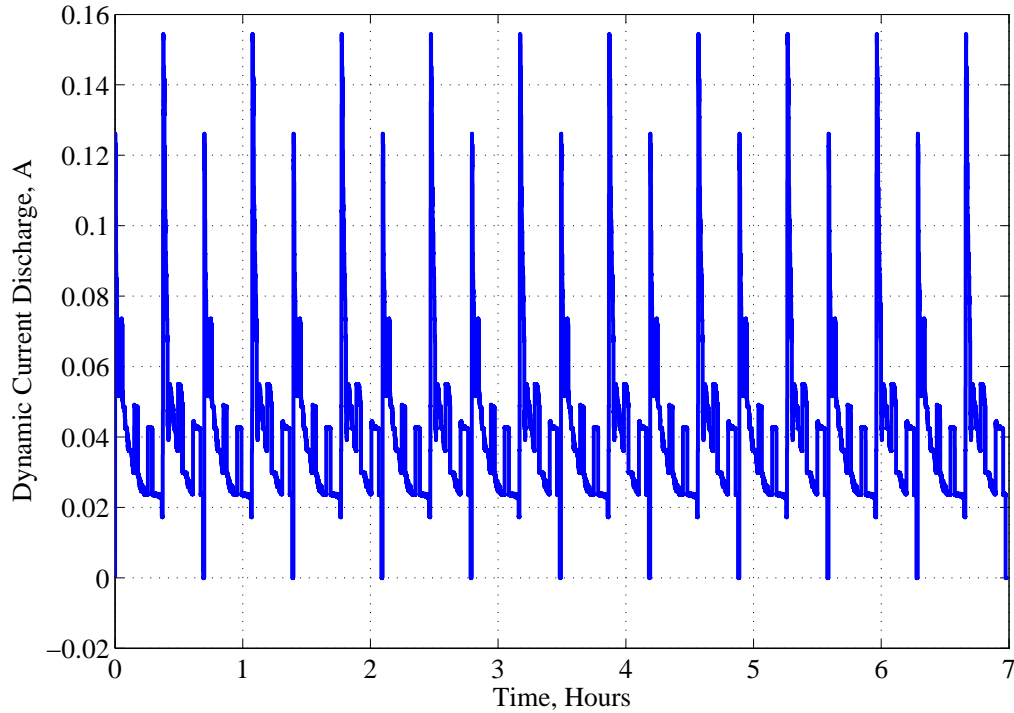
Figure 42: The simulated dynamic current profile per cell for the UDDS drive cycle.

for the estimation of SOC. Table 5 and Table 6 present the results of several tests taken at 22°C and 40°C respectively. The temperature for the tests in Table 6 are kept constant by the use of a temperature control chamber. Note the small percentage error in the SOC estimation at the largely different temperatures, showing the effectiveness of the proposed methodology at varying temperatures. The correlation measures between the SOC and the open-circuit voltage are used from the table in Appendix C. However, note the difference between the parameter values for almost same SOC level at the two different temperatures. The information can be further exploited for the SOH analysis.

It is a known fact that the impedance parameters and open-circuit voltage of a battery is highly susceptible to external factors such as temperature, discharge rate,
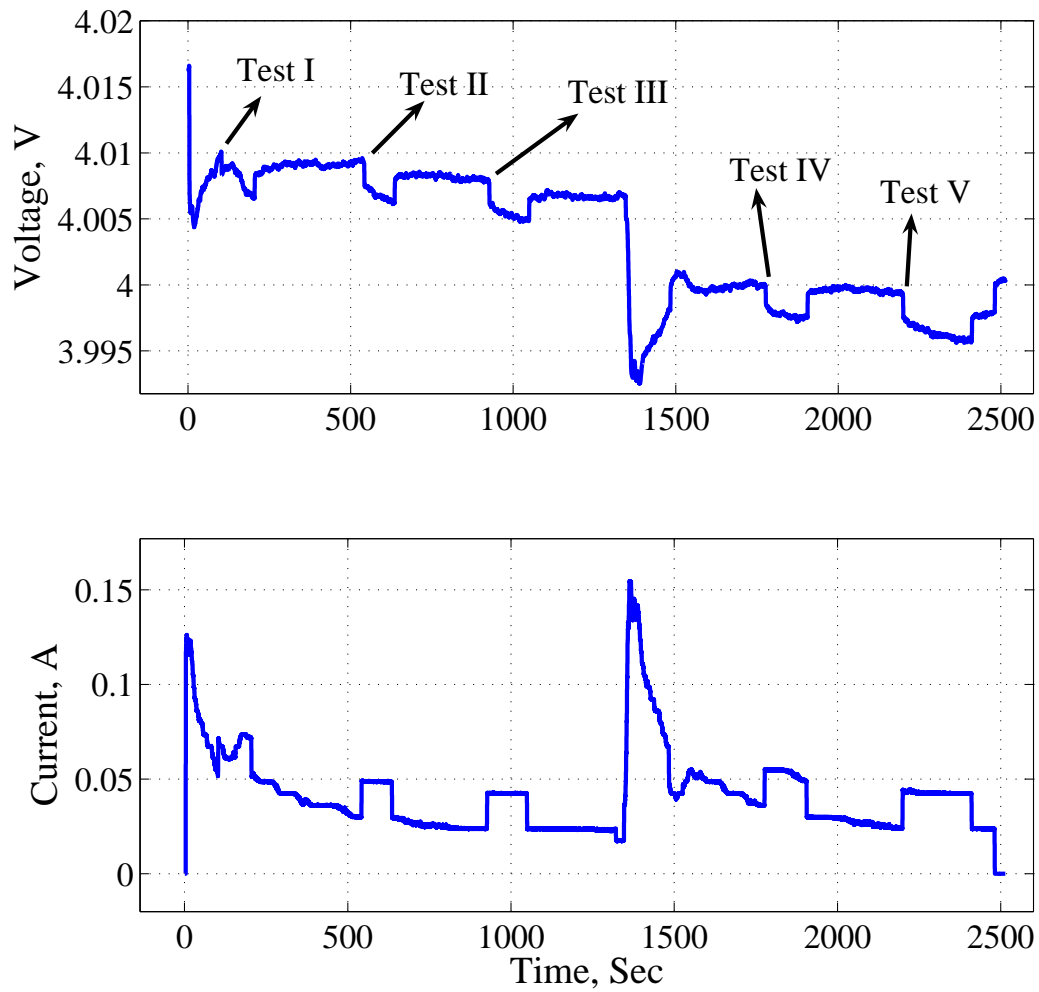
Figure 43: Discharge curve for the simulated current profile for UDDS drive cycle. Several tests are performed. The proposed methodology is used to estimate the open-circuit voltage of the battery. Top trace: The voltage drawn from the battery. Bottom trace: The corresponding current profile from the cell.

aging, and other environmental and structure-based factors. Hence the values of parameters at two different temperatures may be different, and that might give the basis for SOH analysis. In order to study this point, estimations are performed at two different temperatures and the difference in the values of the parameters are studied. The tests are taken one after another immediately so that the SOC level of the battery

Table 5: Experimental Results at 22°C Temperature

| Test No. | $v_B(0)$ | $\hat{V}_{INT}$ | $S\hat{O}C$ | $V_{INT,Calculated}$ | (%) Error |
|----------|----------|-----------------|-------------|----------------------|-----------|
| Test I | 4.0503 V | 4.1833 V | 99.50 % | 4.1675 V | 0.38 % |
| Test II | 3.8845 V | 4.0340 V | 89.50 % | 3.9995 V | 0.86 % |
| Test III | 3.7348 V | 3.8863 V | 77.50 % | 3.8515 V | 0.90 % |
| Test IV | 3.6234 V | 3.7687 V | 65.50 % | 3.7355 V | 0.90 % |
| Test V | 3.5308 V | 3.6557 V | 53.50 % | 3.6335 V | 0.61 % |
| Test VI | 3.3194 V | 3.444 V | 12.75 % | 3.4384 V | 0.16 % |
| Test VII | 2.9386 V | 3.245 V | 1.75 % | 3.279 V | 1.03 % |

Table 6: Experimental Results at 40°C Temperature

| Test No. | $v_B(0)$ | $\hat{V}_{INT}$ | $S\hat{O}C$ | $V_{INT,Calculated}$ | (%) Error |
|----------|----------|-----------------|-------------|----------------------|-----------|
| Test I | 4.0170 V | 4.212 V | 100 % | 4.179 V | 0.79 % |
| Test II | 3.8435 V | 4.0455 V | 94.50 % | 4.0085 V | 0.92 % |
| Test III | 3.7211 V | 3.9238 V | 84.50 % | 3.8835 V | 1.13 % |
| Test IV | 3.6191 V | 3.8244 V | 74.50 % | 3.7881 V | 0.95 % |
| Test V | 3.5281 V | 3.7298 V | 63.50 % | 3.6969 V | 0.89 % |
| Test VI | 3.4405 V | 3.6034 V | 46.50 % | 3.5948 V | 0.24 % |
| Test VII | 3.2407 V | 3.3963 V | 9.50 % | 3.3913 V | 0.15 % |

does not change. A test is performed at 24°C room temperature, and immediately after the first test, a second test is performed inside a controlled temperature chamber of 40°C. The results obtained are shown in Table 7. Note the difference in almost all the parameters value despite the same SOC level.

Table 7: Parameters Values for Tests at 24°C and 40°C at a Constant SOC

| Parameters | At 24°C | At 40°C |
|------------|---------|---------|
| $\hat{R}_1$ | 0.0725 Ω | 0.0780 Ω |
| $\hat{R}_2$ | 0.8937 Ω | 0.5145 Ω |
| $\widehat{R_2C}$ | 110.36 Sec | 107.64 Sec |
| $\hat{V}_{INT}$ | 4.0791 V | 4.0124 V |

## 6.4    Summary

This chapter has summarized the results of parameter extractions and the state estimation of open-circuit voltage of a battery. In this methodology, a non-intrusive test

signal is superimposed on the battery load which triggers transient dynamics inside the battery. The resulting terminal voltage and current are measured and the estimation is done in two parts. First, a non-linear least-squares routine is used to estimate the lumped electrical parameters of the battery model. Second, a $H_\infty$ filter is used to estimate the open-circuit voltage as a dynamic state variable which compensates for its non-linear nature and the uncertainty in the battery model. Experimental results obtained at consistent temperatures demonstrate that the open-circuit voltage and parameter values together can combine to provide state-of-charge and state-of-health measurements.

CHAPTER 7: CONCLUSIONS

Unique challenges of a battery monitoring method are to estimate SOC and SOH accurately in dynamic operating conditions. Such conditions may be cases like the battery is charged, is discharged, has varying charge/discharge rates, is turned-off and turned-on immediately etc. Moreover, characteristics of a battery depend upon temperature, aging, gassing, electrode structures etc. Any monitoring method is still required to provide SOC and SOH despite the battery conditions. Such requirement is a challenge for any methodology unless it is made bulky and computationally expensive. For estimation of SOC and SOH, a thorough analysis of battery kinetics in different operating conditions posits the following key points:

- Open-circuit voltage of a battery is directly proportional to SOC. Any monitoring method has to estimate it dynamically and then the value of SOC can be regressed with available data based on temperature, aging, and charge/discharge conditions. The open-circuit voltage $V_{INT}$ is a dynamic state variable, and estimating it adaptively should be a key target for an effective assessment.

- A robust method to estimate parameters of a battery model can establish a basis for SOH quantitative analysis. Any such method should use easily available data such as voltage and current from a simple load and converges parameters to the global minimum. Comparing parameters from one good cell to those of bad

ones and similarly based on other factors, SOH analysis can be done.

This thesis accomplish the above objectives by presenting an integrated methodology combining a simplified battery model, a transient-based parameter extraction process and adaptive estimation of open-circuit voltage dynamically. The methodology presented in this thesis is done on both lead-acid and lithium-ion battery chemistries with simple battery loads like automobile head lamp, and heater.

## 7.1    Conclusions

The thesis accomplishes the following key tasks.

- A detailed investigation into chemical kinetics of a battery and its equivalent electrical models is done  [68]. The objective of an equivalent lumped circuit is to model the electrochemical behavior of a battery in such a way that its qualitative analysis can be done easily. However, it is difficult to represent entire dynamics exhibited by battery by equivalent electric circuits because of its complex, nonlinear, non-stationary, time-variant and temperature dependent behavior. By approximating most of the dynamics especially in the range of frequency interests, a simplified battery model is presented. The trade-off involved in presenting such a model is among battery discharge/charge characteristics, its transient and steady-state behavior, and an electrical circuit with fewer resistors and capacitors so that it is easy to understand the battery behavior with minimal components. The model is supported by the conventional method of electrochemical impedance spectroscopy.

- A transient based approach to estimation of parameters of equivalent electrical

circuit of a battery model is presented [68, 73]. The method exploits the fact that the battery shows transient dynamics when a load is turned on. This information in the form of voltage and current data is used to estimate parameters of a lumped equivalent electrical model. A non-linear estimation algorithm in the form of Gauss-Newton method with linearization approach is used in this thesis [59]. The method makes sure that the non-linear estimation does not fall into local minima which is an issue with such method. By simulating the residual error by a Taylor-series expansion, the method takes advantage of the fact that the parameters of a non-linear problem are mostly embedded into low order coefficients and hence can be linearized for a small interval. Such arrangement makes sure the optimization achieves the global minimum and runs it repeatedly for entire range of data. Parameters obtained by this method varies with respect to state-of-charge (SOC) of a battery. This could also establish a basis for state-of-health SOH measurements.

- Estimation of a state variable by $H_\infty$ filter is done for dynamic estimation of open-circuit voltage of the battery model. In this procedure, a non-intrusive test signal is superimposed on the battery load which triggers transient dynamics inside the battery. The resulting terminal voltage and current are measured and a non-linear least-squares routine is used to estimate the lumped electrical parameters of the battery model. These parameters along with input data are subsequently sent to a $H_\infty$ filter algorithm to obtain the open-circuit voltage $V_{INT}$. This method is especially suitable as it compensates for the non-linear nature of the open-circuit voltage and the uncertainty in the battery model.

The estimated $V_{INT}$ could form a basis for estimation of SOC in real time.

## 7.2    Directions for Future Work

The directions of future work can go in several ways.

- An automated system comprising of data collection module, nonlinear estimation of parameters, and open-circuit voltage estimation and thereby measure of SOC and SOH can be done.

- Estimation of parameters and open-circuit voltage can be performed for live data from currently available electric vehicles such as Chevy Volt.

- A detailed analysis of battery parameters with respect to temperature, aging, and discharge rates can be done.

- A calibrated SOC vs open-circuit voltage with respect to aging of the battery can be prepared.

- The methodology can be tested for various battery chemistries in varying sizes.

REFERENCES

[1] "The battery market will charge ahead; $[online : http : //www.businessweek.com/lifestyle/content/jul2009/bw2009072 - 953040.htm]$," July 2009.

[2] "Google uncloaks once-secret server; $[online : http : //news.cnet.com/8301 - 1001 - 3 - 10209580 - 92.html]$," April 2009.

[3] "Sony says recall strains battery production; $[online : http : //www.nytimes.com/2006/10/25/technology/25sony.html]$," October 2006.

[4] E. Meissner and G. Richter, "Battery monitoring and electrical energy management precondition for future vehicle electric power systems," *Journal of Power Sources*, vol. 116, pp. 79–98, 2003.

[5] M. Cugnet, J. Sabatier, S. Laruelle, S. Grugeon, B. Sahut, A. Oustaloup, and J. Tarascon, "On lead-acid-battery resistance and cranking-capability estimation," *IEEE Transactions on Industrial Electronics*, vol. 57, pp. 909–917, 2010.

[6] S. M. Lukic, J. Cao, R. C. Bansal, F. Rodriguez, and A. Emadi, "Energy storage systems for automative applications," *IEEE Transactions on Industrial Electronics*, vol. 55, pp. 2258–2267, 2008.

[7] S. Piller, M. Perrin, and A. Jossen, "Methods for state-of-charge determination and their applications," *Journal of Power Sources*, vol. 96, pp. 113–120, 2001.

[8] J. D. Kozlowski, "Electrochemical cell prognostics using online impedance measurements and model-based data fusion techniques," in *Proc. IEEE Aerospace Conference*, vol. 7, pp. 3257–3270, 2003.

[9] F. Huet, "A review of impedance measurements for determination of the state-of-charge or state-of-health of secondary batteries," *Journal of Power Sources*, vol. 70, pp. 59–69, 1998.

[10] "Ieee recommended practice for maintenance, testing, and replacement of large lead storage batteries for generating stations and substations 450, 1987.." IEEE Std. 450, Auguest 1987.

[11] K. Floyd, J. Noworolski, and W. Sokolski, "Assessment of lead-acid battery state of charge by monitoring float charging current," in *Proc. of 16th Int. Tele. Energy Conf.*, pp. 602–608, 1994.

[12] D. Linden and T. B Reddy, *Handbook of Batteries*. New York: McGraw-Hill, 2001.

[13] E. Karden, S. Buller, and R. W. D. Doncker, "A method for measurement and interpretation of impedance spectra for industrial batteries," *Journal of Power Sources*, vol. 85, pp. 72–78, 2000.

[14] R. S. Robinson, "Online battery testing: a reliable method for determining battery health?," in *IEEE Telecommunication Energy Conference*, pp. 654–661, 1996.

[15] E. Karden, S. Buller, and R. W. D. Doncker, "A frequency-domain approach to dynamical modeling of electrochemical power sources," *Journal of Power Sources*, vol. 47, pp. 2247–2356, 2002.

[16] P. Mauracher and E. Karden, "Dynamic modelling of lead/acid batteries using impedance spectroscopy for parameter identification," *Journal of Power Sources*, vol. 67, pp. 69–84, 1997.

[17] M. Hughes, R. T. Barton, S. A. G. R. Karunathilaka, and N. A. Hampson, "The residual capacity estimation of fully sealed 25 ah lead/acid cells," *Journal of Power Sources*, vol. 17, pp. 305–329, 1986.

[18] M. L. Gopikanth and S. Sathyanarayana, "Impedance parameters and the state-of-charge. ii. lead-acid battery," *Journal of Applied Electrochemistry*, vol. 9, pp. 369–379, 1979.

[19] M. Hughes, R. T. Barton, S. A. G. R. Karunathilaka, and N. A. Hampson, "The estimation of the residual capacity of sealed lead-acid cells using the impedance technique," *Journal of Applied Electrochemistry*, vol. 16, pp. 555–564, 1986.

[20] L. Ran, W. Haiying, and L. Gechen, "Prediction of state of charge of lithium-ion rechargeable battery with electrochemical impedance spectroscopy theory," in *IEEE Conference on Industrial Electronics and Applications*, pp. 684–688, 2010.

[21] S. Rodrigues, N. Munichandraiah, and A. K. Shukla, "A review of state-of-charge indication of batteries by means of a.c. impedance measurements," *Journal of Power Sources*, vol. 87, pp. 12–20, 2000.

[22] M. Keddam, Z. Stoynov, and H. Takenouti, "Impedance measurement on pb/h2so4 batteries," *Journal of Applied Electrochemistry*, vol. 7, pp. 539–544, 1977.

[23] R. T. Barton and P. J. Mitchell, "Estimation of the residual capacity of maintenance-free lead-acid batteries. part 1. identification of a parameter for the prediction of state-of-charge," *Journal of Power Sources*, vol. 27, pp. 287–295, 1989.

[24] V. V. Viswanathan, A. J. Salkind, J. J. Kelley, and J. B. Ockerman, "Effect of state of charge on impedance spectrum of sealed cells part ii: Lead acid batteries," *Journal of Applied Electrochemistry*, vol. 25, pp. 729–739, 1995.

[25] A. J. Salkind, P. Singh, A. Cannone, T. Atwater, X. Wang, and D. Reisner, "Impedance modeling of intermediate size lead-acid batteries," *Journal of Power Sources*, vol. 116, pp. 174–184, 2003.

[26] B. Hariprakash, S. K. Martha, A. Jaikumar, and A. K. Shukla, "On-line monitoring of lead-acid batteries by galvanostatic non-destructive technique," *Journal of Power Sources*, vol. 137, pp. 128–133, 2004.

[27] H. Blanke, O. Bohlem, S. Buller, R.W.D. Doncker, B. Fricke, A. Hammouche, D. Linzen, M. Thele, and D. U. Sauer, "Impedance measurements on lead-acid batteries for state-of-charge, state-of-health and cranking capability prognosis in electric and hybrid electric vehicles," *Journal of Power Sources*, vol. 144, pp. 418–425, 2005.

[28] M. Ceraolo and G. Pede, "Techniques for estimating the residual range of an electric vehicle," *IEEE Transactions on Vehicular Technology*, vol. 50, pp. 109–115, 2001.

[29] S. Pang, J. Farrell, J. Du, and M. Barth, "Battery state-of-charge estimation," in *Proceedings American Control Conference*, vol. 2, pp. 1644–1649, June 2001.

[30] D. J. Deepti and V. Ramanarayanan, "State of charge of lead acid battery," in *IEEE Conference on Power Electronics*, pp. 89–93, 2006.

[31] O. Caumont, P. L. Moigne, C. Rombaut, X. Muneret, and P. Lenain, "Energy gauge for lead-acid batteries in electric vehicles," *IEEE Transactions on Energy Conversion*, vol. 15, pp. 354–360, 2000.

[32] B. S. Bhangu, P. Bentley, D. A. Stone, and C. M. Binghamr, "Nonlinear observers for predicting state-of-charge and state-of-health of lead-acid batteries for hybrid-electric vehicles," *IEEE Transaction on Vehicular Technology*, vol. 54, pp. 783–794, 2005.

[33] J. Chiasson and B. Vairamohan, "Estimating the state of charge of a battery," *IEEE Transactions on Control Systems Technology*, vol. 3, pp. 465–470, 13.

[34] M. Knauff, C. Dafis, and D. Niebur, "A new battery model for use with an extended kalman filter state of charge estimator," in *American Control Conference*, pp. 1991–1996, 2010.

[35] R. Klein, N. A. Chaturvedi, J. Christensen, J. Ahmed, R. Findeisen, and A. Kojic, "State estimation of a reduced electrochemical model of a lithium-ion battery," in *American Control Conference*, pp. 6618–6623, 2010.

[36] M. Charkhgard and M. Farrokhi, "State-of-charge estimation for lithium-ion batteries using neural networks and ekf," *IEEE Transactions on Industrial Electronics*, vol. 57, pp. 4178–4187, 2010.

[37] D. V. Do, C. Forgez, K. e. Benkara, and G. Friedrich, "Impedance observer for a li-ion battery using kalman filter," *IEEE Transactions on Vehicular Techonology*, vol. 58, pp. 3930–3937, 2009.

[38] D. Simon, *Optimal State Estimation.* New York: Wiley-Interscience, 2006.

[39] C. S. C. Bose and F. C. Laman, "Battery state of health estimation through coup de fouet," in *IEEE Telecommunication Energy Conference*, pp. 597–601, 2000.

[40] P. E. Pascoe and A. H. Anbuky, "Vrla battery capacity estimation using soft computing analysis of the coup de fouet region," in *IEEE Telecommunication Energy Conference*, pp. 589–596, 2000.

[41] S. P. Schooling, P. E. Wellstead, L. Denny, and J. Edmonds, "The use of system identification technology in the development of a battery test instrument a technology transfer case study," in *IEEE International Conference on Control Applications*, pp. 791–796, 2000.

[42] D. H. J. Baert and A. A. K. Varvaet, "A new method for the measurment of the double layer capacitance for the estimation of battery capacity," in *IEEE Telecummunication Energy Conference*, pp. 733–738, Oct. 2003.

[43] P. E. Pascoe and A. H. Anbuky, "Vrla battery discharge reserve time estimation," *IEEE Transactions on Power Electronics*, vol. 19, pp. 1515–1522, 2004.

[44] P. Rong and M. Pedram, "An analytical model for predicting the remaining battery capacity of lithium-ion batteries," *IEEE Transactions on Very Large Scale Integration (VLSI) Systems*, vol. 14, pp. 441–451, 2006.

[45] I. Snihir, W. Rey, E. Verbitskiy, A. Belfdhel-Ayeb, and P. H. L. Notten, "Battery open-circuit voltage estimation by a method of statistical analysis," *Journal of Power Sources*, vol. 159, pp. 1484–1487, 2006.

[46] M. Coleman, C. B. Zhu, C. K. Lee, and W. G. Hurley, "A combined soc estimation method under varied ambient temperature for a lead-acid battery," in *IEEE Applied Power Electronics Conference and Exposition*, pp. 991–997, 2005.

[47] M. Coleman, C. K. Lee, C. Zhu, and W.G. Hurley, "State-of-charge determination from emf voltage estimation: using impedance, terminal voltage, and current for lead-acid and lithium-ion batteries," *IEEE Transactions on Industrial Electronics*, vol. 54, pp. 2550–2557, 2007.

[48] M. Ragsdale, J. Brunet, and B. Fahimi, "A novel battery identification method based on pattern recognition," in *IEEE Vehicle Power and Propulsion Conference*, pp. 1–6, 2008.

[49] A. Szumanowski and Y. Chang, "Battery management system based on battery nonlinear dynamics modeling," *IEEE Transactions on Vehicular Technology*, vol. 57, pp. 1425–1432, 2008.

[50] A. Banaei, A. Khoobroo, and B. Fahimi, "Online detection of terminal voltage in li-ion batteries via battery impulse response," in *IEEE Vehicle Power and Propulsion Conference*, pp. 194–198, 2009.

[51] S. Tian and M. Ouyang, "An experimental study and nonlinear modeling of discharge i-v behavior of valve-regulated lead-acid batteries," *IEEE Transactions on Energy Conversion*, vol. 24, pp. 452–458, 2009.

[52] V. Agarwal, K. Uthaichana, R. A. DeCarlo, and L. H. Tsoukalas, "Development and validation of a battery model useful for discharging and charging power control and lifetime estimation," *IEEE Transactions on Energy Conversion*, vol. 25, pp. 821–835, 2010.

[53] B. Saha, S. Poll, K. Goebel, and J. Christophersen, "An integrated approach to battery health monitoring using bayesian regression and state estimation," in *IEEE Autotestcon*, pp. 646–653, 2007.

[54] S. Saha, B. Saha, A. Saxena, and K. Goebel, "Distributed prognostic health management with gaussian process regression," in *IEEE Aerospace Conference*, pp. 1–8, 2010.

[55] F. Rufus Jr., S. Lee, and A. Thakker, "Health monitoring algorithms for space application batteries," in *IEEE International Conference on Prognostics and Health Management*, pp. 1–8, 2008.

[56] L. Gao, S. Liu, and R. A. Dougal, "Dynamic lithium-ion battery model for system simulation," in *IEEE Trans. on Components and Packaging Technology*, vol. 125, pp. 495–505, 2002.

[57] J. S. Newman, *Electrochemical Systems.* New York: Prentice-Hill, 1991.

[58] S. Shaw, *System identification and modeling for nonintrusive load diagnostics.* PhD thesis, Massachusetts Institute of Technology, Cambridge, MA, 2000.

[59] S. R. Shaw and C. R. Laughman, "A method for nonlinear least squares with structured residuals," *IEEE Transactions on Automatic Control*, vol. 51, pp. 1704–1708, 2006.

[60] D. Domenico, G. Fiengo, and A. Stefanopoulou, "Lithium-ion battery state of charge estimation with a kalman filter based on a electrochemical model," in *IEEE Intl. Conf. on Control Applications*, pp. 702–707, 2008.

[61] G. L. Plett, "Extended kalman filter for battery management systems of lipb-based hev battery packs part 2. modeling and identification," *Journal of Power Sources*, vol. 134, pp. 262–276, 2004.

[62] H. He, R. Xiong, X. Zhang, F. Sun, and J. X. Fan, "State-of-charge estimation of the lithium-ion battery using an adaptive extended kalman filter based on an improved thevenin model," *IEEE Transactions on Vehicular Technology*, vol. 60, pp. 1461–1469, 2011.

[63] M. Charkhgard and M. Farrokhi, "State-of-charge estimation for lithium-ion batteries using neural networks and ekf," *IEEE Transactions on Industrial Electronics*, vol. 57, pp. 4178–4187, 2010.

[64] G. L. Plett, "Extended kalman filter for battery management systems of lipb-based hev battery packs part 3. state and parameter estimation," *Journal of Power Sources*, vol. 134, pp. 277–292, 2004.

[65] I. Kim, "Nonlinear state of charge estimator for hybrid electric vehicle battery," *IEEE Transactions on Power Electronics*, vol. 23, pp. 2027–2034, 2008.

[66] K. A. Smith, C. D. Rahn, and C. Y. Wang, "Model-based electrochemical estimation and constraint management for pulse operation of lithium ion batteries," *IEEE Transactions on Control Systems Technology*, vol. 18, pp. 654–663, 2010.

[67] J. Yan, G. Xu, Y. Xu, and B. Xie, "Battery state-of-charge estimation based on h-infinity filter for hybrid electric vehicle," in *IEEE Intl. Conf. on Control, Automation, Robotics, and Vision*, pp. 464–469, 2008.

[68] L. P. Mandal and R. W. Cox, "A transient based approach to estimation of electrical parameters of a lead-acid battery model," in *IEEE Energy Conversion Congress Exposition*, pp. 4238–4242, 2010.

[69] "Doe advanced technology development program for lithium-ion batteries: Ineel gen 1 final report; [*online* : $http://avt.inel.gov/battery/pdf/atd-gen1final-report-10-8-01.pdf$]," July 2009.

[70] G. M. Ehrlich2002, *Handbook of Batteries*. New York: McGraw-Hill, 2002.

[71] "Epa urban dynamometer driving schedule; [*online* : $http://www.epa.gov/oms/standards/light-duty/udds.htm$]," July 2011.

[72] Y. Gao and M. Ehsani, "Design and control methodology of plug-in hybrid electric vehicles," *IEEE Transactions on Industrial Electronics*, vol. 57, pp. 633–640, 2010.

[73] L. P. Mandal and R. W. Cox, "A transient based approach for estimating the electrical parameters of a lithium-ion battery model," in *IEEE Energy Conversion Congress Exposition*, 2011.

[74] K. J. Astrom and B. Wittenmark, *Computer-Controlled Systems Theory and Design*. New York: Prentice Hall, 1997.

APPENDIX A: SAMPLING OF A CONTINUOUS-TIME SYSTEM

How to represent a continuous-time system in digital domain connected to a computer via analog-to-digital converter (ADC) and digital-to-analog converter (DAC) is an important issue. Consider a system shown in Fig. 44.
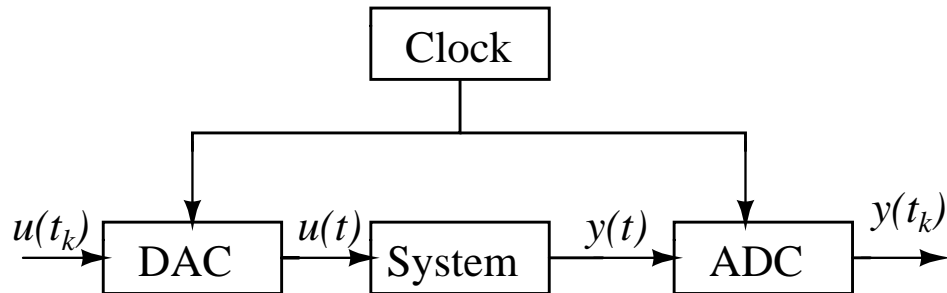


Figure 44: Block diagram of a continuous-time system connected to ADC and DAC [74].

The signals in the computer are the sequences $u(t_k)$ and $y(t_k)$. The key problem is to find the relationship between these sequences. To find the discrete-time equivalent of a continuous-time is called *sampling a continuous-time system.* To obtain desired descriptions, it is necessary to describe the converters and the system. Assume that the continuous-time system is given in the state-space by the Eq. 132.

$$\frac{dx}{dt} = Ax + Bu(t)$$
$$y(t) = Cx(t) + Du(t)$$
(132)

The above equation represents a continuous-time system in the state-space form in which the system has $r$ inputs, $p$ outputs, and is of the order $n$.

The component DAC is so constructed that it holds the analog signal constant until a new conversion is commanded. This is called *zero-order hold circuit.* At sampling

instants, $t_k$, the control changes. Because the control signal is discontinuous, it is necessary to specify its behavior at discontinuities. The convention that the signal is continuous from the right is adopted. The control signal is thus represented by the sampled signal $\{u(t_k) : k = ...., -1, 0, 1, ....\}$. Given the state at the sampling time $t_k$, the state as some future time $t$ is obtained by solving the Eq. 132. The state at time $t$, where $t_k \leq t \leq t_{k+1}$ is thus given by Eq. 133.

$$
\begin{aligned}
x(t) &= e^{A(t-t_k)}x(t_k) + \int_{t_k}^{t} e^{A(t-s')}Bu(s')ds' \\
&= e^{A(t-t_k)}x(t_k) + \int_{t_k}^{t} e^{A(t-s')}Bds'u(t_k) \\
&= e^{A(t-t_k)}x(t_k) + \int_{0}^{t-t_k} e^{As}dsBu(t_k) \\
&= \Phi(t,t_k)x(t_k) + \Gamma(t,t_k)u(t_k)
\end{aligned}
\tag{133}
$$

The second equality follows because $u$ is constant between the sampling instants. The state vector at time $t$ is thus a linear function of $x(t_k)$ and $u(t_k)$. If the ADC and DAC in Fig. 44 is perfectly synchronized and if the conversion times are negligible, the input $u$ and the output $y$ can be regarded as being sampled at the same instants.The system equation of the sampled system at the sampling instants is then

$$
\begin{aligned}
x(t_{k+1}) &= \phi(t_{k+1},t_k)x(t_k) + \Gamma(t_{k+1},t_k)u(t_k) \\
y(t_k) &= Cx(t_k) + Du(t_k)
\end{aligned}
\tag{134}
$$

where $\Phi(t_{k+1},t_k) = e^{A(t_{k+1}-t_k)}$ and $\Gamma(t_{k+1},t_k) = \int_{0}^{t_{k+1}-t_k} e^{As}dsB$.

The relationship between the sampled signals thus can be expressed by the linear difference equation of Eq. 134 and it does not involve any approximations. It gives the exact values of the state variables and the output at the sampling instants. The

model in Eq. 134 is therefore called a zero-order-hold sampling of the system in Eq. 132.

For periodic sampling with period $T$, we have $t_k = kT$ and the model of Eq. 134 simplifies to the time invariant system

$$x(kT + T) = \Phi \ x(kT) + \Gamma \ u(kT)$$
$$y(kT) = C \ x(kT) + D \ u(kT)$$

(135)

where $\Phi = e^{AT}$ and $\Gamma = \int_0^T e^{As}ds B$.

For example, consider a first-order system of state equation of the form

$$\frac{dx}{dt} = \alpha x + \beta u$$

(136)

with $\alpha \neq 0$. Applying Eq. 134, we get $\Phi = e^{\alpha T}$ and $\Gamma = \int_0^T e^{\alpha s}ds \beta = \frac{\beta}{\alpha}(e^{\alpha T} - 1)$. The sampled system thus becomes

$$x(kT + T) = e^{\alpha T}(kT) + \frac{\beta}{\alpha}(e^{\alpha T} - 1)u(kT).$$

(137)

The above relationship can be used to convert a continuous-time system into the equivalent discrete-time system.

APPENDIX B: MATLAB CODE


B.1: Conversion.m

% The following module converts the raw input data into prepared data.

```
x = load('test10');

n = length(x);

delvol = 2.5 *2/power(2,12);

delcur = 0.625 *2/power(2,12);

deltemp = 1.25 * 2/power(2,12);

deldiffvol = 0.625*2/power(2,12);

vol = -2.5 + delvol * x(:,1);

cur = -0.625 + delcur * x(:,2);

temp = -1.25 + deltemp * x(:,3);

surgvol = -0.625 + deldiffvol * x(:,4);

%for voltage signal SecCurrent = vol/100;

PriCurrent = SecCurrent/2.5;

SensedVoltage = PriCurrent * 1438;

% for current signal SecCur = cur/98.1;

SensedCurrent = SecCur * 1000;

% for temperature rating SensedTemp = temp/0.01; % for surge voltage DiffVoltage

= surgvol/4.03; % Gain of diff. amplifier is 4.03

SecSurgeVoltage = DiffVoltage/2; % Gain of op amp is 2

SecCurrent = SecSurgeVoltage/100;
```

PriCurrent = SecCurrent/2.5;

SurgeVoltage = PriCurrent * 1438;

%for plotting with respect to time fsampling = 100;

t = [0:1:length(x)-1];

t = t * 1/fsampling; % in second

subplot(4,1,1);

plot(t,SensedVoltage),ylabel('Voltage,V'),xlabel('Time,Sec'),title('Channel 1')

subplot(4,1,2);

plot(t,SensedCurrent),ylabel('Current,A'),xlabel('Time,Sec'),title('Channel 2')

subplot(4,1,3);

plot(t,SensedTemp),ylabel('Temp,Celcius'),xlabel('in second'),title('Channel 3')

subplot(4,1,4);

plot(t,SurgeVoltage),ylabel('Voltage,V'),xlabel('Time,Sec'),title('Channel 4')

## B.2: Chrismethod.m

% Module for nonlinear least-square estimation

if (exist('v') == 0)

load v.mat;

end

if (exist('t') == 0)

load t.mat;

end

if (exist('i') == 0)

```
load i.mat;

end

N = length(v);

%the pre-estimate of parameters are as follow:

Mu = [0.0073;0.0143;0.0704];

K = 1; Kvec = [];iter = [];

mu = Mu;

while(K¡N)

yhat = battery-model(mu,t,N,zeros(size(t)),i);

interval = findk(v(K:N),yhat(K:N),0.2);

K = min([N K+interval]);

Kvec = [Kvec; K];

mu = GNL('battery-model',mu,t,K,v,i);

end
```

<div align="center">B.3: battery-model.m</div>

```
% Module for giving residual vector

function err = battery-model(mu,t,N,v,i)

t = t(1:N);

v = v(1:N);

i = i(1:N);

Vc = diff45(mu,N,t,i);

R1 = mu(3);

Vb0 = 3.9397; % The starting value of Vb0 for the given estimation problem
```

yhat = ( 3.9397 - Vc - i* R1);

err = (yhat - v);

## B.4: diff45.m

% Module for sending right data for solving differential equations.

function Y = diff45(mu,N,it,i)

Tspan = it;

Vc0 = 0;

$[T, Y]$ = ode45(@(t,y) myode(t,y,it,i,mu),Tspan,Vc0);

## B.5: myode.m

% Module solving the differential equations

function dydt = myode(t,y,it,i,mu)

alp1 = mu(1);

alp2 = mu(2);

f = interp1(it,i,t);

dydt = alp1* f - y* alp2;

## B.6: GNL.m

% Module for Gauss-Newton update

function $[theta]$ = GNL(theta0,t,k,v,i)

theta = theta0;

% limiting tolerances

xtol = 1e-4;

ftol = 1e-4;

```
gtol = eps;

maxiter = 100*length(theta);

% initializing stuff

fvec = feval(f,theta,varargin:);

oldnorm = norm(fvec);

info = ' ';

iter = 0;

while(info==' ')

[fjac, fvec] = fdjac2(theta,t,k,v,i);

fjac = [fjac; .1 * eye(length(theta))];

fvec = [fvec; .1 * (theta(:) - theta0(:))];

iter = iter + 1;

[u, s, v] = svd(fjac,0);

utf = u'* fvec;

% eliminates the almost zero singular values

s = diag(diag(s) .* ( 1 - ( diag(s)¡ sqrt(eps))));

dx = diag(s)==0;

delta = -v * diag((1 -dx)./(diag(s) + dx)) * utf;

jcnorms = sqrt(diag(v * s * s * v'));

theta = theta + delta;

%compute norm of the scaled gradient

gnorm = 0;

if ( oldnorm ≠ 0)
```

dx = delta/oldnorm ;

gnorm = max(abs(dx .* (jcnorms $\cong$ 0)./(jcnorms + (jcnorms==0))));

end

% is gradient norm less than gtol?

if( gnorm < gtol)

info = sprintf('gradient norm = %.3e, less than gtol = %.3e',gnorm,gtol);

return

end

% too many iterations?

if (iter $\geq$ maxiter)

info = sprintf('number of funcion evaluation exceeds %d',maxiter);

return

end

% is step in parameter space less than xtol * norm(theta)?

if (norm(delta) $\leq$ xtol * norm(theta))

info = sprintf('maximum relative step less than %.3e',xtol);

return

end

end

B.7: fdjac2.m

% Module for calculating the Jacobian matrix

function $[fjac, fvec]$ = fdjac2(f,theta,varargin)

```
small = sqrt(eps);

fvec = feval(f,theta,varargin:);

fjac = zeros(size(fvec,1),size(theta,1));

maxstep = 0.1;

for i = 1:size(fjac,2)

smu = theta(i);

h = sign(theta(i)) * min([max(abs(smallsmall * smu)) maxstep]);

theta(i) = theta(i) + h;

fjac(:,i) = (feval(f,theta,varargin:) - fvec)/h;

theta(i) = smu;

end
```

B.8: findk.m

```
% Module for finding the largest linear growth in the residual

function [K, mu] = findk(yobs,yhat,ltol)

N = length(yhat);

if(N < 4)

K=N;

return

end

for K = 4:N

t = linspace(0,1,K)';

A = [ones(K,1) t t.*t];
```

err = yobs(1:K) - yhat(1:K);

mu = A \ err;

if(abs(mu(2))>sqrt(eps) && abs(mu(2))*ltol ≤ abs(mu(3)))

K = min([K N]);

return

end

end

## B.9: Hinffilter.m

% This module estimates the open-circuit voltage. function $[K, Vint, Vc]$ =Hinf-Filter(v,t,i,mu)

N = length(v);

T = t(2) - t(1);

%For the given problem, the related functions are

Fk = $[1 − mu(2) * T \ 0; \ 0 \ 1]$;

Bk = $[mu(1) * T − mu(1) * mu(2) * (T^2)/2; 0]$;

Hk = $[−1 \ 1]$;

Dk = -1* mu(3);

%Let's choose the positive definite symmetric metrices for cost function

% P0 is the estimation error x0 - x0-cap, which keeps getting updated.

P0 = diag([1;1]);

% Qk is based on user's known if any 'a priori'. Suppose if the second element of noise's smaller, then Qk(2,2) should be chosen smaller.

```
Qk = diag([.0017,.0017]);

% Rk is chosen based on any priori for measurement noises.

Rk = 0.0010;

% Sk is based on the user's interest in obtaining a particular accurate state

Sk = diag([3,3]);

Lk = diag([1,1]);

%Let's choose the performace bound as follow

theta = .28;

Gain = [];

%Let's define the initial states

Vc0 = 0;

Vint0 = v(1) - i(1)*mu(3);

x = [Vc0; Vint0];

xhat = x;

xhatarray = [];

for k=1:1:N

Sk-bar = Lk'*Sk*Lk;

K = P0 * inv( 1 - theta * Sk-bar * P0 + Hk' * inv(Rk) * Hk * P0 )* Hk'* inv(Rk);

xhat = Fk * xhat + Bk * [i(k)] + Fk * K * [v(k) - Hk * xhat - Dk * i(k)];

Pk-new = Fk * P0 * inv( 1 - theta * Sk-bar * P0 + Hk' * inv( Rk) * Hk * P0 )* Fk'

+ Qk;

Hinf-cond = eig(inv(P0) - theta * Sk-bar + Hk' * inv(Rk) * Hk);

for num =1:2
```

if(Hinf-cond(num) < 0)

disp(['Hinfinity filter condition fails. Hinf condition is ', num2str(Hinf-cond(num)),'

The index is ', num2str(k)]);

return;

end

end

xhatarray = [xhatarray xhat];

P0 = Pk-new;

Gain = [Gain K];

## B.10: ConvertSOC.m

% This module is used to find SOC vs open-circuit voltage table

function [SOC,Vint] = ConvertSOC(v,t,i)

Qtotal = trapz(t,i);

soc = [1:-.01:0]';

Qspent = Qtotal *(1-soc);

N = length(t);

SOC = [];

Vint =[];

nextnum=2;

for j=1:101

Qtemp = Qspent(j);

for k = nextnum:1:N

```
z = trapz(t(1:k),i(1:k));

if((z == Qtemp)| (abs(z-Qtemp) <0.001))

SOC=[SOC soc(j)];

Vint = [Vint v(k)];

nextnum=k;

break;

end

end

end

NewVint = Vint(end:-1:1);

plot(fliplr(100*SOC),NewVint)

set(gca,'XDir','reverse');
```

B.11: FindSOC.m

```
% Module used to find SOC from coulumb counting method

function [SOC,Volt] = FindSOC(t,v,i)

%The total charge in Ah of a freshly charged 100% soc value is

Qtotal = 3.0560;

soc = [1:-.0001:0.76]';

% SOC from 100% to 76 %

Qspent = Qtotal *(1-soc);

Volt =[v(1)];

NextRank =1;
```

```
SOC =[.885];

%For the CarSim-3 Data, the begining Voltage Vint = 4.016 and hence the correpond-

ing SOC = 88% and Qspent = 0.3667 and the remaining charge Qbegin = 2.6893;

Qarray = [.3667 ];

for k = 2:1:length(i)

z = trapz(t(1:k),i(1:k))/3600; %in Ah

NetQ = 0.3667 + z;

Qarray = [Qarray NetQ];

for j=NextRank:1:length(Qspent)

Qtemp = Qspent(j);

if((NetQ == Qtemp)| (abs(NetQ - Qtemp)<.01))

SOC=[SOC soc(j)];

Volt = [Volt v(k)];

NextRank =j;

break;

end

end

end

figure(1),plot(t,100*SOC), ylabel('SOC '), xlabel('Time, Sec');

figure(2),plot(t,Qarray - 0.3667),ylabel('Cumulative Charge'), xlabel('Time, Sec');
```

B.12: udds-power.m

% Module for simulating power for UDDS cycle

function [PosInd,Ifinal]=udds-power(t,v)

%t is in seconds for the acceleration calculation

V = v*1610/3600; % Velocity in m/s

%Input Data for Simulation

M = 1700; %Mass in kg

fr = 0.01; %Rolling resistance coefficient

g= 9.81; % gravity $(m/s^2)$

row-a = 1.205; % Air mass density $(kg/m^3)$

C-D = 0.3; % Aerodynamic drag coefficient of the vehicle

A-f = 2.2; % Front area of the vehicle $(m^2)$

delta = 1.05; % Rotational inertia factor

i = 0; % Grade of the road. For the flat road, i = 0

a = [0];

Pt = [0];

PosCur = [];

NegCur = [];

PosInd =[];

NegInd =[];

for j=2:length(v)

accel = v(j) - v(j-1);

% The traction power of a vehicle measured on drive wheels can be expressed

Pow = V(j) * ( M*g*fr + 1/2*row-a*C-D*A-f*V(j)*V(j) + M*delta*accel + M*g*i

); % In Watt. Based on IEEE Journal (Ref:Ehsani2010).

Pt = [Pt Pow];

a = [accel a];

end

% Let the efficiency from the motor shaft to motor drive be 90%

%Then the required motor power would be given by

Pm = Pt/0.9;

% LEt the efficiency of the motor be 85%, then

Pmore = Pm/.85;

% LEt the efficincy of the power electronics system be 90%, then the final battery

power would be

Pbatt = Pmore/.9;

%Taking the example of Chevy Volt, suppose the voltage of the battery module is

at 42 V, and 8 modules is used, keeping one as a spare of total 9 modules, the total

current in the module will be

Itotal = Pbatt/(8*42);

% For the above design criteria, the combination of batteries would be 12 in series

with 3 parallel strings. Hence the the current from each string would be

Ib = Itotal/3;

%This would be output

figure(1)

```
plot(t,Ib)

figure(5)

plot(t,Pbatt/1000)

for k=1:length(Ib)

if(Ib(k) ≥ 0)

PosCur = [PosCur Ib(k)];

PosInd = [PosInd t(k)];

else if(Ib(k) < 0)

NegCur = [NegCur Ib(k)];

NegInd = [NegInd t(k)];

end

end

end

PosPow =[PosCur(1)];

NegPow =[NegCur(1)];

TimeInt = [PosInd(1)];

for k=2:1:length(PosCur)

TempPower = trapz(PosInd(1:k),PosCur(1:k));

PosPow = [PosPow TempPower];

TempTime = trapz(PosInd(1:k));

TimeInt = [TimeInt TempTime];

end

for k=2:1:length(NegCur)
```

```
TempPower = trapz(NegInd(1:k),-1*NegCur(1:k));

NegPow = [NegPow TempPower];

end

figure(2),plot(PosInd,PosPow),hold on, plot(NegInd,NegPow)
```

% Assume that only 20% of regenerative power is converted and charged back into battery, the final profile of energy consumed by the UDDS speed profile per Li-ion cell would be

```
RegPow = linspace(NegPow(1),NegPow(end),length(PosPow) - 20);

Ebatt = [PosPow(1:20) (PosPow(21:end) - 0.15*RegPow)]; % Ebatt is the total charge
```

consumed by the current profile in Coulumb

```
figure(3),plot(PosInd,Ebatt)

Ifinal = Ebatt(2:end)./TimeInt(2:end);

figure(4),plot(PosInd(1:end-1),Ifinal)

csvwrite('udds-test.csv',Ifinal');
```

APPENDIX C: SOC VS $V_{INT}$ TABLE

The Table 8 shows $V_{INT}$ vs SOC values for freshly charged 18650-type lithium-ion battery. The discharge was performed at C/55 rate. Table 8 is generated at room temperature of 22°C. Similarly, Table 9 presents the results at 40°C.

Table 8: SOC vs $V_{INT}$ Chart for 18650-type Li-ion battery at C/55

| SOC (%) | $V_{INT}$(V) | SOC (%) | $V_{INT}$(V) | SOC (%) | $V_{INT}$(V) |
|---|---|---|---|---|---|
| 100 | 4.1988 | 66 | 3.7705 | 32 | 3.5739 |
| 99 | 4.1708 | 65 | 3.7635 | 31 | 3.5739 |
| 98 | 4.1567 | 64 | 3.7495 | 30 | 3.5669 |
| 97 | 4.1357 | 63 | 3.7425 | 29 | 3.5669 |
| 96 | 4.1216 | 62 | 3.7354 | 28 | 3.5599 |
| 95 | 4.1076 | 61 | 3.7214 | 27 | 3.5529 |
| 94 | 4.0935 | 60 | 3.7144 | 26 | 3.5529 |
| 93 | 4.0795 | 59 | 3.7073 | 25 | 3.5529 |
| 92 | 4.0654 | 58 | 3.6933 | 24 | 3.5458 |
| 91 | 4.0584 | 57 | 3.6863 | 23 | 3.5388 |
| 90 | 4.0374 | 56 | 3.6793 | 22 | 3.5318 |
| 89 | 4.0303 | 55 | 3.6652 | 21 | 3.5248 |
| 88 | 4.0163 | 54 | 3.6582 | 20 | 3.5178 |
| 87 | 4.0022 | 53 | 3.6512 | 19 | 3.5107 |
| 86 | 3.9882 | 52 | 3.6442 | 18 | 3.5037 |
| 85 | 3.9812 | 51 | 3.6442 | 17 | 3.4897 |
| 84 | 3.9671 | 50 | 3.6371 | 16 | 3.4827 |
| 83 | 3.9531 | 49 | 3.6301 | 15 | 3.4686 |
| 82 | 3.9391 | 48 | 3.6301 | 14 | 3.4546 |
| 81 | 3.932 | 47 | 3.6231 | 13 | 3.4475 |
| 80 | 3.918 | 46 | 3.6161 | 12 | 3.4335 |
| 79 | 3.911 | 45 | 3.6161 | 11 | 3.4265 |
| 78 | 3.8969 | 44 | 3.6161 | 10 | 3.4195 |
| 77 | 3.8829 | 43 | 3.609 | 9 | 3.4124 |
| 76 | 3.8759 | 42 | 3.609 | 8 | 3.4054 |
| 75 | 3.8618 | 41 | 3.602 | 7 | 3.3984 |
| 74 | 3.8548 | 40 | 3.602 | 6 | 3.3914 |
| 73 | 3.8408 | 39 | 3.595 | 5 | 3.3844 |
| 72 | 3.8267 | 38 | 3.595 | 4 | 3.3633 |
| 71 | 3.8197 | 37 | 3.595 | 3 | 3.3212 |
| 70 | 3.8127 | 36 | 3.588 | 2 | 3.2509 |
| 69 | 3.7986 | 35 | 3.588 | 1 | 3.1597 |
| 68 | 3.7916 | 34 | 3.581 | 0 | 3.0052 |
| 67 | 3.7776 | 33 | 3.581 | | |

Table 9: SOC vs $V_{INT}$ Chart for 18650-type Li-ion battery at 40°C

| SOC (%) | $V_{INT}$(V) | SOC (%) | $V_{INT}$(V) | SOC (%) | $V_{INT}$(V) |
|---|---|---|---|---|---|
| 100 | 4.1392 | 66 | 3.7425 | 32 | 3.5616 |
| 99 | 4.1269 | 65 | 3.7389 | 31 | 3.5570 |
| 98 | 4.1041 | 64 | 3.7337 | 30 | 3.5523 |
| 97 | 4.0865 | 63 | 3.7214 | 29 | 3.5476 |
| 96 | 4.0760 | 62 | 3.7056 | 28 | 3.5476 |
| 95 | 4.0619 | 61 | 3.6968 | 27 | 3.5388 |
| 94 | 4.0461 | 60 | 3.6863 | 26 | 3.5336 |
| 93 | 4.0374 | 59 | 3.6793 | 25 | 3.5265 |
| 92 | 4.0251 | 58 | 3.6740 | 24 | 3.5195 |
| 91 | 4.0093 | 57 | 3.6635 | 23 | 3.516 |
| 90 | 3.9987 | 56 | 3.6529 | 22 | 3.5125 |
| 89 | 3.9935 | 55 | 3.6424 | 21 | 3.509 |
| 88 | 3.9847 | 54 | 3.6336 | 20 | 3.502 |
| 87 | 3.9706 | 53 | 3.6284 | 19 | 3.4932 |
| 86 | 3.9531 | 52 | 3.6231 | 18 | 3.4853 |
| 85 | 3.9320 | 51 | 3.6161 | 17 | 3.4774 |
| 84 | 3.9233 | 50 | 3.6134 | 16 | 3.4669 |
| 83 | 3.9180 | 49 | 3.6108 | 15 | 3.4511 |
| 82 | 3.9039 | 48 | 3.6082 | 14 | 3.4423 |
| 81 | 3.8881 | 47 | 3.6055 | 13 | 3.430 |
| 80 | 3.8811 | 46 | 3.6029 | 12 | 3.4177 |
| 79 | 3.8671 | 45 | 3.6003 | 11 | 3.4037 |
| 78 | 3.8478 | 44 | 3.5976 | 10 | 3.3966 |
| 77 | 3.8443 | 43 | 3.5950 | 9 | 3.3896 |
| 76 | 3.8355 | 42 | 3.5924 | 8 | 3.3808 |
| 75 | 3.8302 | 41 | 3.5897 | 7 | 3.380 |
| 74 | 3.8197 | 40 | 3.5871 | 6 | 3.3791 |
| 73 | 3.8004 | 39 | 3.5845 | 5 | 3.3668 |
| 72 | 3.7951 | 38 | 3.5818 | 4 | 3.3475 |
| 71 | 3.7898 | 37 | 3.5792 | 3 | 3.3124 |
| 70 | 3.7828 | 36 | 3.5766 | 2 | 3.2509 |
| 69 | 3.7705 | 35 | 3.5739 | 1 | 3.1737 |
| 68 | 3.760 | 34 | 3.5704 | 0 | 3.0649 |
| 67 | 3.7442 | 33 | 3.5616 | | |